UNIVERSITY OF MINNESOTA
ST. ANTHONY FALLS LABORATORY
Engineering, Environmental and Geophysical Fluid Dynamics

PROJECT REPORT 476

Hydraulic Model Study of the Stilling Basin with a Baffled Chute

By

Omid Mohseni, Luke Carlson and Matthew Lueker

Prepared for
MWH Americas, Inc.
Denver, Colorado

August 2006
Minneapolis, Minnesota

Abstract

The existing stilling basin is filled with backfill sand to counteract the excessive pore pressure from seepage water. To make the existing stilling basin operational a new design was proposed by MWH Americas, Inc. The new design comprises a baffled chute and no stilling basin, i.e. the bed elevation of the existing stilling basin was raised by 14 ft to avoid any backfill sand in the stilling basin. The goal of this physical model study was to assess the performance of the new outlet structure under the probable maximum flood, standard project flood, and the reservoir draw down discharge conditions and different tailwater levels, and to determine the velocity magnitudes downstream of the stilling basin to design the necessary protection measures. The physical model included the spillway, the chute, the stilling basin and about 220 ft of the channel downstream. The model was built at a scale of 1:16.

The physical model study showed that under a series of flow conditions and tailwater levels rolling waves were transported downstream and the channel exhibited unsatisfactory hydraulic conditions. Therefore, several modifications were proposed by MWH, which were incorporated in the physical model and were evaluated. The final design consisted of a baffled chute ending in a stilling basin with a bed elevation 6.5 ft below the channel invert.

Eight test series were conducted on the final design. The test series showed that under the probable maximum flood condition with a tailwater level of 14.5 ft above the datum, the maximum average velocity and the maximum velocity were about 8.8 and 13 fps, respectively. Under the standard project flood condition with a tailwater of 13.3 ft above the datum, the maximum average velocity and the maximum velocity were about 9.3 and 13 fps, respectively. Under the drawdown flood condition with a tailwater of 11.5 ft above the datum, the maximum average velocity and the maximum velocity were about 8.4 and 10 fps, respectively. However, under the drawdown flood condition with no tailwater, a hydraulic drop occurred at the downstream end of the stilling basin and the flow regime became supercritical with a maximum average velocity and a maximum velocity of 8.7 and 16 fps, respectively.

Acknowledgements

The work reported herein was supported by MWH Americas Inc. Craig Harris from MWH Americas Inc. was the project manager and Mr. John Haapala was the project engineer. We also thank Richard Christopher, Mike Plante, Ben Erickson and Alex Ding of St. Anthony Falls Laboratory for their contribution to the model construction and documentation.

Table of Contents

List of Figures

List of Tables

1. Introduction

After initial evaluation of the existing stilling basin downstream of the outlet structure of the cooling water reservoir under several flow conditions and a range of tailwater conditions (Mohseni et al., 2005), MWH Americas Inc. requested a physical model study of a new design of the stilling basing. The existing stilling basin has a bed elevation of 7 ft below the datum (-7 ft) and in order to counteract the excessive pore pressure from seepage water, the stilling basin is currently filled with backfill sand. To avoid the backfill in the stilling basin and to make the stilling basin operational, a new design was proposed by MWH, which is comprised of a baffled chute ending in the 250-ft wide channel downstream at an elevation of 7 ft above the datum. To evaluate the performance of the baffle blocks which were designed at three different sizes, increasing in the downstream direction, the original model of the stilling basin was modified and several series of tests were conducted. The flow conditions of interest are the probable maximum flood (PMF), the standard project flood (SPF) and the reservoir drawdown flood (RDD), which are estimated to be at 4296 cfs, 3369 cfs and 2300 cfs, respectively. Table 1.1 gives the production tests under which the proposed design was evaluated.

Table 1.1. Target discharges and tailwaters of the production tests

Reservoir Elevation (feet)	**Spillway Discharge (cfs)**	**Tailwater Level (ft)**	**Tailwater Level (ft)**
52.1	**4296**	**14.5 (50 year flood)**	**16.0 (500-year flood)**
50.5	**3369**	**13.3 (5-10 year flood)**	**16.0 (500-year flood)**
49.0	**2300**	**7.0 (No tailwater from Colorado River)**	**14.5 (50 year flood)**

2. Model Construction

The model was built at St. Anthony Falls Laboratory at a scale of 1:16. Using a 1:16 scale Froude similarity, model parameters were scaled as follows:

Length	1:16
Area	1:256
Volume	1:4096
Flow rate	1:1024
Velocity	1:4
Time	1:4

2.1. General Features of the Physical Model

The new design proposed by MWH is shown in Figure 2.1. The upstream end of the original model, i.e. the reservoir, the gated ogee spillway and part of the chute with a slope of 22:1, and the downstream end of the model, i.e. a section of the tailrace channel and the leaf drop gate for controlling the tailwater condition, were maintained as in the original model (Mohseni et al., 2005). In the new design, most of the chute downstream of the ogee spillway and the stilling basin were modified. All modifications were built from plywood and lumber (Figure 2.2 and 2.3), painted and sealed.

The physical model construction accuracy was maintained at 0.01 feet (one eighth of an inch), which corresponds to 0.16 feet in the prototype. The construction accuracy of the baffle blocks was at 0.005 ft, which corresponds to 0.08 feet for the prototype.

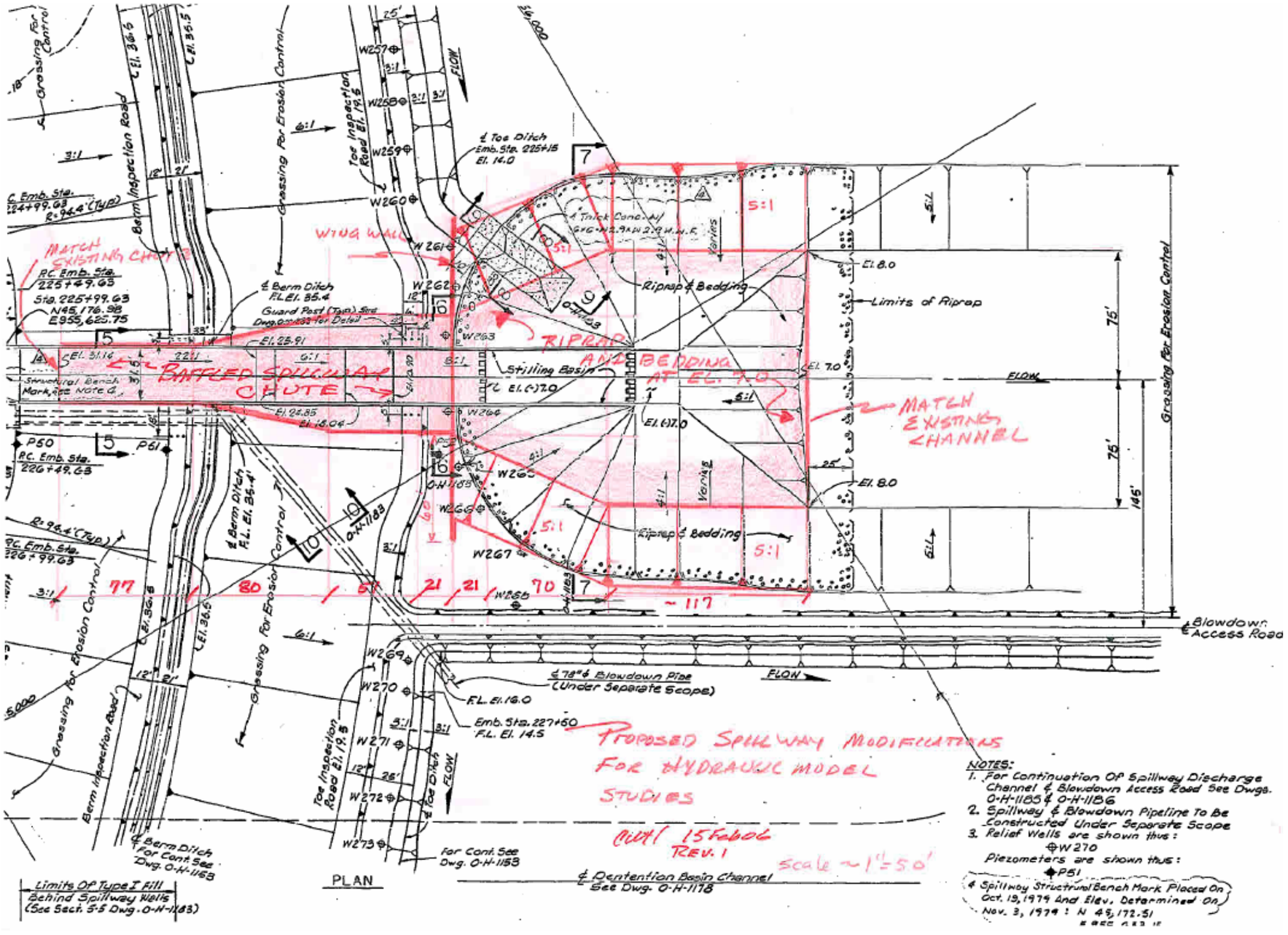

Figure 2.1. Plan view of the existing prototype reservoir outlet structure with the proposed design in red.

Figure 2.2. Modifications made to the downstream channel using lumber.

Figure 2.3. The model was built from lumber and plywood and sealed.

2.2. Instrumentation

To measure water surface elevations upstream of the spillway, i.e. in the reservoir, and downstream in the tailrace two wet wells were provided. The upstream wet well was connected to a pressure tap via a ¼-inch plastic tube to the head tank. The downstream well was connected to the bottom of the channel at several locations close to the middle of each cross-section via pressure taps, ¼-inch plastic tubes, and a series of valves. Water levels in the wet wells were measured using point gages with a precision of 0.001 ft. The zero points of all gages were surveyed.

To measure water velocity, a two-dimensional Sontek FlowTracker Acoustic Doppler Velocimeter (ADV) was mounted on a carriage (Figure 2.4) to measure the velocity of a cylindrical sampling volume (0.24″ diameter, 0.35″ height) located 4 inches away from the probe with an accuracy of +/-1.0%. All velocity measurements were taken at 20% and 80% of the total water depth, measured from the bed, when the water depth was 4 inches or more. For water depths less than 4 inches, velocities were measured at 60% of the water depth measured from the bed. The ADV sampled velocities at a frequency of 1 Hz over 60 seconds in the model, equal to 4 minutes in the prototype. Mean standard errors were below 0.1 fps in the model.

To measure total flow through the model, the sharp-crested weir which had been previously installed in the head tank was recalibrated, i.e. the wet well readings were calibrated to flow rates using the SAFL weigh tanks. Figure 2.5 shows the results of the calibration.

Flow patterns along the baffled chute and downstream of the chute were documented using digital video cameras; the video clips on DVDs are enclosed.

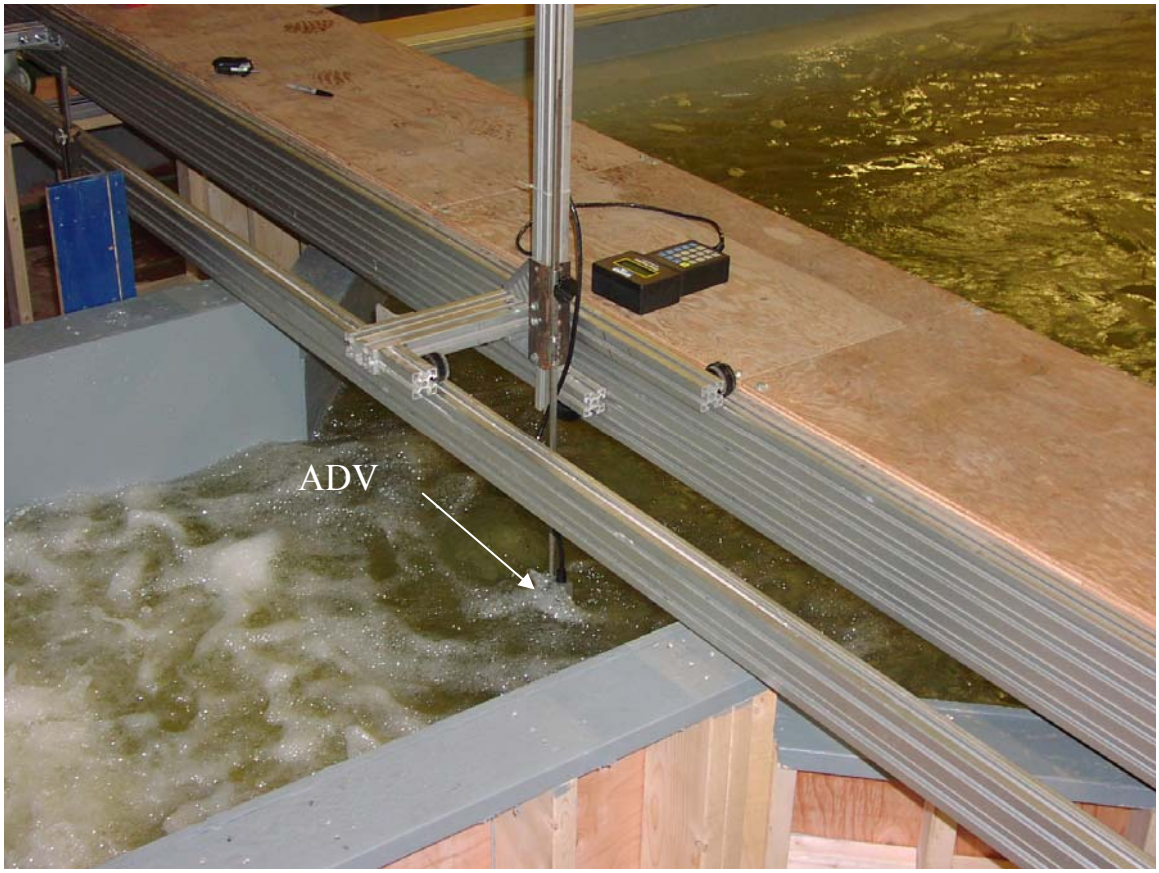

Figure 2.4. A 2-dimensional Acoustic Doppler Velocimeter (ADV) mounted on the carriage to measure flow velocities across the width and depth of the tailrace channel.

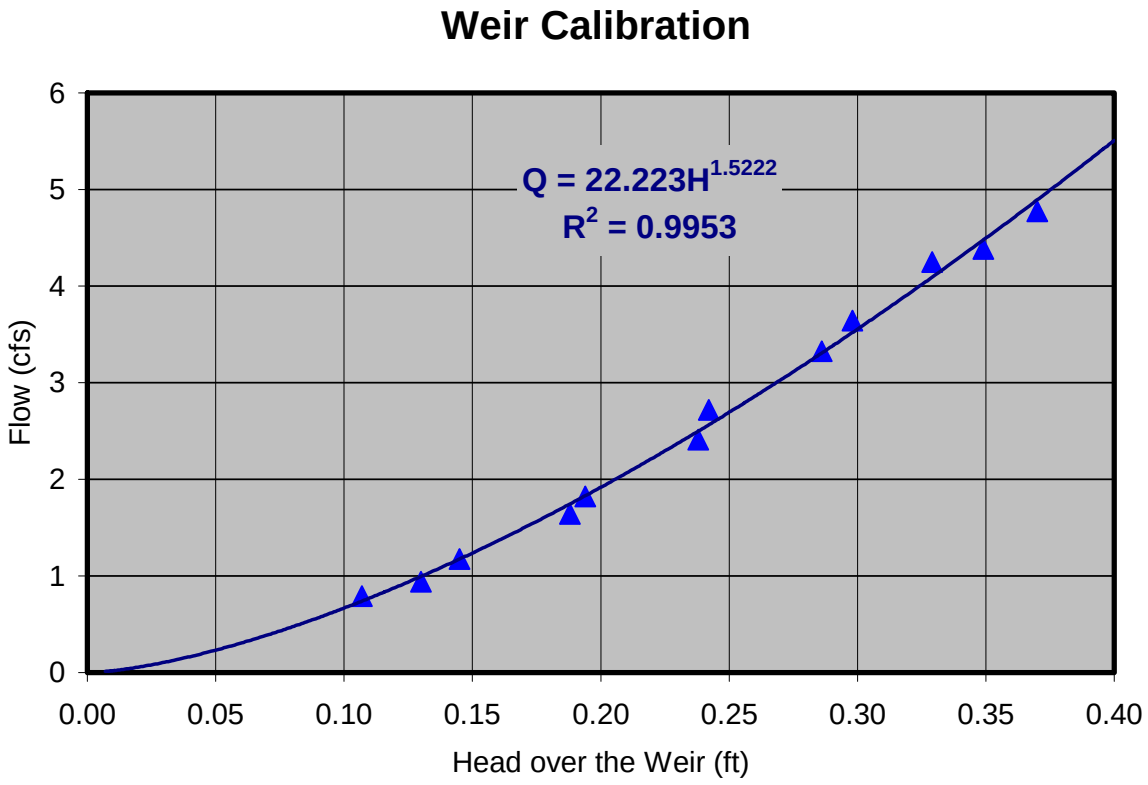

Figure 2.5. To calibrate the graduated wet well against flow over the weir, the measured flows using the SAFL weigh tanks were plotted versus the wet well readings (gage pressure).

3. Modifications and Test Series

Several modifications were proposed by MWH to determine the hydraulically acceptable design for an outlet structure which could efficiently dissipate the energy of the outflow into the downstream channel. After making each modification, the flow conditions over the chute and in the downstream channel were visually evaluated and if it seemed acceptable a test series was conducted. This test series which was labeled the "initial test series" in the Scope of Work document consisted of a series of velocity measurements downstream of the chute under a flow condition of 4296 cfs with a tailwater of 14.5 ft (the 50-year flood level) and a reservoir elevation of 52.1 above the datum. After the final modifications, the production tests were conducted as outlined in Table 1.1.

Most test series were documented using a digital video camera. In the following sections each design and the associated test results are presented.

3.1. Baffled Chute with 90-Degree Wingwalls and No Stilling Basin

The first modification proposed by MWH is shown in Figure 3.1, where the chute extended 157 ft at a slope of 22:1 from the toe of the ogee spillway and then for an additional 57 ft at a slope of 3:1 until it reached the elevation of 7 ft above the datum where water was discharged into the downstream channel. In addition, 77 ft from the toe of the spillway, the width of the chute gradually expanded from 31.5 ft to 70 ft. The length of the expansion was 80 ft and it ended where the bed slope changed to 3:1. Three types of baffle blocks were considered for this design. The configuration of the baffle blocks is shown in Figure 3.1. The corresponding model was constructed as shown in Figure 3.2. The model was built such that the baffle blocks could be reconfigured over the expansion area and the 70-ft wide section of the chute. It was decided that the small baffle blocks on the upper 77-ft section of the chute, where the width was 31.5 ft would not be installed, until after the flow quality over the downstream baffle blocks had been observed and evaluated. Therefore, only six rows of small baffle blocks, six rows of medium size baffle blocks and seven rows of large blocks were installed (Figure 3.2).

Following is the summary of the visual assessment of the flow conditions:

- The baffle blocks were effective in dissipating the energy of the outflow.

- There was no need to install the small baffle blocks on the upper 77-ft of the chute.
- Under high flow conditions, the jet out of the first row of the large baffle blocks located at the end of the 22:1 sloped reach of the chute skipped the second row of the large blocks which were located at the beginning of the 3:1 slope of the chute.
- A strong flow separation was evident near the wing walls where flow entered the downstream channel where the width expanded to 250 ft. Subsequently, the flow velocities in the middle section of the channel seem to be too high to be protected by riprap.
- In addition, it was noted that this design would interfere with several existing relief pressure wells.

It was decided that the initial test series with this modification would not be conducted, but that the design would be modified to improve the hydraulic conditions over the baffle blocks and in the tailrace channel.

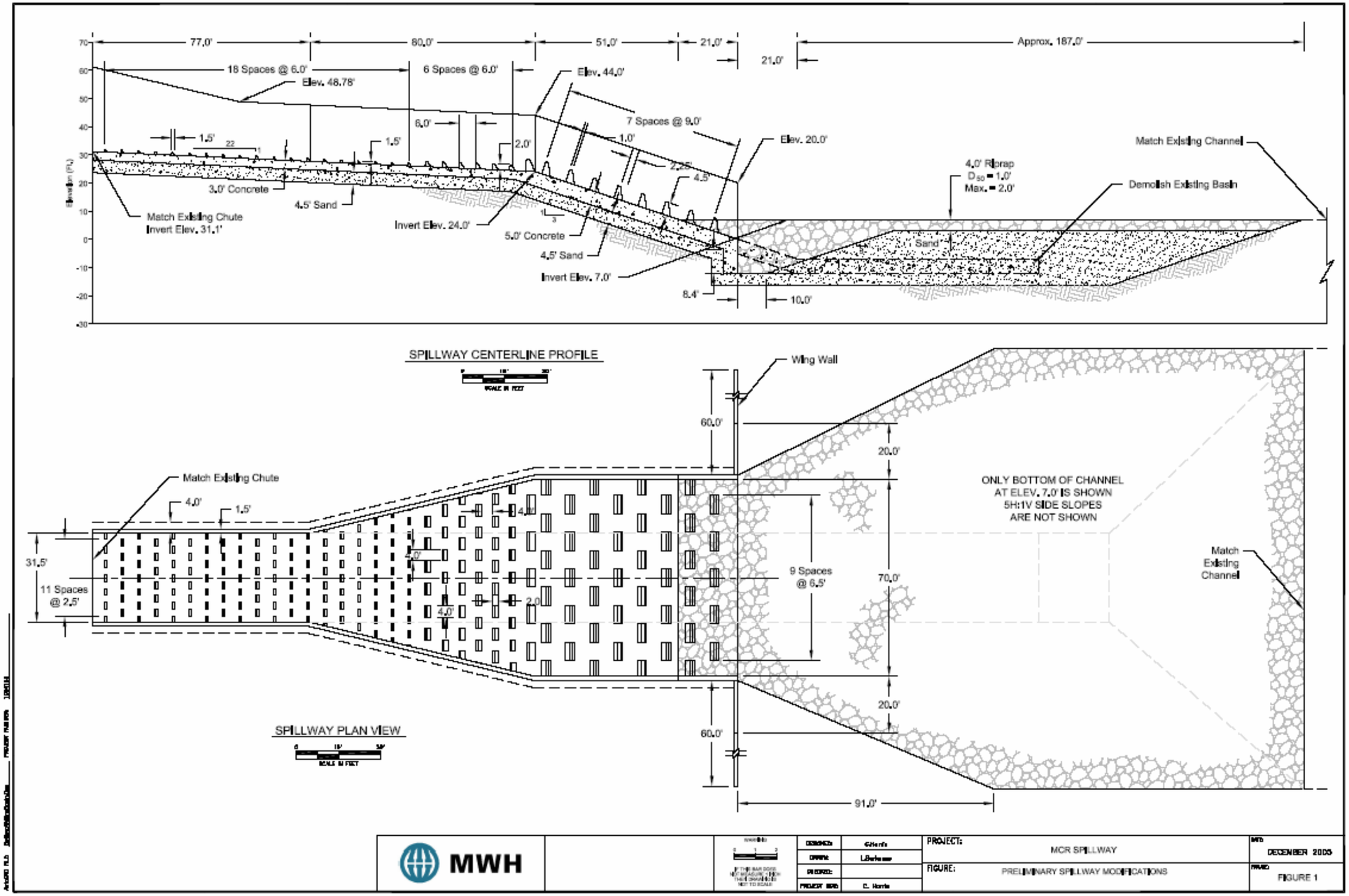

Figure 3.1. First proposed modification to the outlet structure.

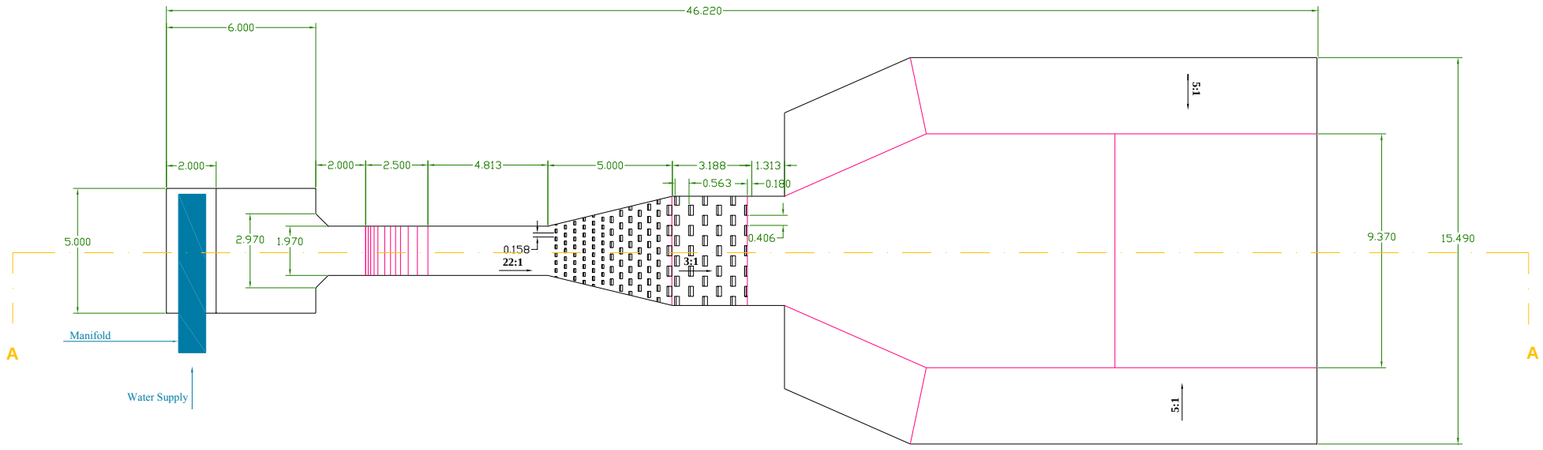

PLAN VIEW

All dimensions are in feet

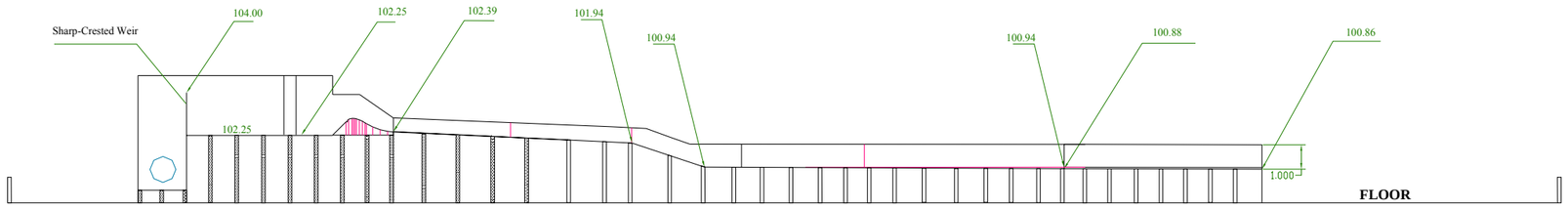

Section A-A

All dimensions are in feet

Figure 3.2. Plan view and longitudinal cross-section of the model layout of the first modification to the outlet structure.

3.2. Baffled Chute with Flared Wingwalls and No Stilling Basin

In this modification, MWH proposed to adjust the distance between the first (on the section with a 22:1 slope) and the second (on the section with a 3:1 slope) rows of the large baffle blocks, and remove the last two rows of the medium sized baffle blocks replacing them with one new row of the large baffle blocks. Therefore, the number of rows of the medium sized baffle blocks dropped to four, while the number of rows of large baffle blocks rose to eight. In addition, to avoid any interruption to the existing pressure relief wells, the channel downstream of the chute was extended for another 21 ft and then its wingwalls were flared (Figure 3.3 the prototype and Figure 3.4 the model).

With these modifications, a test series was conducted meeting the initial test series conditions. The measured flow was at 4209 cfs and the tailwater level was at 14.5 ft above the datum. The X- and Y-components of the velocities were measured at the cross-sections and locations shown in Figure 3.5. In addition, the water surface profile along the centerline of the channel was measured using the wet wells. As shown in Figure 3.6, the water surface dropped around cross-section A and a hydraulic jump occurred upstream of the expansion in the tailrace channel. The flow regime was subcritical throughout the tailrace channel. However, rolling waves transported downstream creating swirls and rough surface in the channel. The water depth at cross-section A was too small to provide any meaningful velocity measurement using ADV.

The X- and Y-components of the velocities at cross-sections B to E are displayed in Figures 3.7 to 3.14. Figure 3.7 shows that the velocity distribution was not symmetrical at cross-section B due to unsteady characteristic of the swirls. Figures 3.8 to 3.10 show that there was a return flow (negative velocities) at 20% depth due to the transport of the rolling waves downstream. Y-components of velocity at the above cross-sections showed no symmetry (Figures 3.11 to 3.14). It was clear that this design did not provide favorable hydraulic conditions in the tailrace channel, therefore, new modifications were proposed as described in Section 3.3.

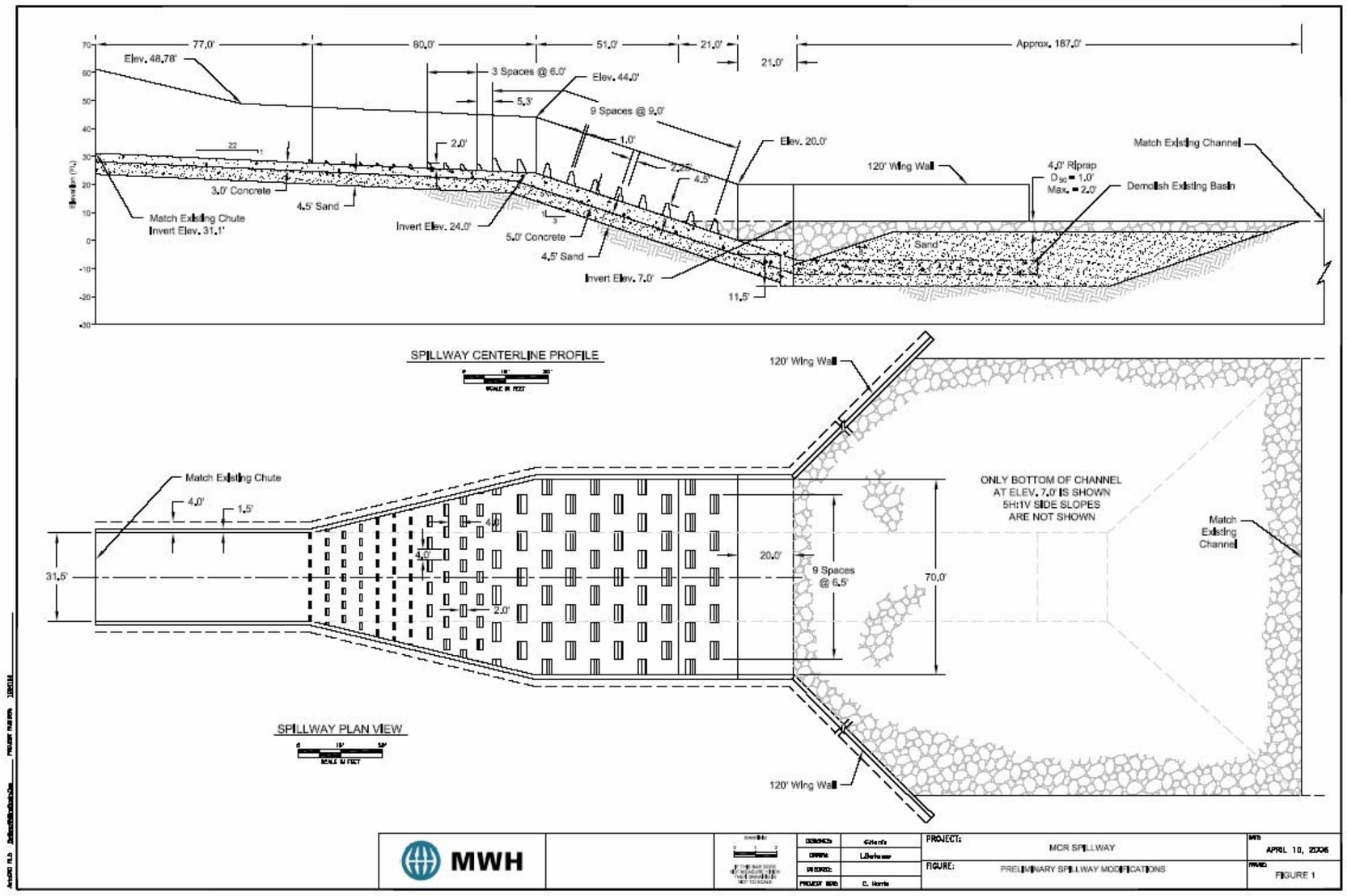

Figure 3.3. Second proposed modification to the outlet structure with flared wingwalls at the upstream end of the tailrace channel.

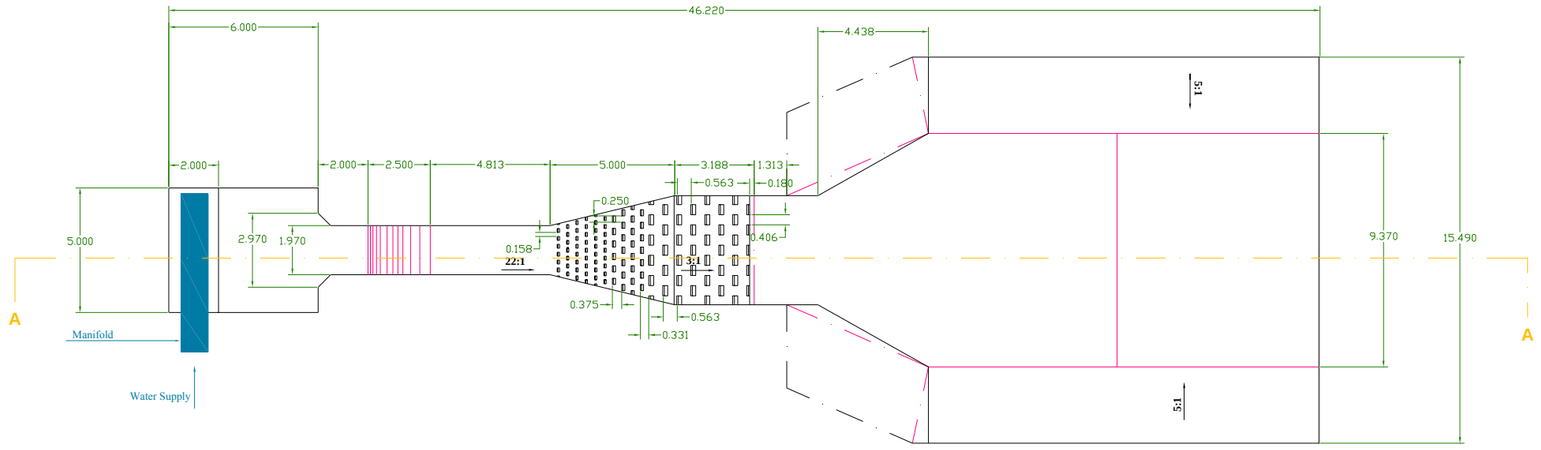

PLAN VIEW

All dimensions are in feet

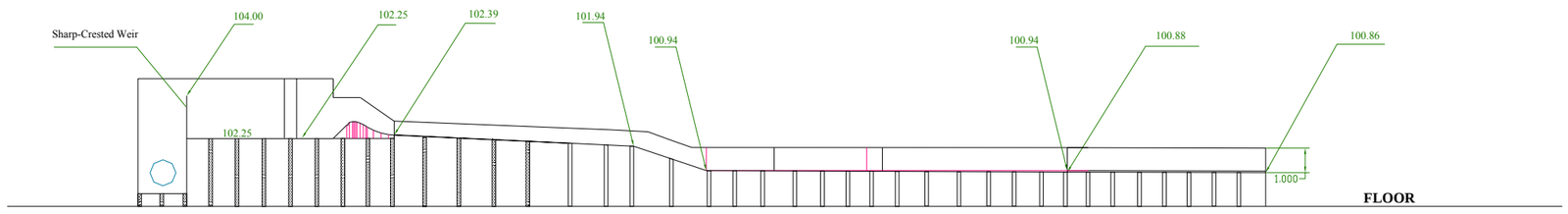

Section A-A

All dimensions are in feet

Figure 3.4. Plan view and longitudinal cross-section of the model layout of the second modification to the outlet structure with flared wingwalls.

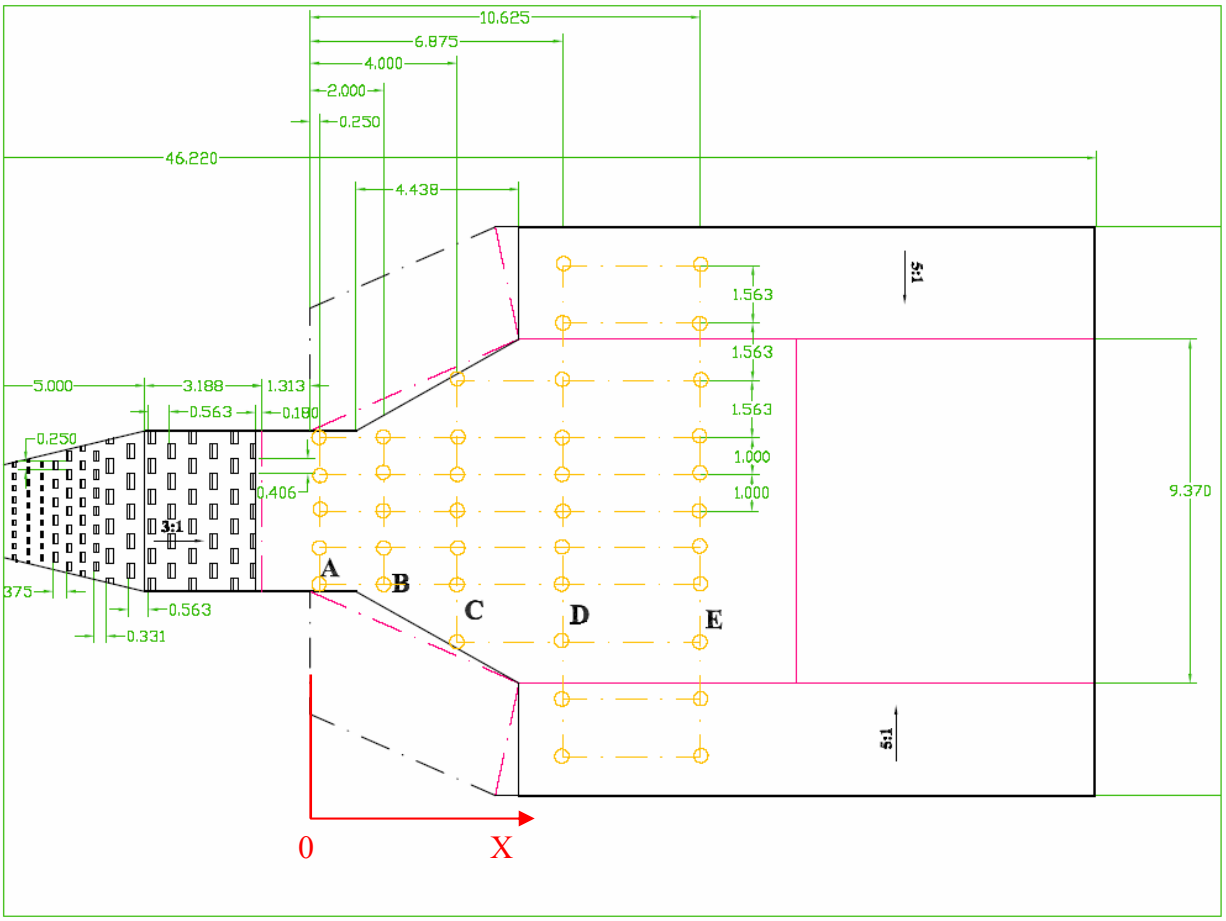

Figure 3.5. Cross-sections A through E and locations where flow velocities were measured. Dimensions are in feet (model).

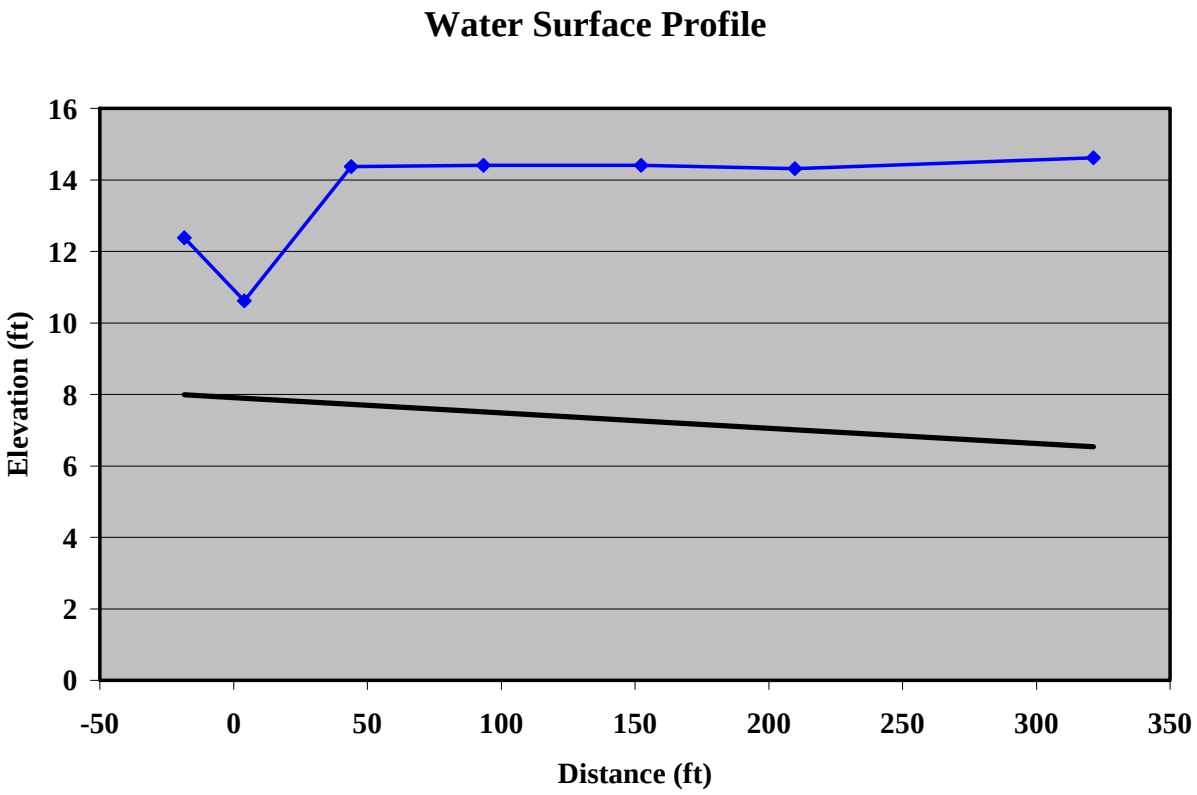

Figure 3.6. Water surface profile along the center of the channel downstream of the chute. X=0 is shown in Figure 3.5, which is 4 ft upstream of cross-section A.

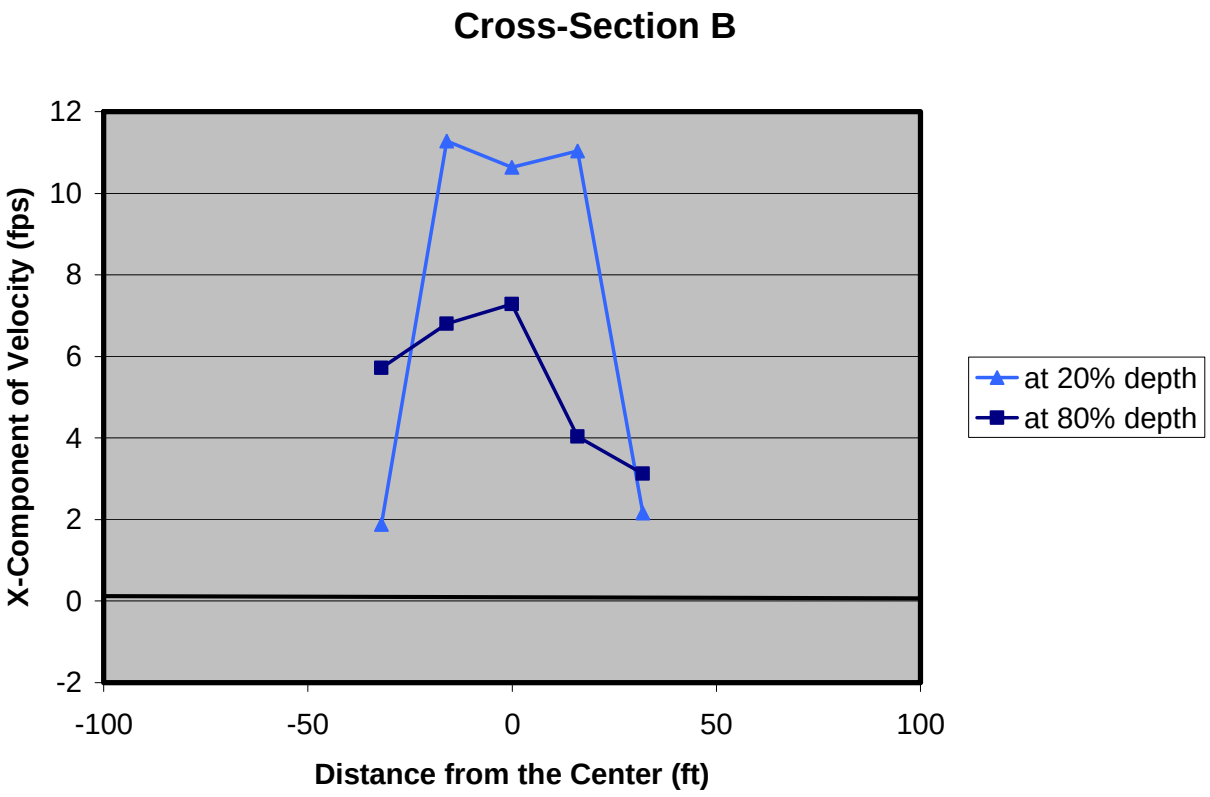

Figure 3.7. X-component of velocity distribution measured at cross-section B under a flow condition of 4209 cfs and a tailwater level of 14.5 ft above the datum.

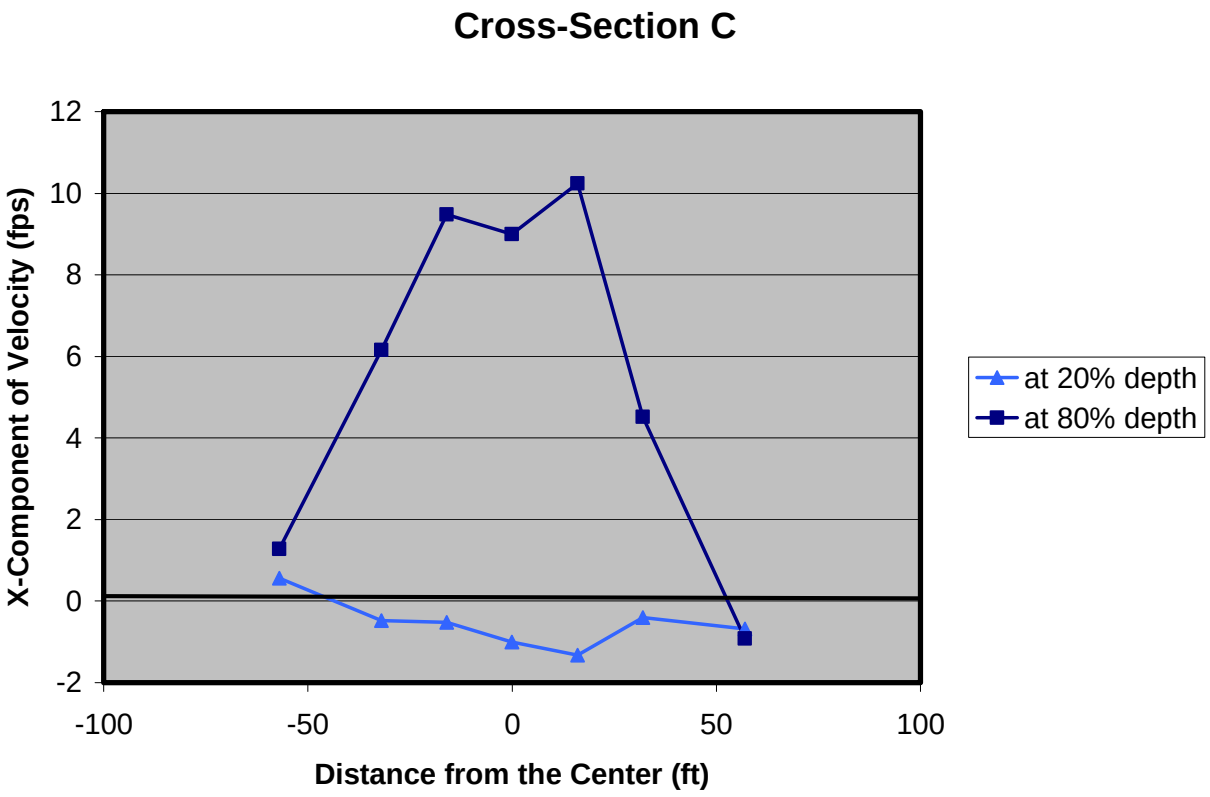

Figure 3.8. X-component of velocity distribution measured at cross-section C under a flow condition of 4209 cfs and a tailwater level of 14.5 ft above the datum.

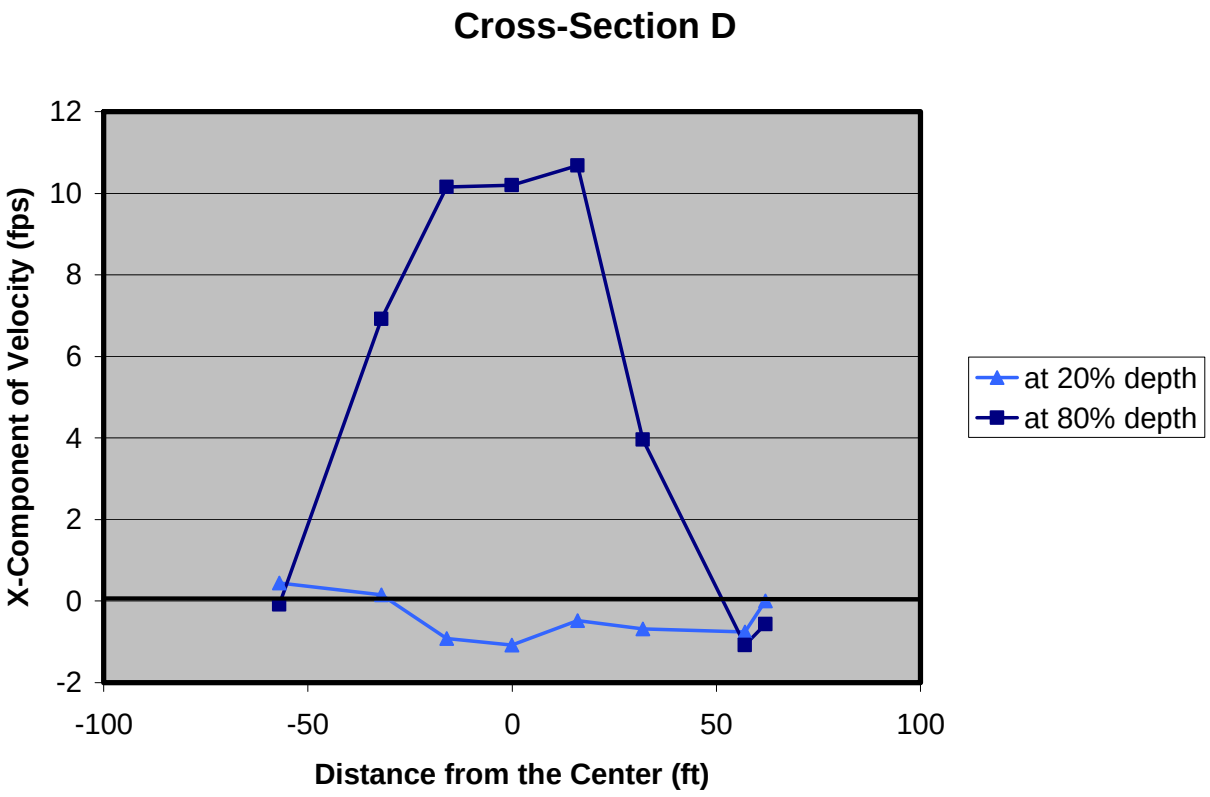

Figure 3.9. X-component of velocity distribution measured at cross-section D under a flow condition of 4209 cfs and a tailwater level of 14.5 ft above the datum.

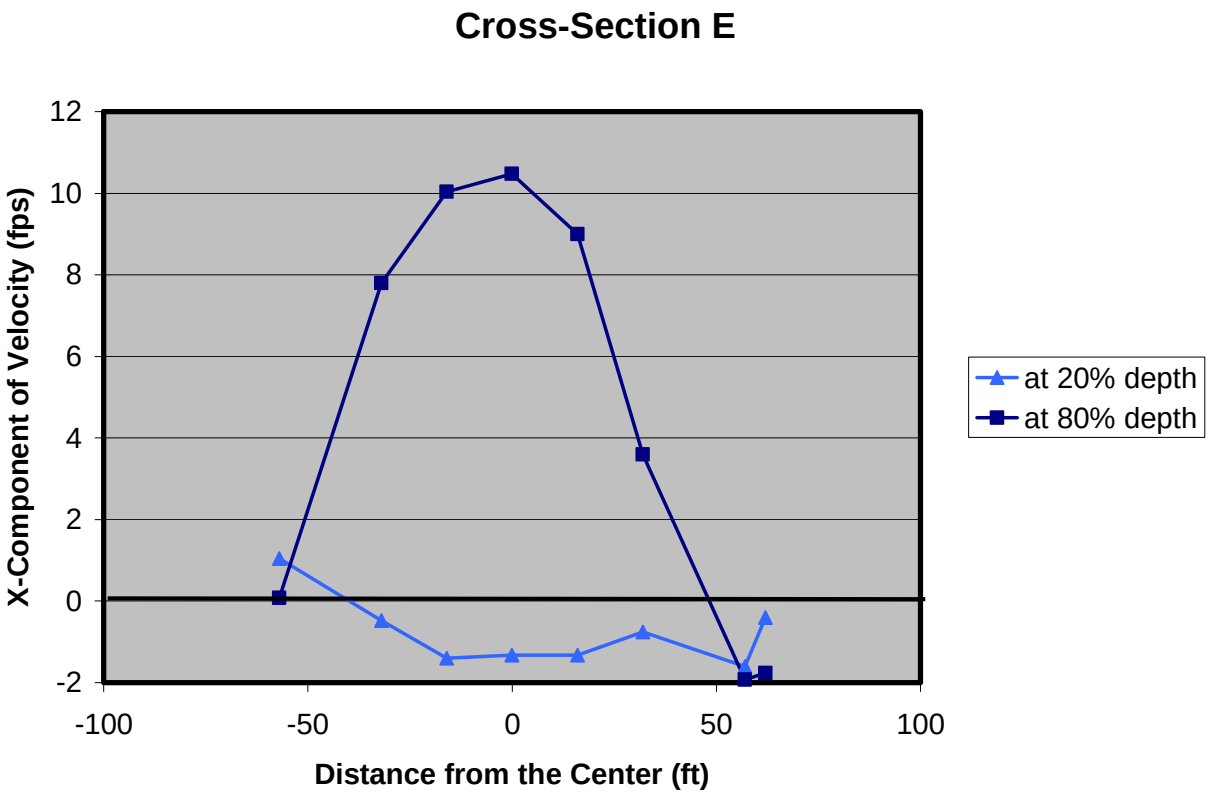

Figure 3.10. X-component of velocity distribution measured at cross-section E under a flow condition of 4209 cfs and a tailwater level of 14.5 ft above the datum.

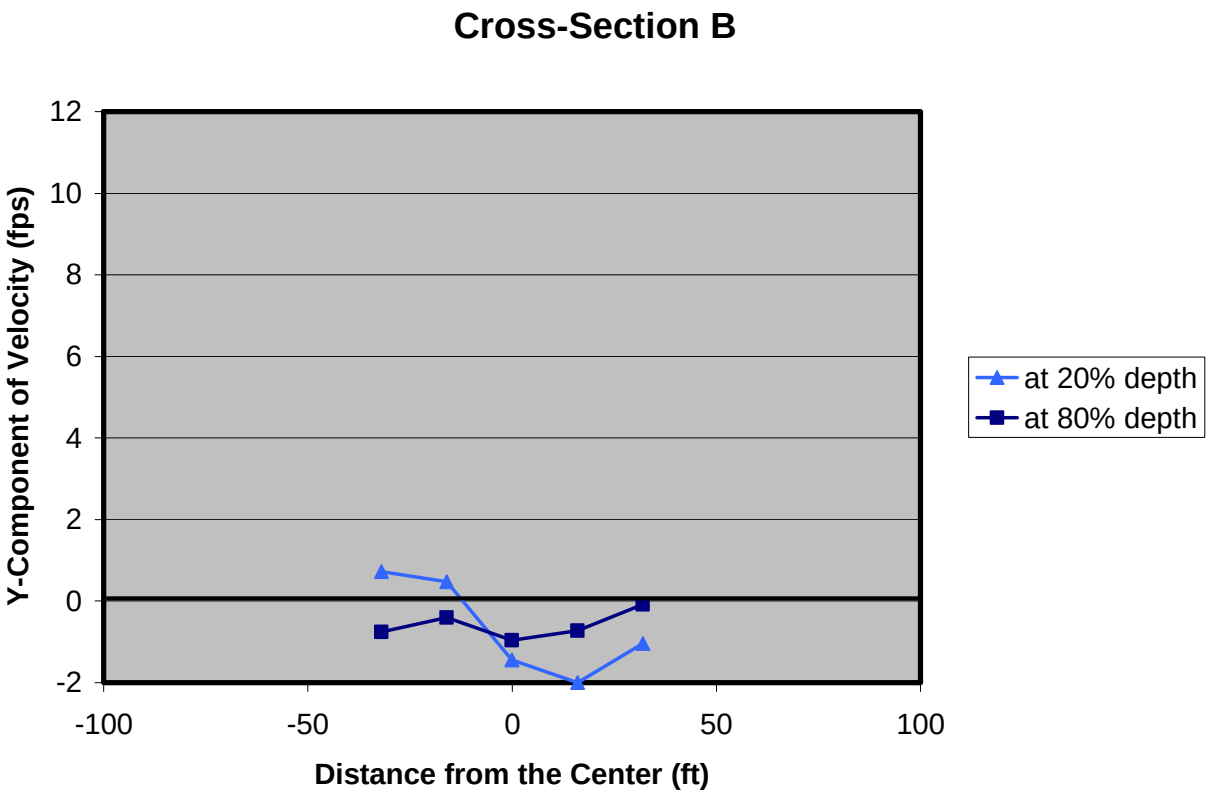

Figure 3.11. Y-component of velocity distribution measured at cross-section B under a flow condition of 4209 cfs and a tailwater level of 14.5 ft above the datum

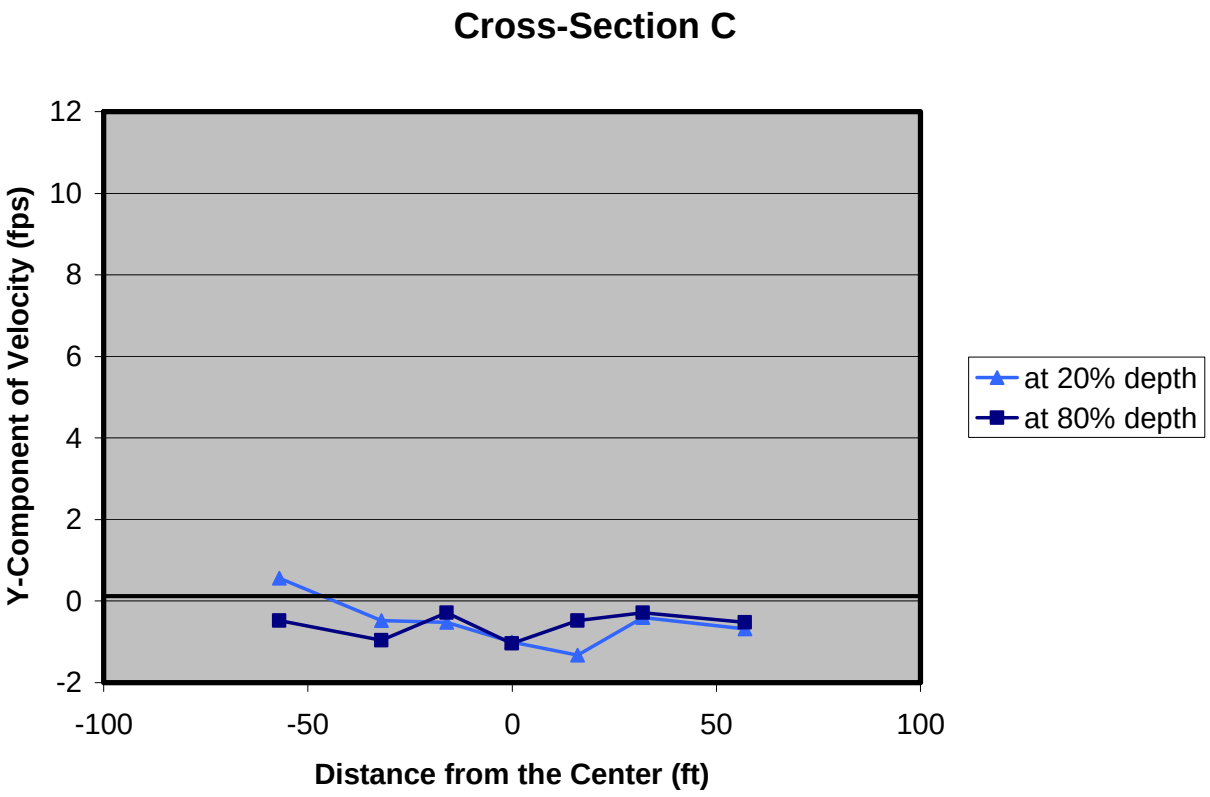

Figure 3.12. Y-component of velocity distribution measured at cross-section C under a flow condition of 4209 cfs and a tailwater level of 14.5 ft above the datum

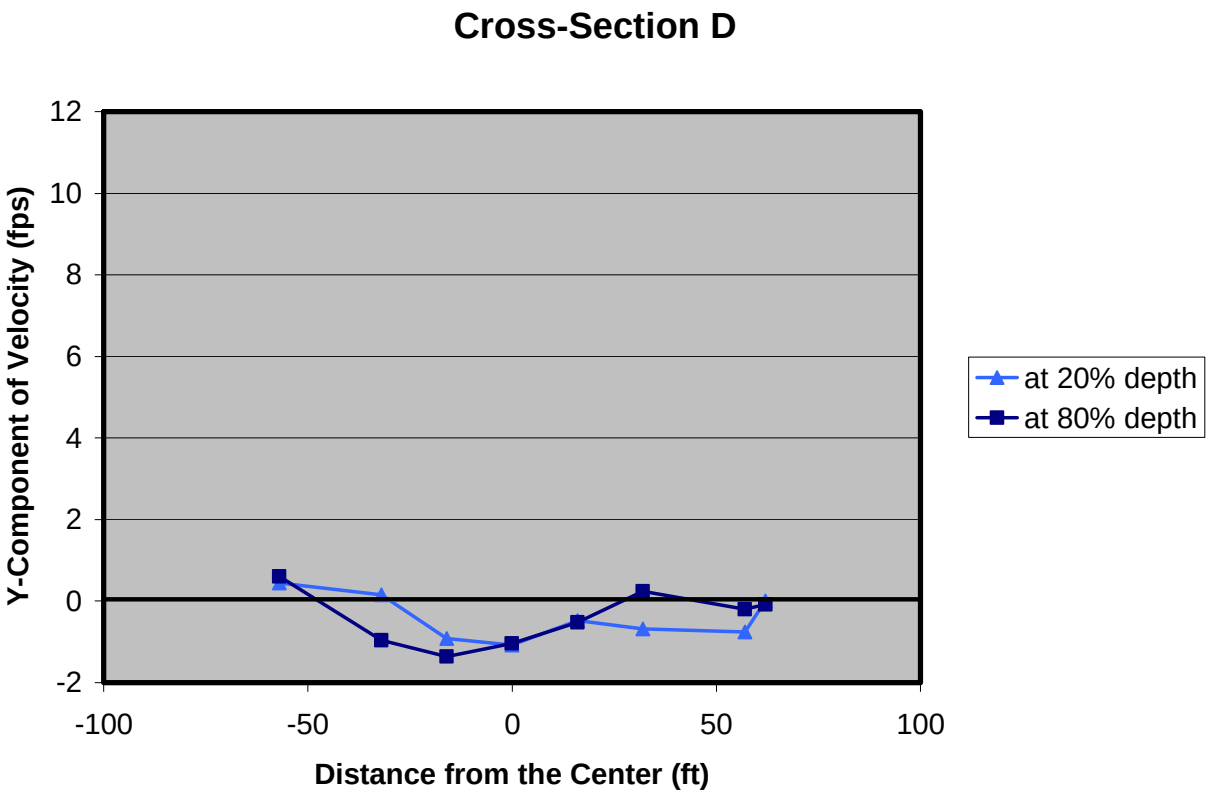

Figure 3.13. Y-component of velocity distribution measured at cross-section D under a flow condition of 4209 cfs and a tailwater level of 14.5 ft above the datum

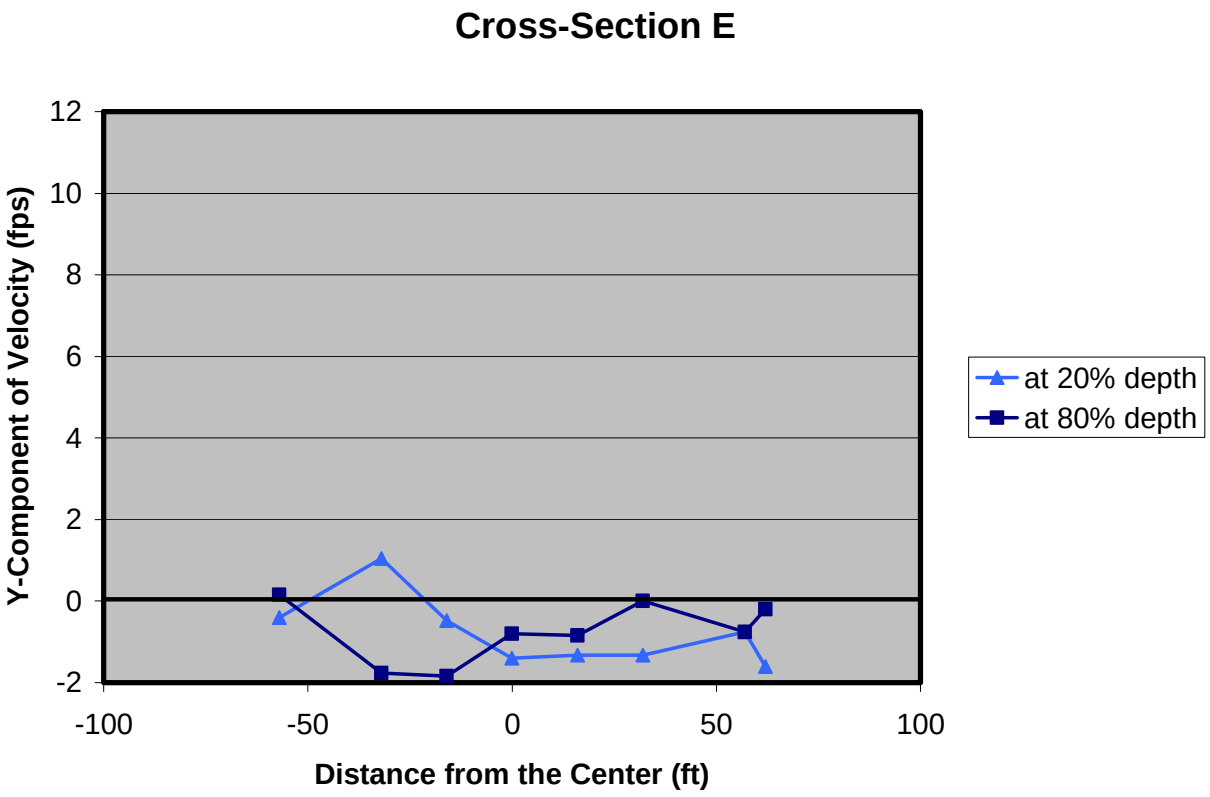

Figure 3.14. Y-component of velocity distribution measured at cross-section E under a flow condition of 4209 cfs and a tailwater level of 14.5 ft above the datum

3.3. Baffled Chute with Additional Baffle Blocks and No Stilling Basin

At this stage, it was decided that a couple of minor modifications would be made to the structure and that the flow patterns would be documented using a digital video camera before making any substantial modifications. The modifications were (1) adding two rows of baffle blocks at the upstream end of the 70-ft wide section of the tailrace channel, and (2) removing the flared wingwalls, i.e. making 90-degree wingwalls similar to Section 3.1, with the two new rows of baffle blocks in place. Flow conditions, were visually evaluated under three flow conditions with relatively low tailwater levels which could exacerbate the hydraulic condition in the downstream channel. The results are summarized in Table 3.1.

Table 3.1. Qualitative assessment of the flow conditions

Target Discharge (cfs)	Tailwater (ft)	Condition 1	Condition 2	Condition 3
		No baffle block in the tailrace channel with flared wing walls	Two rows of baffle block in the tailrace channel with flared wingwalls	Two rows of baffle block in the tailrace channel with no flared wingwalls
2300	8.5	Hydraulic jump moved downstream	Hydraulic jump moved downstream	Hydraulic Jump moved downstream
3369	11.6	Strong swirls in the downstream channel	Swirls in the downstream channel	Hydraulic jump upstream of the expansion; swirls in the downstream channel
4296	12.2	Very strong swirls in the downstream channel	Very strong swirls in the downstream channel	Hydraulic jump upstream of the expansion; very strong swirls in the downstream channel

Condition 1 in Table 3.1 gives the qualitative assessment of the tests done with the modification described in Section 3.2. The actual flows were 2284, 3297 and 2284 cfs and the tailwater levels were 8.5, 11.5 and 12.3 ft above the datum, respectively.

For Condition 2, under a 2300 cfs flow and a tailwater of 8.5 ft above the datum, the flow regime was subcritical in the 70-ft wide section of the tailrace channel. At the beginning of the expansion, a hydraulic drop occurred and the flow regime became supercritical, i.e. flow exhibited very high velocities, and the hydraulic jump moved downstream as shown schematically in Figure 3.15. Under higher flow conditions, the hydraulic jump occurred in the

70-ft wide section of the tailrace channel but slightly further downstream in comparison to Condition 1 (Figure 3.16). Condition 3, i.e. removing the flared wingwalls and shortening the 70-ft wide section of the channel, did not improve the hydraulic conditions under any of the three flow conditions.

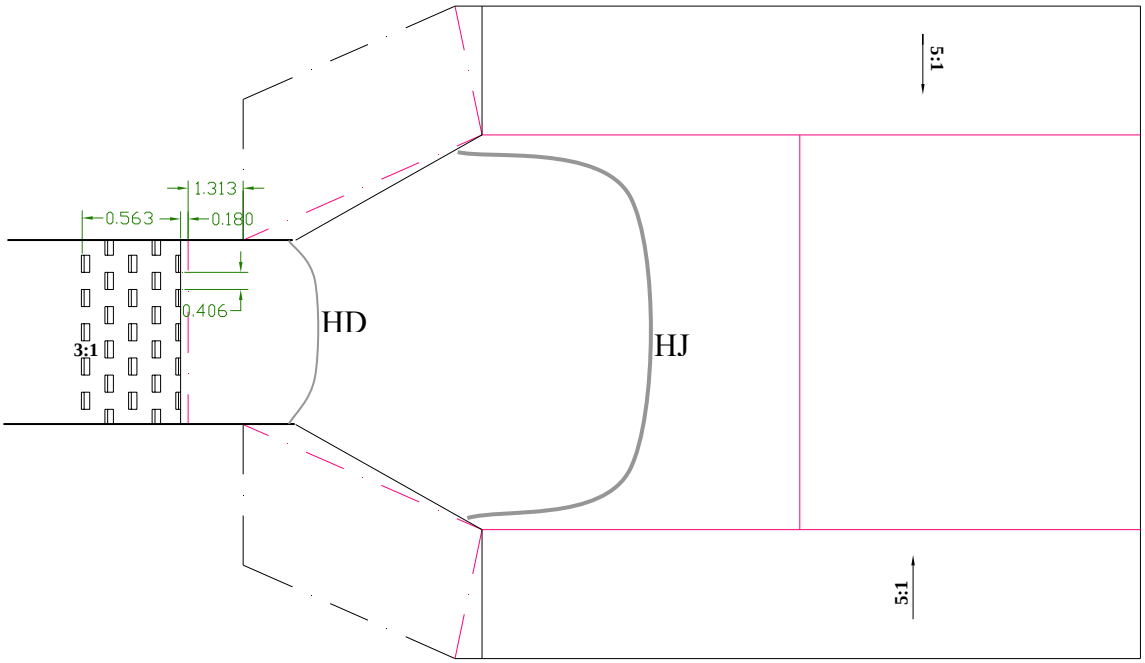

Figure 3.15. Schematic location of the hydraulic jump (HJ) in the downstream channel under the flow condition of 2300 cfs and a tailwater of 8.5 ft above the datum. HD stands for hydraulic drop.

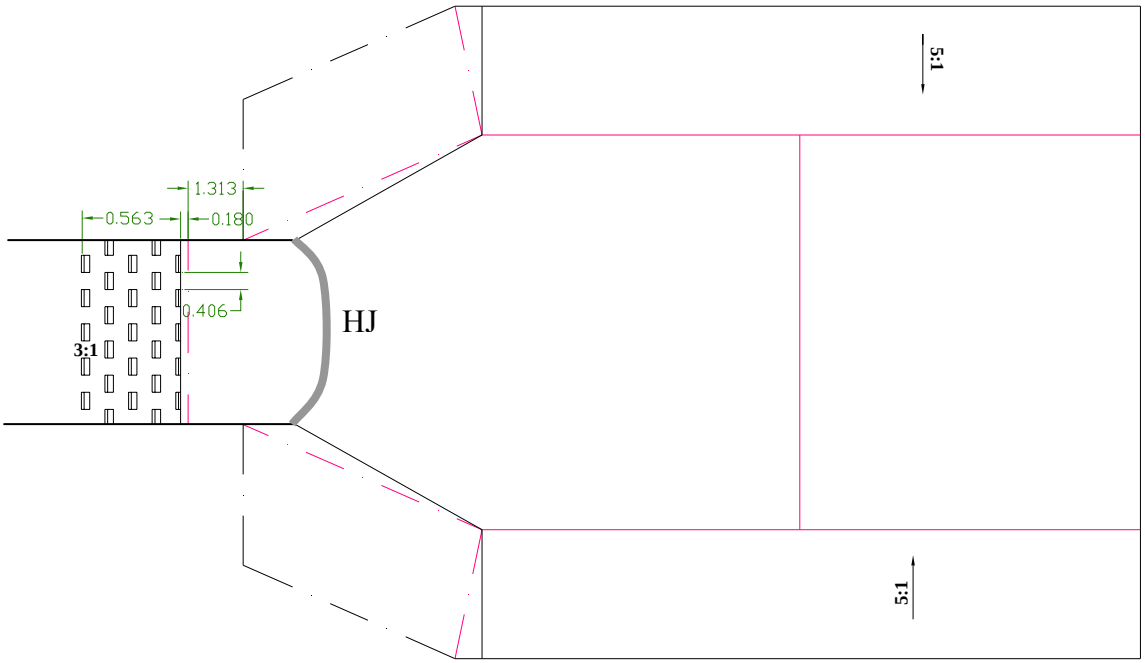

Figure 3.16. Schematic location of the hydraulic jump (HJ) in the downstream channel under the flow condition of 4296 cfs and a tailwater of 12.2 ft above the datum.

3.4. Baffled Chute with a Stilling Basin

In order to avoid the occurrence of a hydraulic jump in the downstream channel, MWH proposed a deep stilling basin at the downstream end of the chute. The bed elevation of the stilling basin was set at 1.5 ft above the datum. In addition, the chute downstream of the spillway was modified. The chute extended 115 ft at a slope of 22:1 from the toe of the ogee spillway and then it expanded over a distance of 69 ft from a width of 31.5 ft to 70 ft with a slope of 6:1, and finally it was extended another 34 ft with a slope of 3:1 at a constant width of 70-ft until it reached the stilling basin at an elevation of 1.5 ft above the datum (Figure 3.17). The stilling basin was 48 ft long with an end-sill at its downstream end. The baffle blocks were also rearranged with four rows of small baffle blocks at the end of the 22:1 slope chute, four rows of the mid size baffle blocks on the expansion section of the chute, and 10 rows of large baffle blocks on the remaining length of the chute. In addition, 45-degree wingwalls were provided exactly downstream of the stilling basin.

The model layout is shown in Figure 3.18 and the constructed model is shown in Figures 19a and 19b. The model chute was built such that the mid size and large baffle blocks could be reconfigured. In addition, provisions were made to easily lower the bed elevation of the model stilling basin by one ft (the white board shown in Figure 19b), i.e. providing a bed elevation of 0.5 ft above the datum. With the bed elevation at 0.5 ft, the model stilling basin would become slightly shorter.

The initial test series (a flow condition of 4296 and a tailwater elevation of 14.5 ft) was repeated with the stilling bed elevation at 1.5 ft. The water surface profile in the downstream channel is shown in Figure 3.20. Distances were measured from the downstream end of the stilling basin. No hydraulic jump moved out of the basin under this flow condition. The hydraulic jump occurred at the upstream end of the stilling basin.

Velocities were measured at the cross-sections and locations given in Figure 3.21. The X-components of velocities at cross-sections A to E are shown in Figures 3.22 to 3.26. At cross-section A (Figure 3.22), lower velocities were exhibited at the mid point of the cross-section, which were due to the presence of a baffle block at the mid point of the last row of large baffle blocks (Figures 3.17 and 3.18). The velocity distributions across the width were relatively

symmetrical (Figures 3.22 to 3.26). Very weak flow separation was exhibited along the 45-degree wing walls (Figure 3.23). Downstream of the wingwalls, however, the flow separation region became larger (Figures 3.24 and 3.25) due to the sudden expansion of the cross-section (Figures 3.17 and 3.18). At about 180 ft downstream of the stilling basin, i.e. at cross-section E, flow velocity was uniformly distributed across most of the width; nevertheless, the flow separation was still evident near the banks (Figure 3.26).

With the new design, the overall hydraulic condition in the downstream channel under the flow condition of 4296 cfs and a tailwater level of 14.5 ft above the datum was significantly improved. However, to determine if a deeper stilling basin under the drawdown flood condition, i.e. 2300 cfs, would have a better hydraulic performance, two test series were conducted under two different bed elevations for the stilling basin. The results of these two tests are presented in the following subsections.

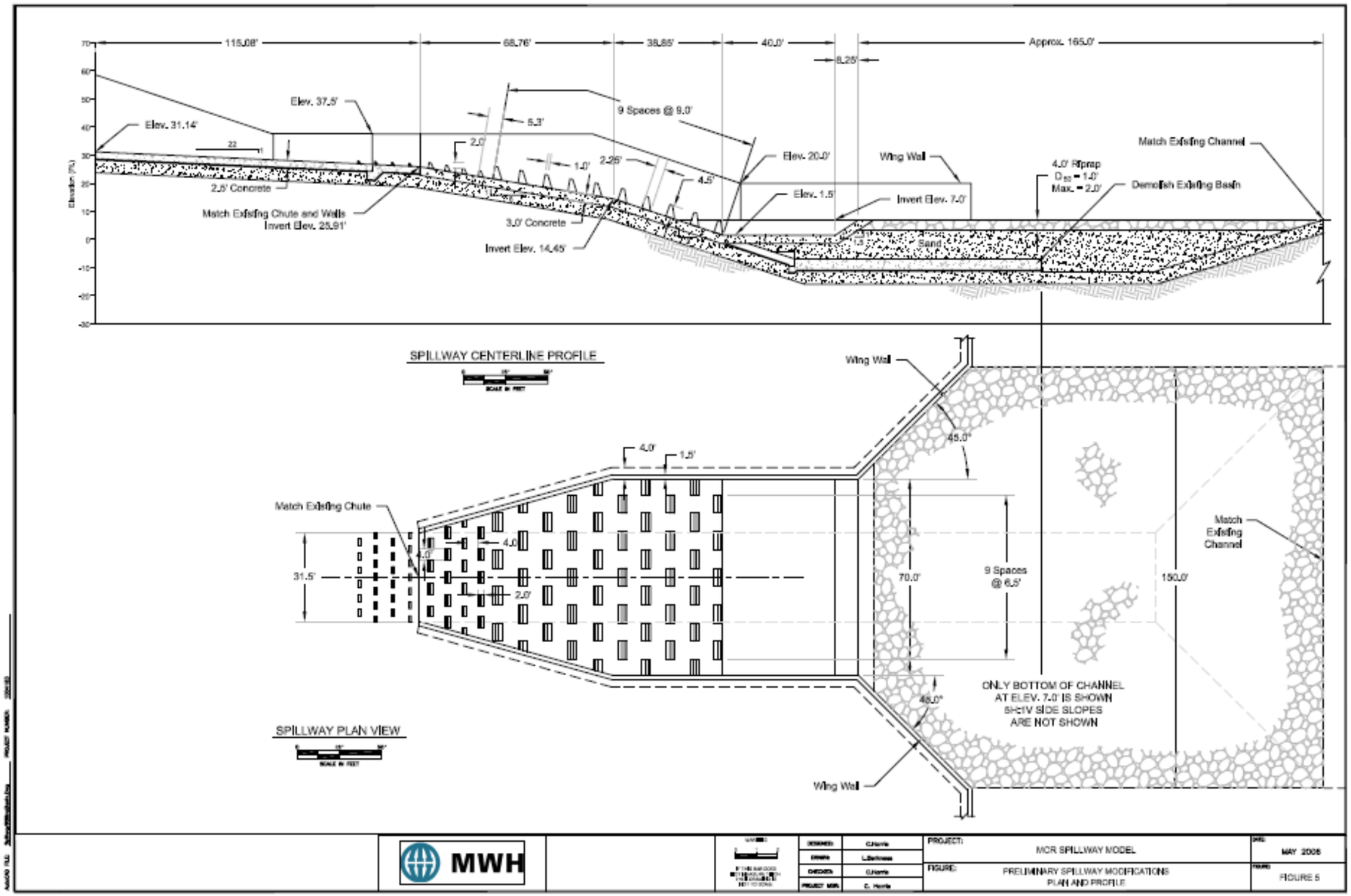

Figure 3.17. The final proposed modification to the outlet structure with a stilling basin at an elevation of 1.5 ft above the datum.

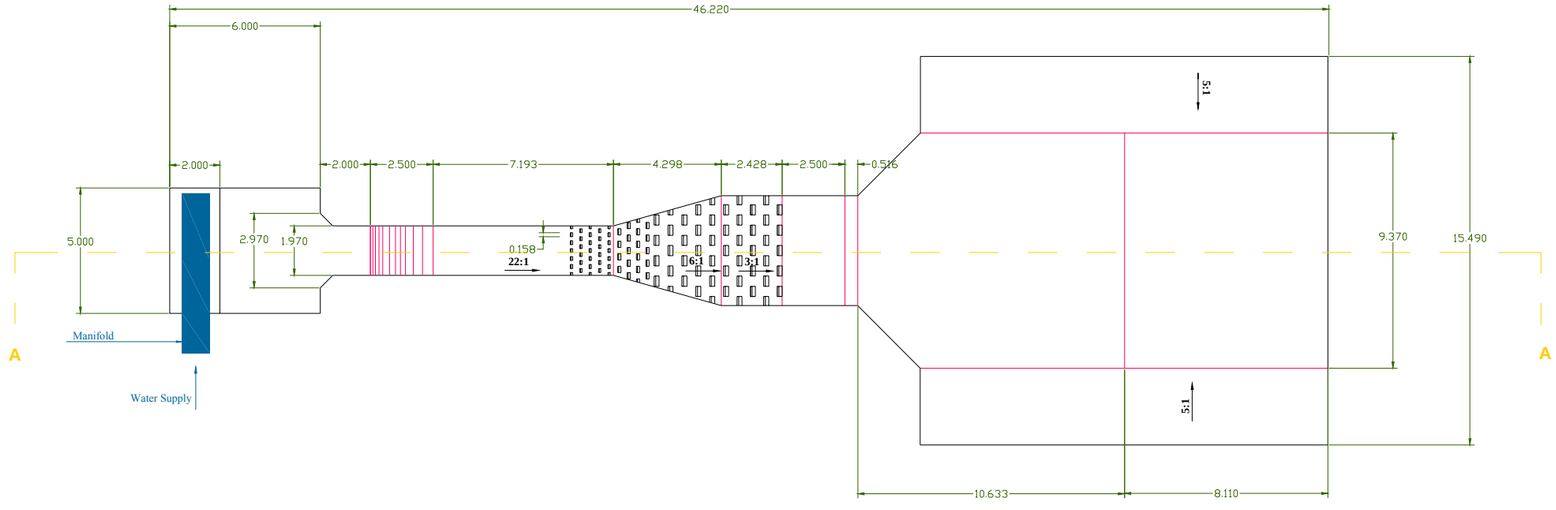

PLAN VIEW

All dimensions are in feet

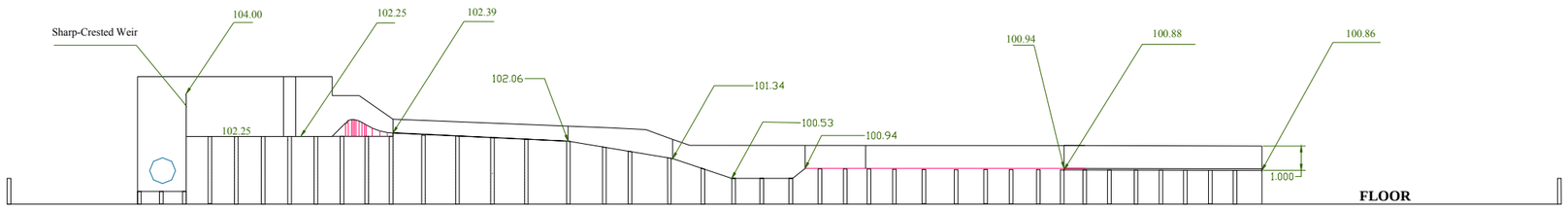

Section A-A

All dimensions are in feet

Figure 3.18. Plan view and longitudinal cross-section of the model layout of the final proposed modification to the outlet structure.

(a)

(b)

Figure 3.19. Photos of the final design of the stilling basin (a) looking downstream prior to the installation of the baffle blocks, and (b) looking upstream after the installation of the baffle blocks. The white boards underneath of the blocks and inside the stilling basin were removable.

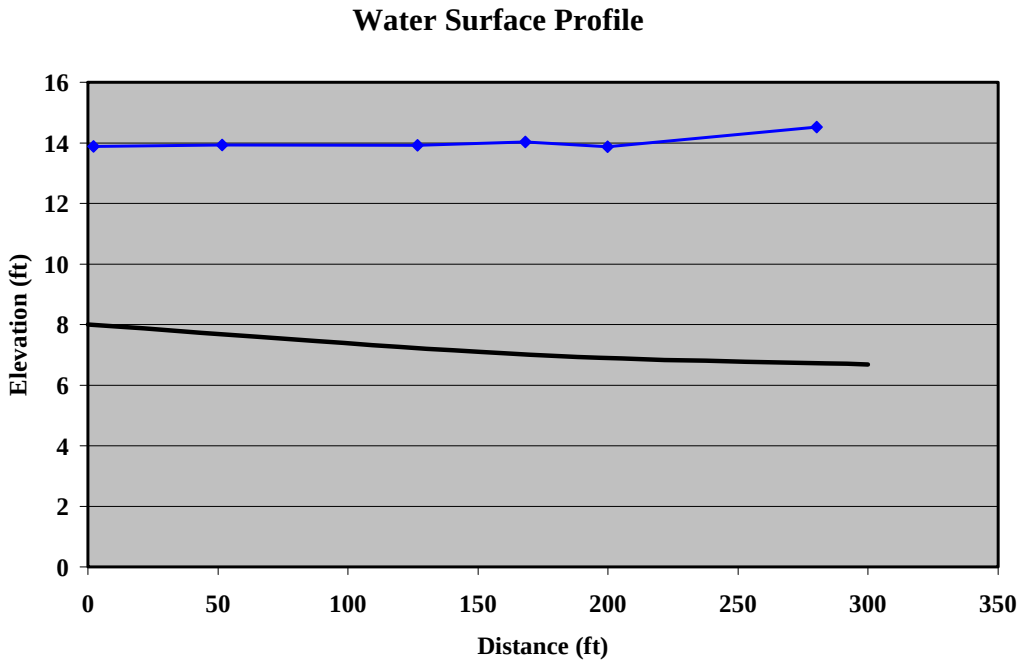

Figure 3.20. Water surface profile under a flow condition of 4307 cfs and a tailwater of 14.5, with the stilling bed elevation at 1.5 ft above the datum. The coordinate is shown in Figure 3.21.

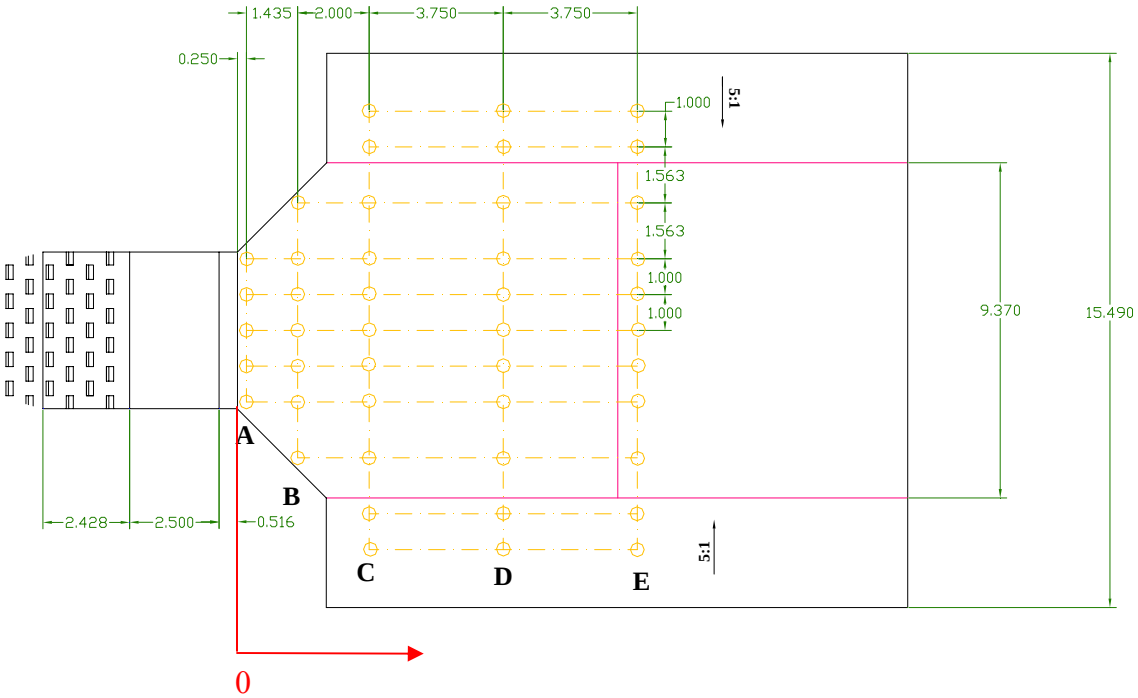

Figure 3.21. Cross-sections A through E and locations where flow velocities were measured. Dimensions are in feet (model).

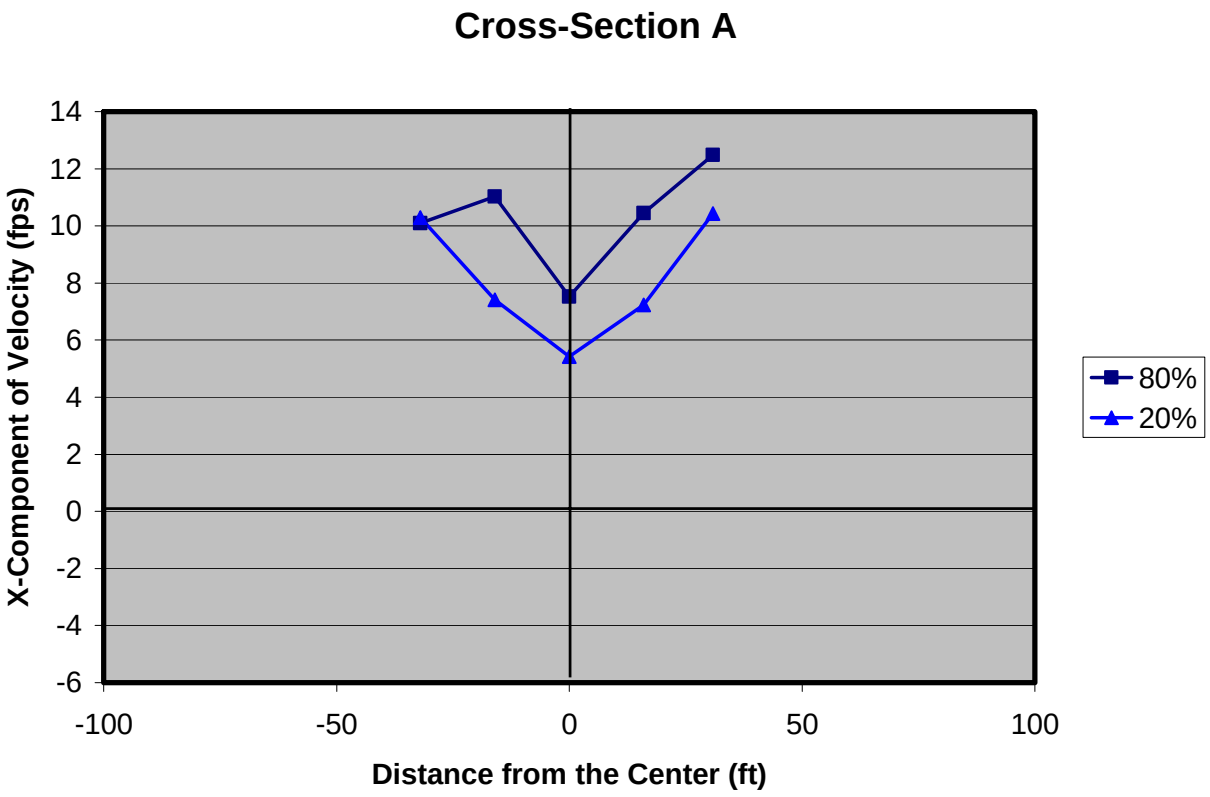

Figure 3.22. X-component of velocity distribution measured at cross-section A under a flow condition of 4307 cfs and a tailwater level of 14.5 ft above the datum. The stilling basin elevation was at 1.5 ft above the datum.

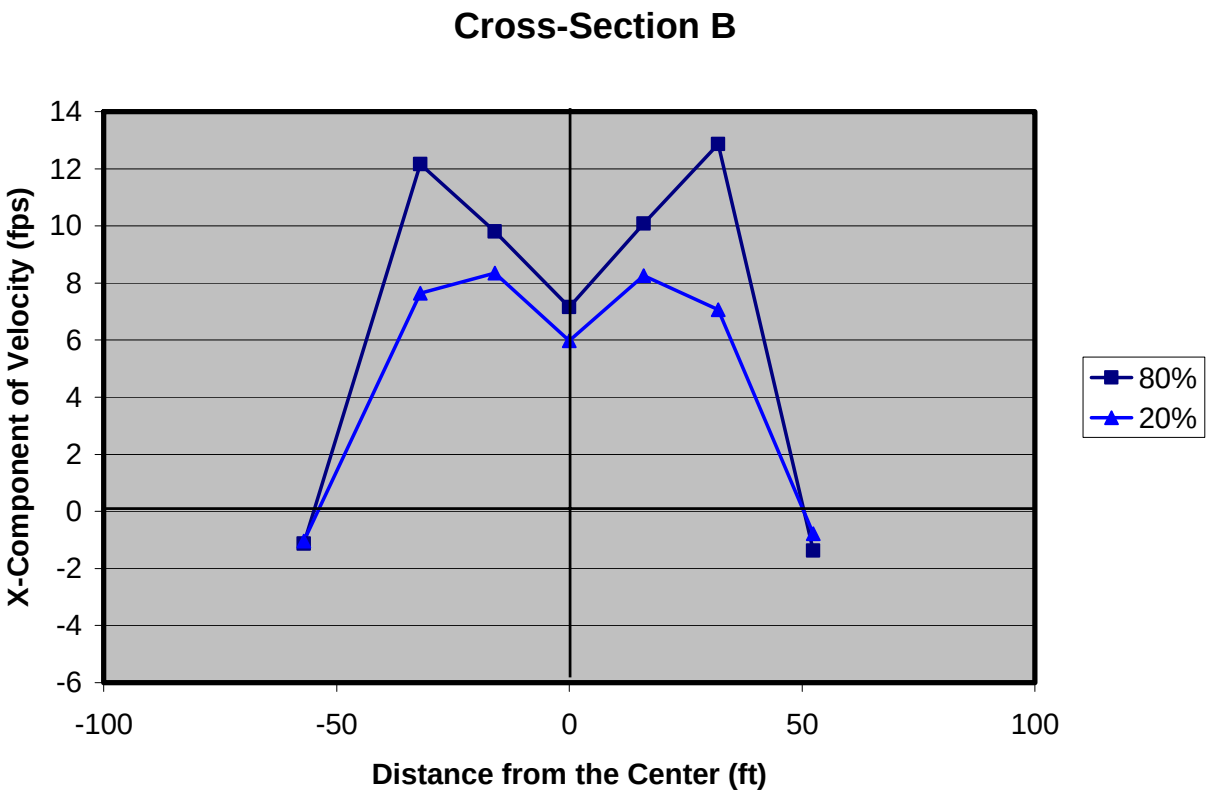

Figure 3.23. X-component of velocity distribution measured at cross-section B under a flow condition of 4307 cfs and a tailwater level of 14.5 ft above the datum. The stilling basin elevation was at 1.5 ft above the datum.

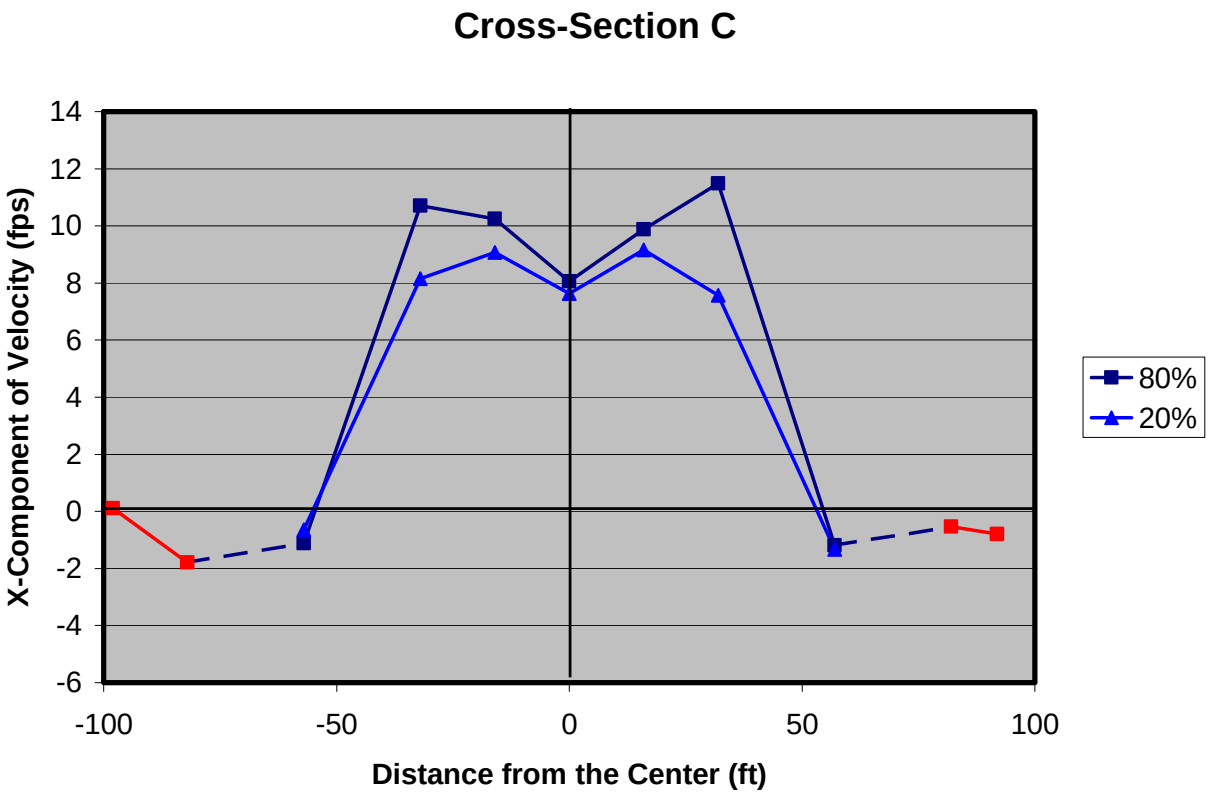

Figure 3.24. X-component of velocity distribution measured at cross-section C under a flow condition of 4307 cfs and a tailwater level of 14.5 ft above the datum. The stilling basin elevation was at 1.5 ft above the datum. The red markers were measured at 60% depth.

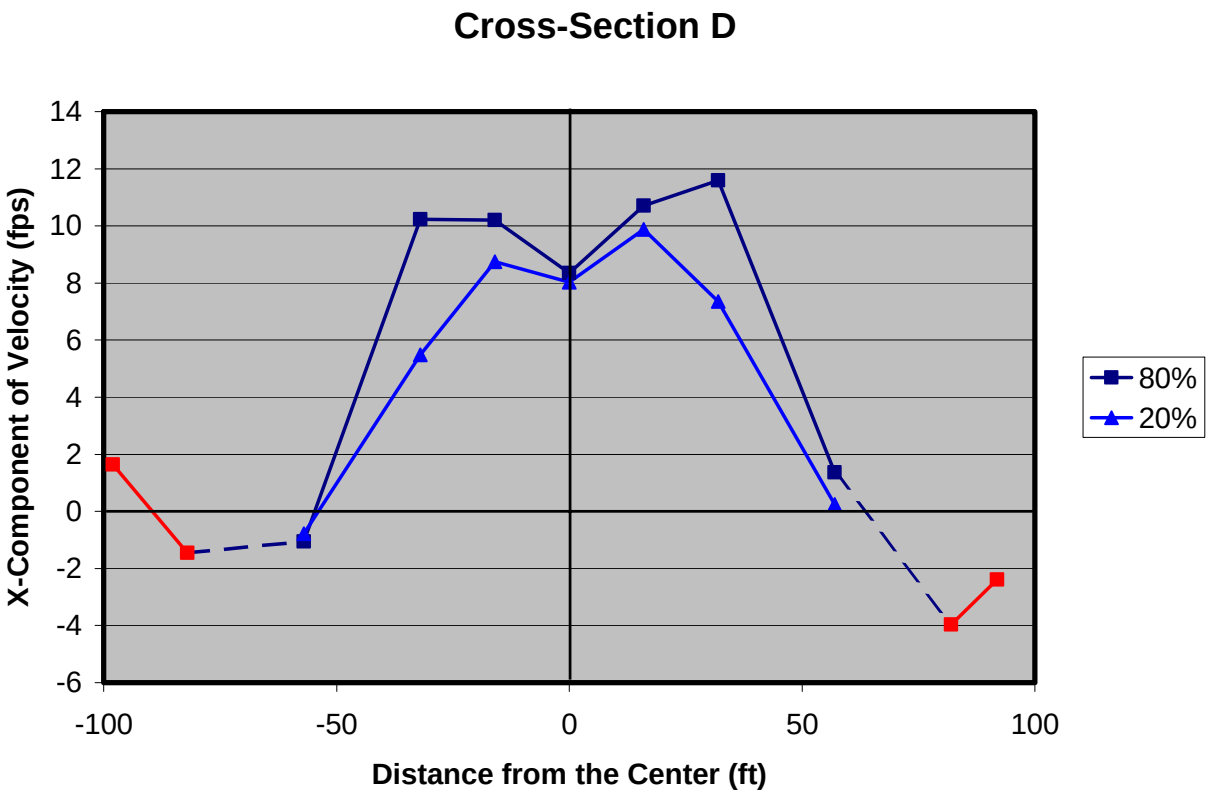

Figure 3.25. X-component of velocity distribution measured at cross-section D under a flow condition of 4307 cfs and a tailwater level of 14.5 ft above the datum. The stilling basin elevation was at 1.5 ft above the datum. The red markers were measured at 60% depth.

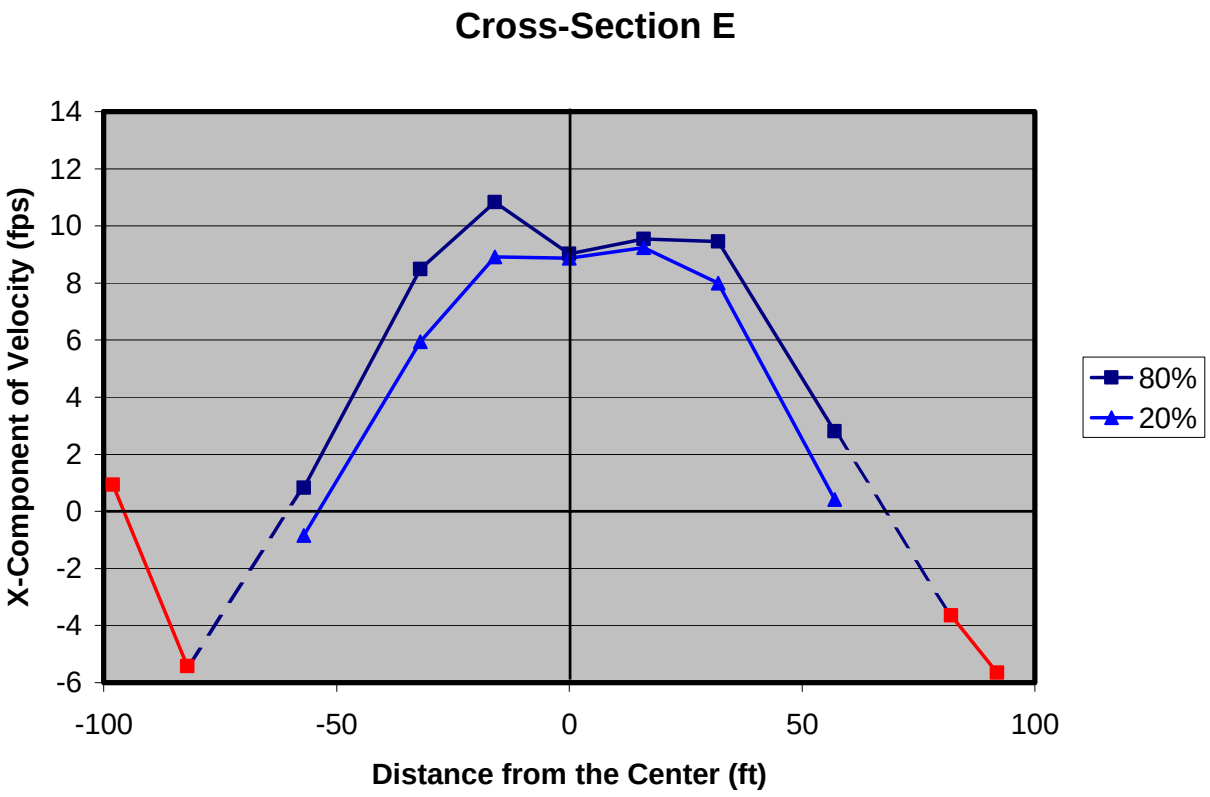

Figure 3.26. X-component of velocity distribution measured at cross-section E under a flow condition of 4307 cfs and a tailwater level of 14.5 ft above the datum. The stilling basin elevation was at 1.5 ft above the datum. The red markers were measured at 60% depth.

3.4.1. Test Results for the Stilling Basin Bed Elevation at 1.5 ft above the Datum

This test was conducted under the flow condition of 2300 cfs and a tailwater condition of 11.5 ft above the datum. Since the 2300 cfs flow condition corresponds to the drawdown flood as a reservoir management practice, it was decided to conduct the test under a tailwater condition for which the hydraulic jump does not occur outside of the basin. The measured discharge was 2271 cfs. For this test, the stilling basin bed elevation was set at 1.5 ft above the datum.

The velocities were measured at the cross-sections and locations shown in Figure 3.21. The water surface profile resulting from this test is shown in Figure 3.27 and the X-components of velocities are shown in Figures 3.28 to 3.32. The velocity distributions across the width were relatively uniform and symmetrical. A very weak flow separation[1] was evident near the wingwalls with very small Y-components of velocity recorded at cross-sections A and B (Figures 3.33 and 3.34). A stronger flow separation was evident downstream of the wingwalls due to the sudden expansion of the cross-section. The maximum X-component of velocity at cross-section A was approximately 10 fps which decreased to 9 fps at cross-section E. The area integrated average velocity at cross-sections A and E were estimated to be 8.7 and 5.2 fps, respectively.

[1] The open channel flow separation at the upstream end of expansions is the detachment of flow streamlines from the boundary layer near the wall. This phenomenon is different from the flow detachment at spillways. This detachment dose not form vacuum cavity but creates a recirculating flow region. As is evident in the velocity profiles (Figures 3.29 to 3.34), the velocities are negative near the wall. The velocities near the separation zone are too small to cause cavitation but they increase the head loss which is not an issue in this case study.

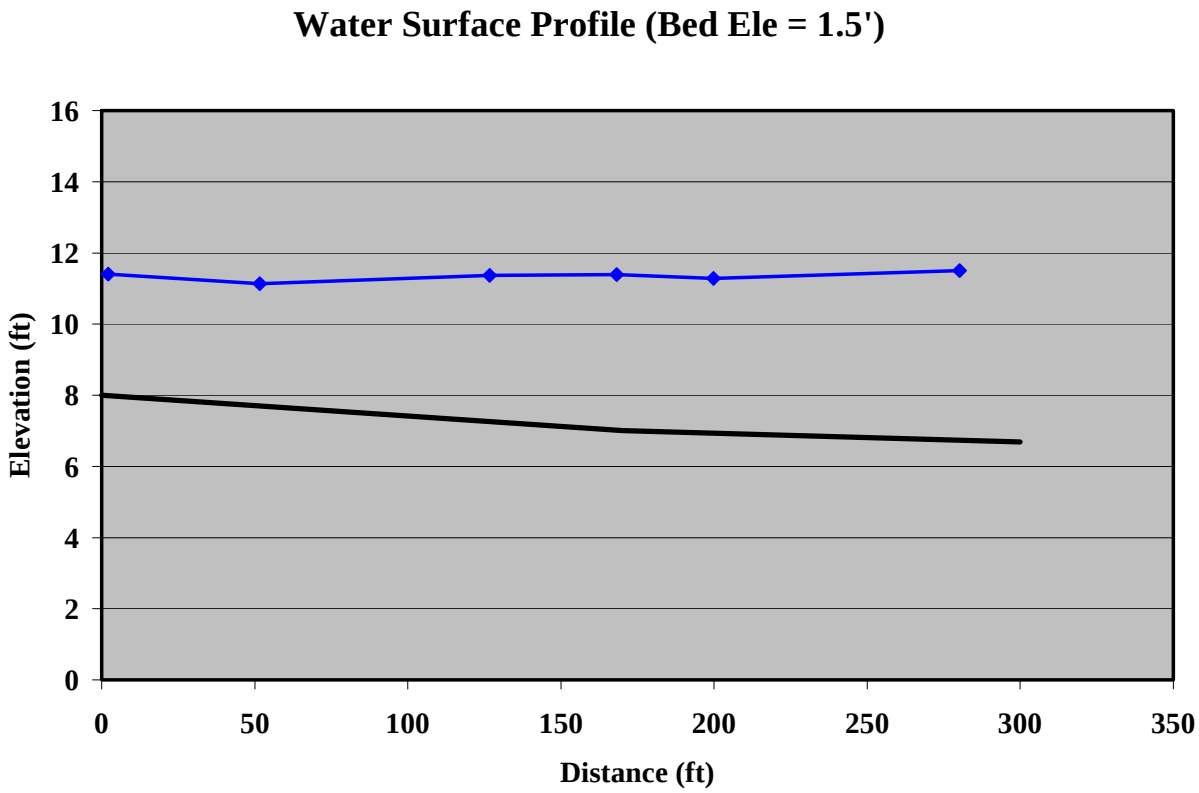

Figure 3.27. Water surface profile in the channel downstream of the stilling basin under a flow condition of 2271 cfs and a tailwater of 11.5, with the stilling bed elevation at 1.5 ft above the datum. The X-coordinate is shown in Figure 3.21.

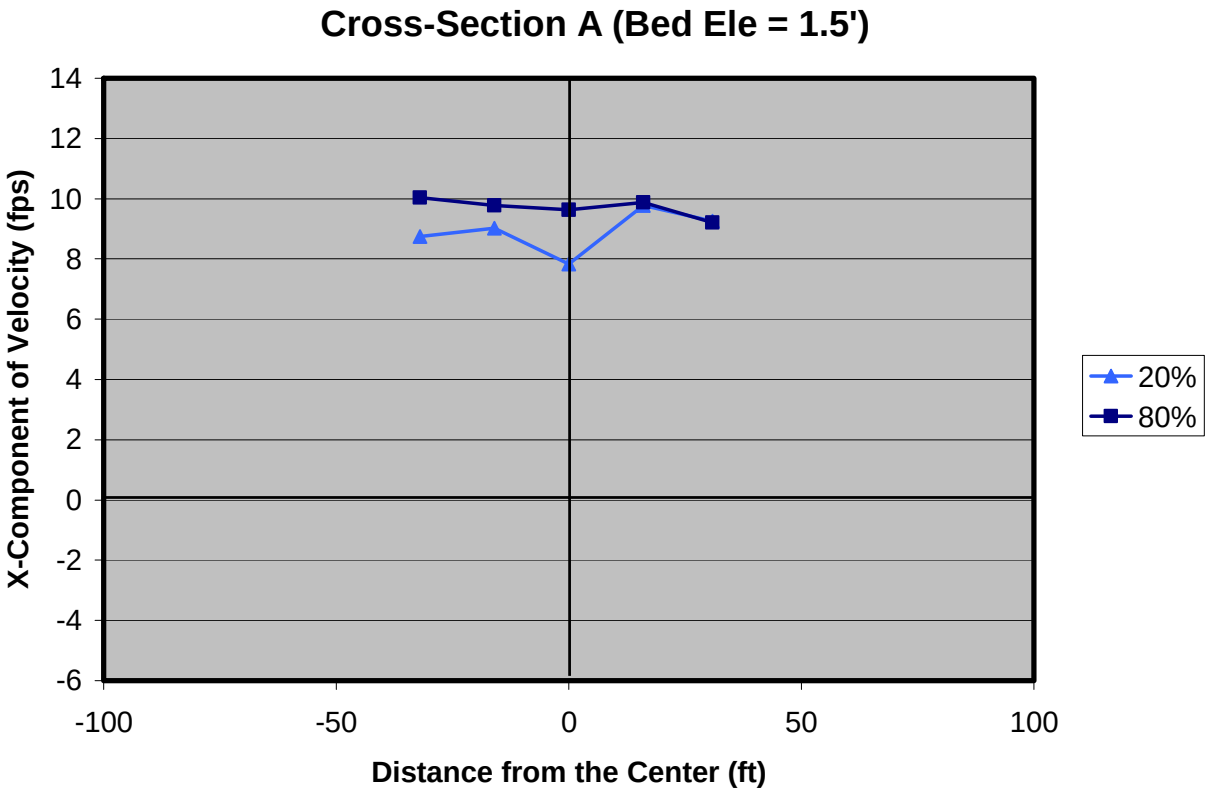

Figure 3.28. X-component of velocity distribution measured at cross-section A under a flow condition of 2271 cfs and a tailwater level of 11.5 ft above the datum. The stilling basin elevation was at 1.5 ft above the datum.

Figure 3.29. X-component of velocity distribution measured at cross-section B under a flow condition of 2271 cfs and a tailwater level of 11.5 ft above the datum. The stilling basin elevation was at 1.5 ft above the datum.

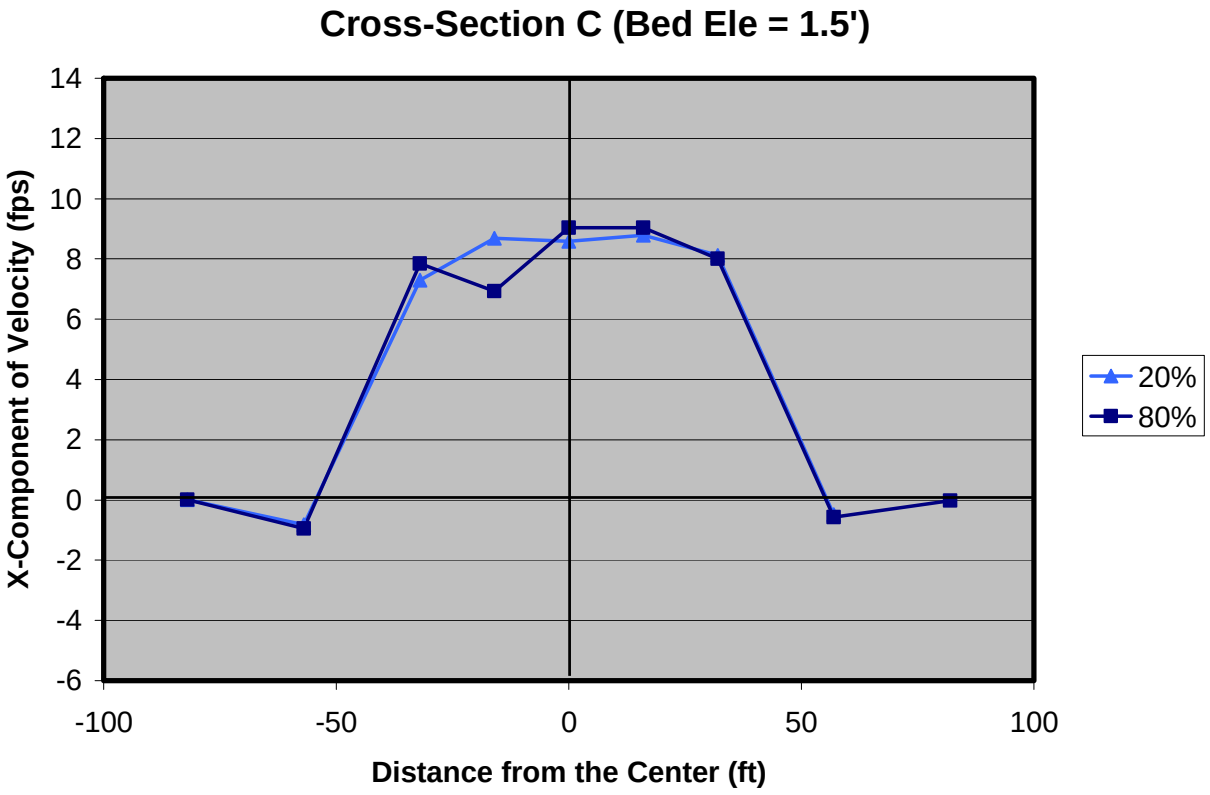

Figure 3.30. X-component of velocity distribution measured at cross-section C under a flow condition of 2271 cfs and a tailwater level of 11.5 ft above the datum. The stilling basin elevation was at 1.5 ft above the datum.

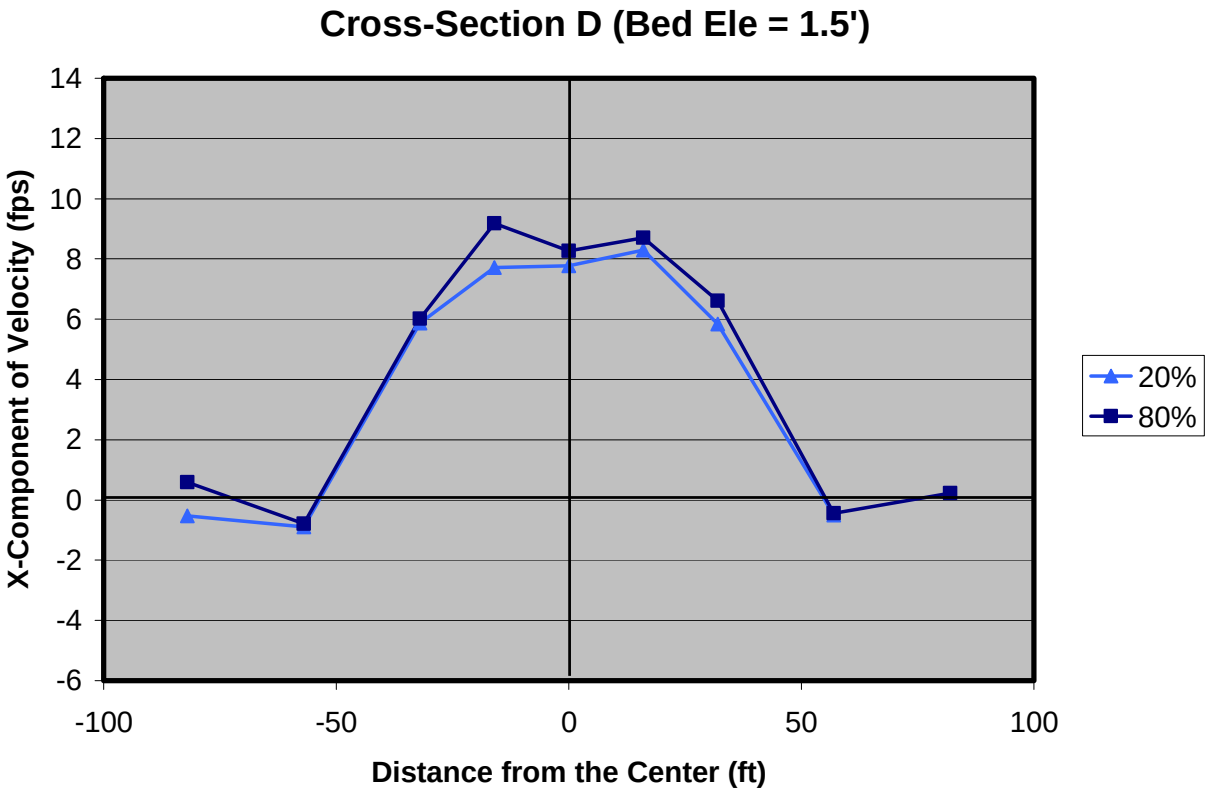

Figure 3.31. X-component of velocity distribution measured at cross-section D under a flow condition of 2271 cfs and a tailwater level of 11.5 ft above the datum. The stilling basin elevation was at 1.5 ft above the datum.

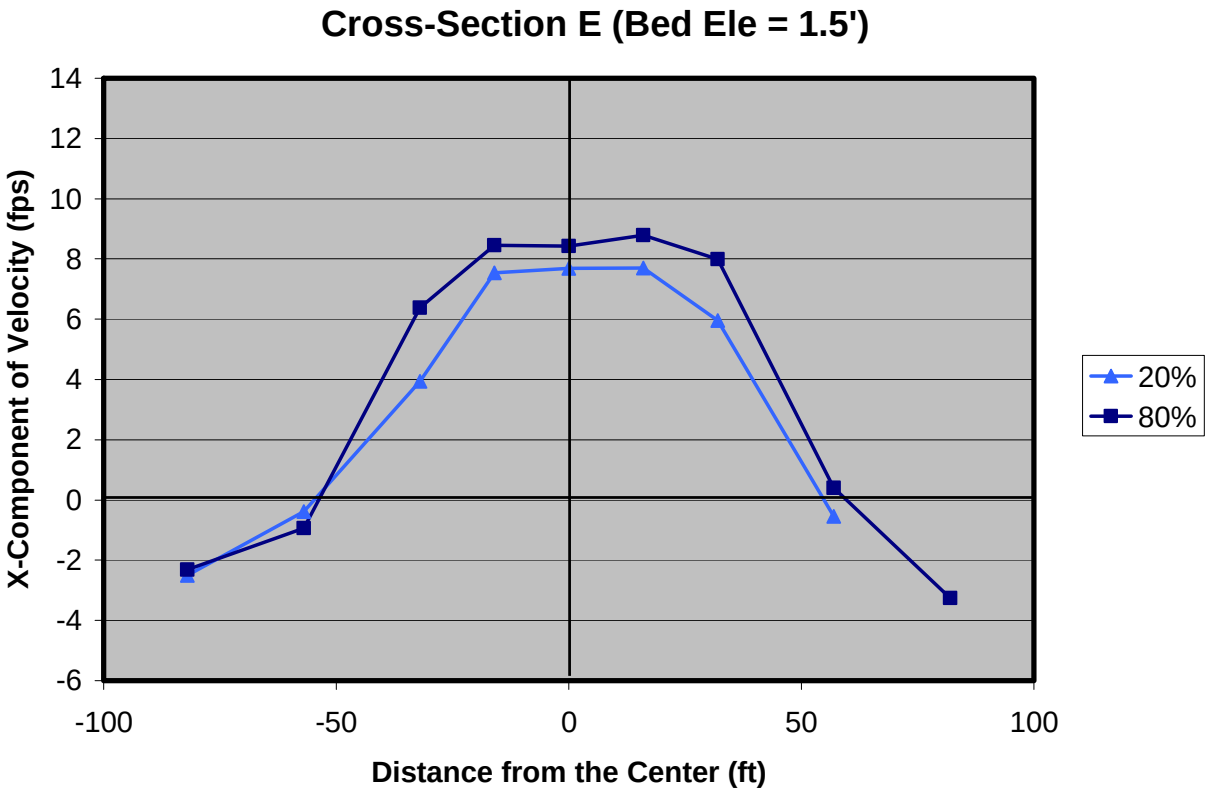

Figure 3.32. X-component of velocity distribution measured at cross-section E under a flow condition of 2271 cfs and a tailwater level of 11.5 ft above the datum. The stilling basin elevation was at 1.5 ft above the datum.

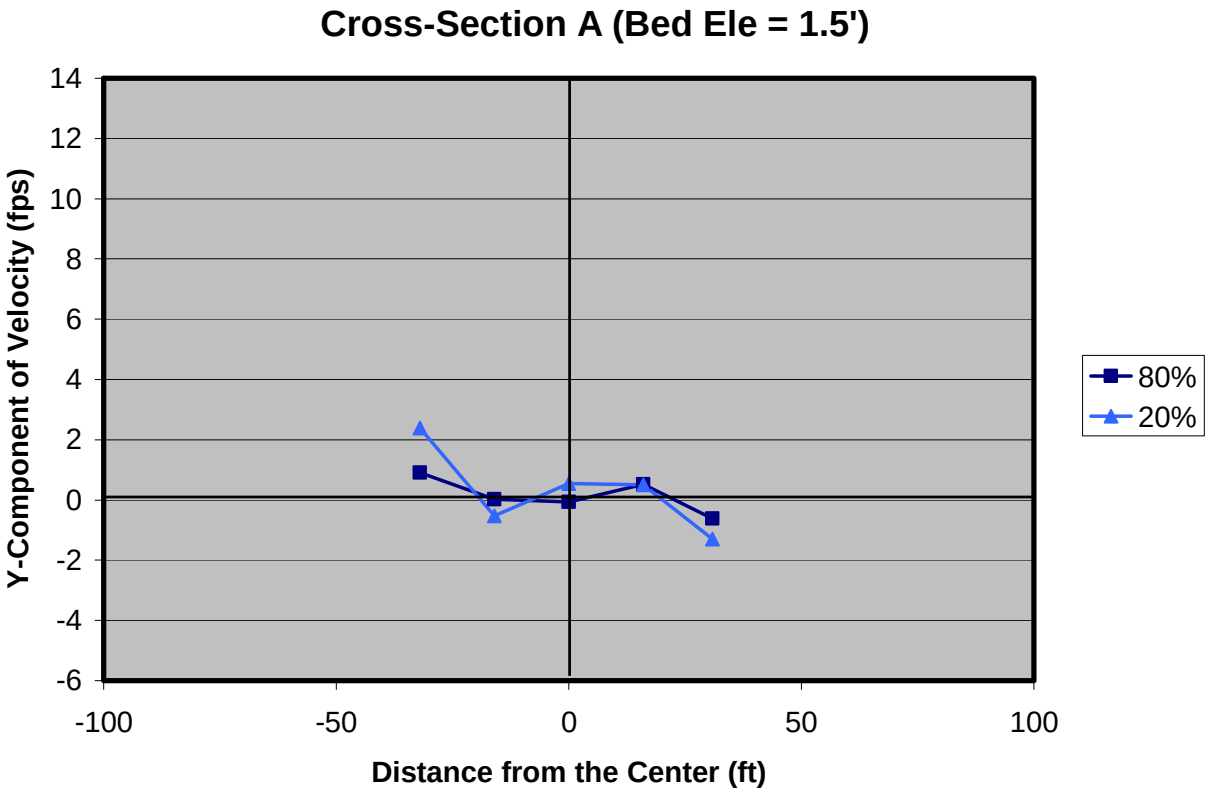

Figure 3.33. Y-component of velocity distribution measured at cross-section A under a flow condition of 2271 cfs and a tailwater level of 11.5 ft above the datum. The stilling basin elevation was at 1.5 ft above the datum.

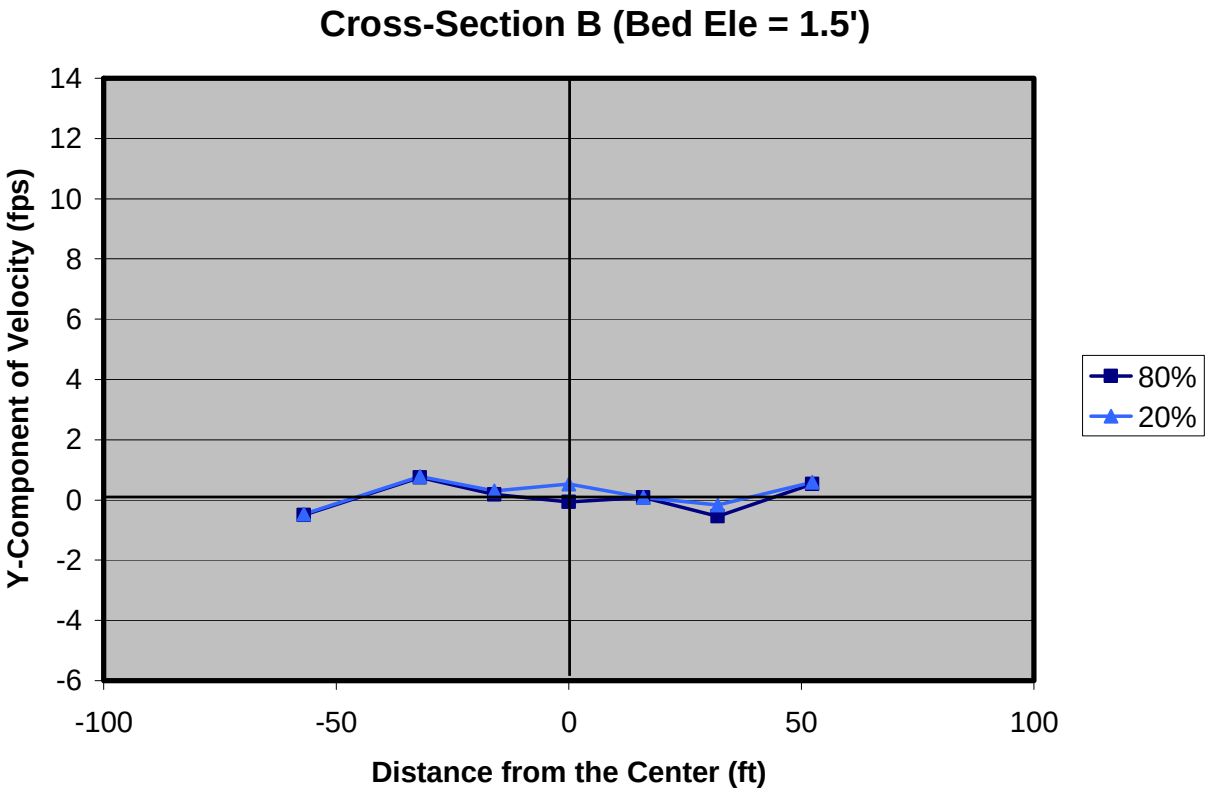

Figure 3.34. Y-component of velocity distribution measured at cross-section B under a flow condition of 2271 cfs and a tailwater level of 11.5 ft above the datum. The stilling basin elevation was at 1.5 ft above the datum.

3.4.2. Test Results for the Stilling Basin Bed Elevation at 0.5 ft above the Datum

This test was also conducted under the flow condition of 2300 cfs and a tailwater condition of 11.5 ft above the datum. The measured discharge was 2286 cfs. For this test, the stilling basin bed elevation was set at 0.5 ft above the datum, i.e. 1 ft lower than the previous test.

The water surface profile resulting from this test is shown in Figure 3.35 which was similar to the test done with the stilling basin bed elevation at 1.5 ft. The X-components of velocities are shown in Figures 3.36 to 3.40. The velocity distributions across the width were relatively similar to the previous test. Similarly, a very weak flow separation was evident near the wingwalls with small Y-components of velocity recorded at cross-sections B (Figures 3.41) and a stronger flow separation was evident downstream of the wingwalls. The Y-component of velocity at cross-section E is shown in Figure 3.42. The maximum X-component of velocity at cross-section A was approximately 10 fps which decreased to 9 fps at cross-section E.

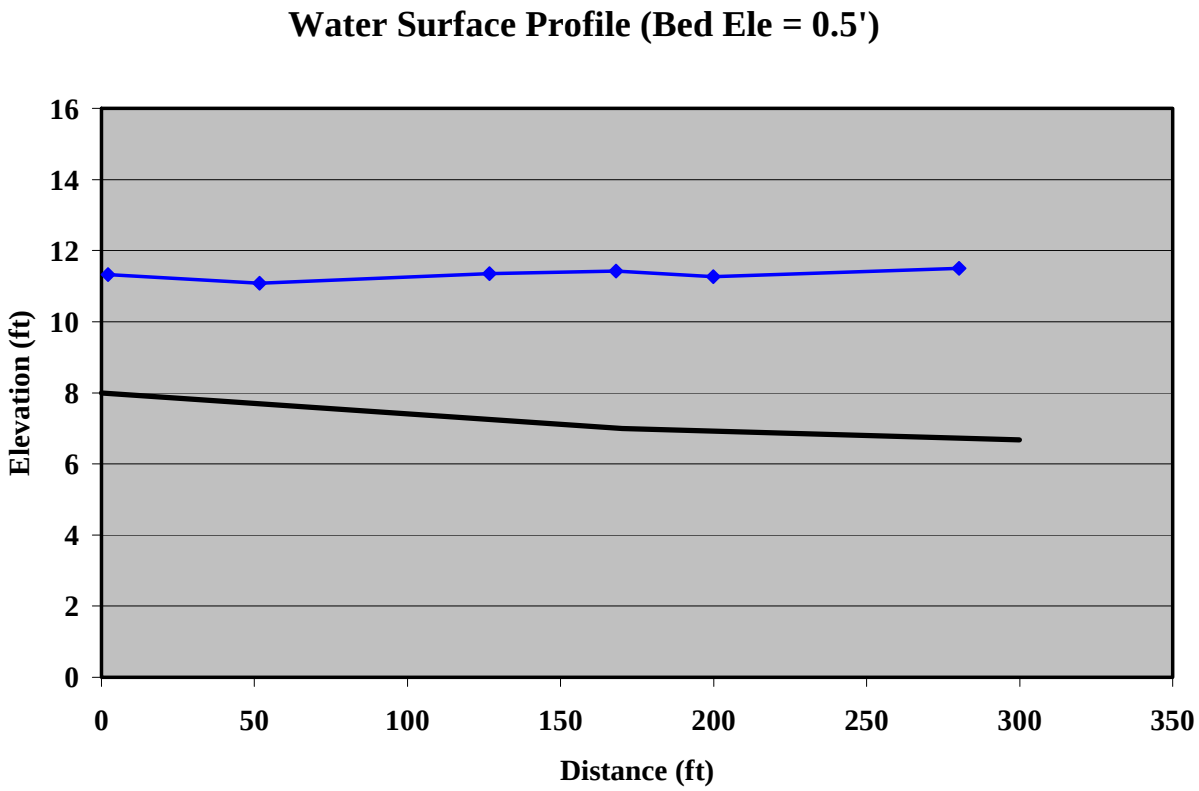

Figure 3.35. Water surface profile in the channel downstream of the stilling basin under a flow condition of 2286 cfs and a tailwater of 11.5, with the stilling bed elevation at 1.5 ft above the datum. The X-coordinate is shown in Figure 3.21.

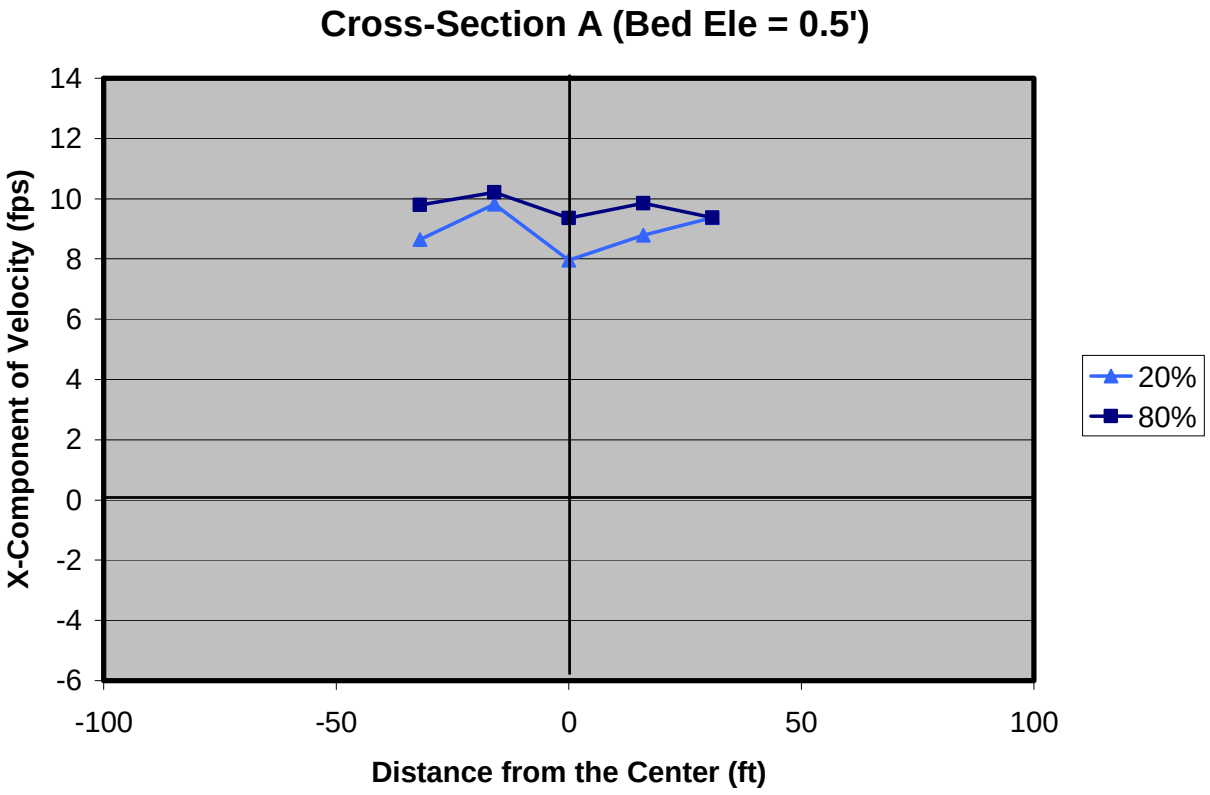

Figure 3.36. X-component of velocity distribution measured at cross-section A under a flow condition of 2285 cfs and a tailwater level of 11.5 ft above the datum. The stilling basin elevation was at 0.5 ft above the datum.

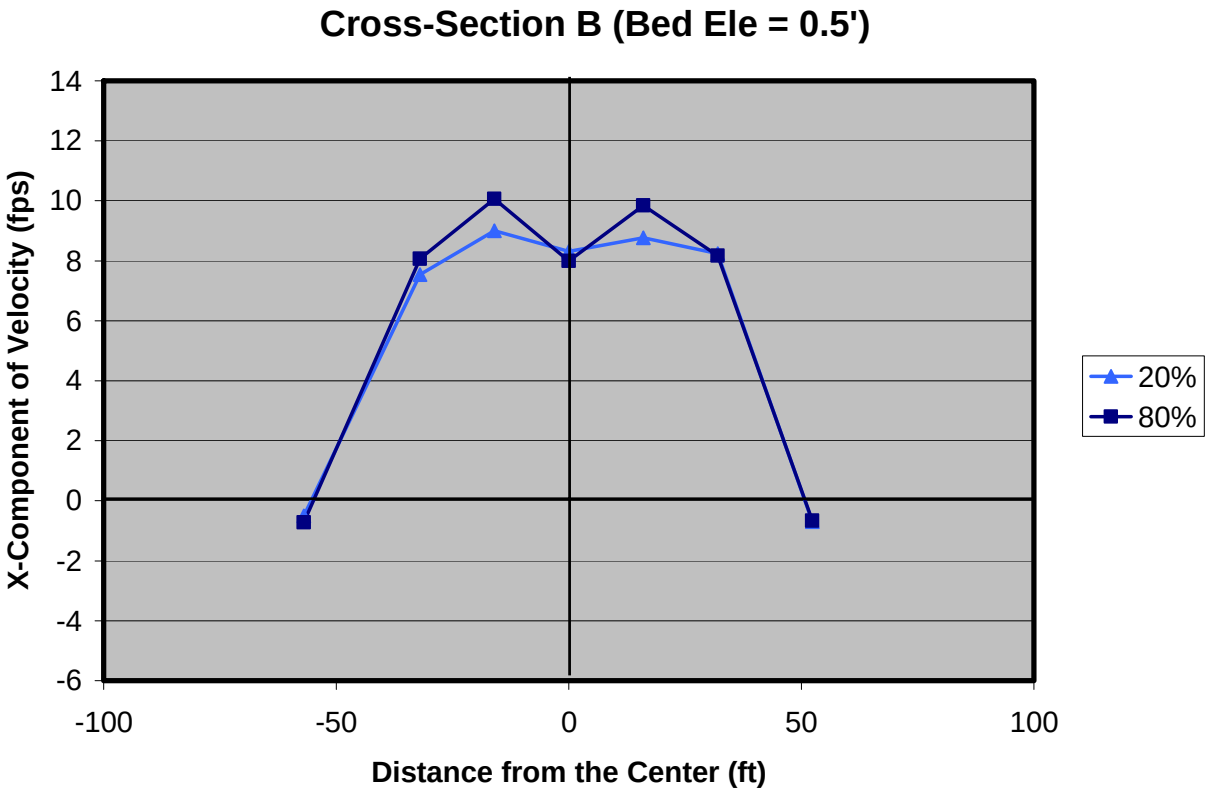

Figure 3.37. X-component of velocity distribution measured at cross-section B under a flow condition of 2285 cfs and a tailwater level of 11.5 ft above the datum. The stilling basin elevation was at 0.5 ft above the datum.

Figure 3.38. X-component of velocity distribution measured at cross-section C under a flow condition of 2285 cfs and a tailwater level of 11.5 ft above the datum. The stilling basin elevation was at 0.5 ft above the datum.

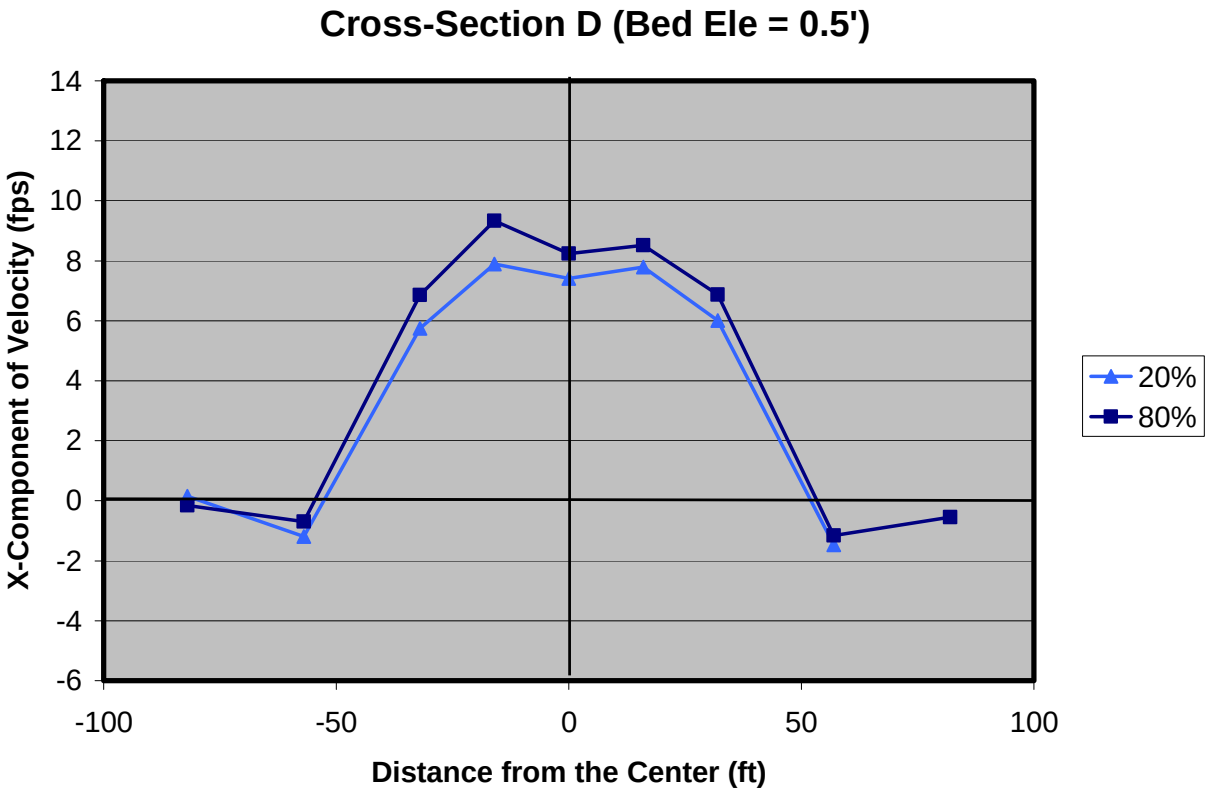

Figure 3.39. X-component of velocity distribution measured at cross-section D under a flow condition of 2285 cfs and a tailwater level of 11.5 ft above the datum. The stilling basin elevation was at 0.5 ft above the datum.

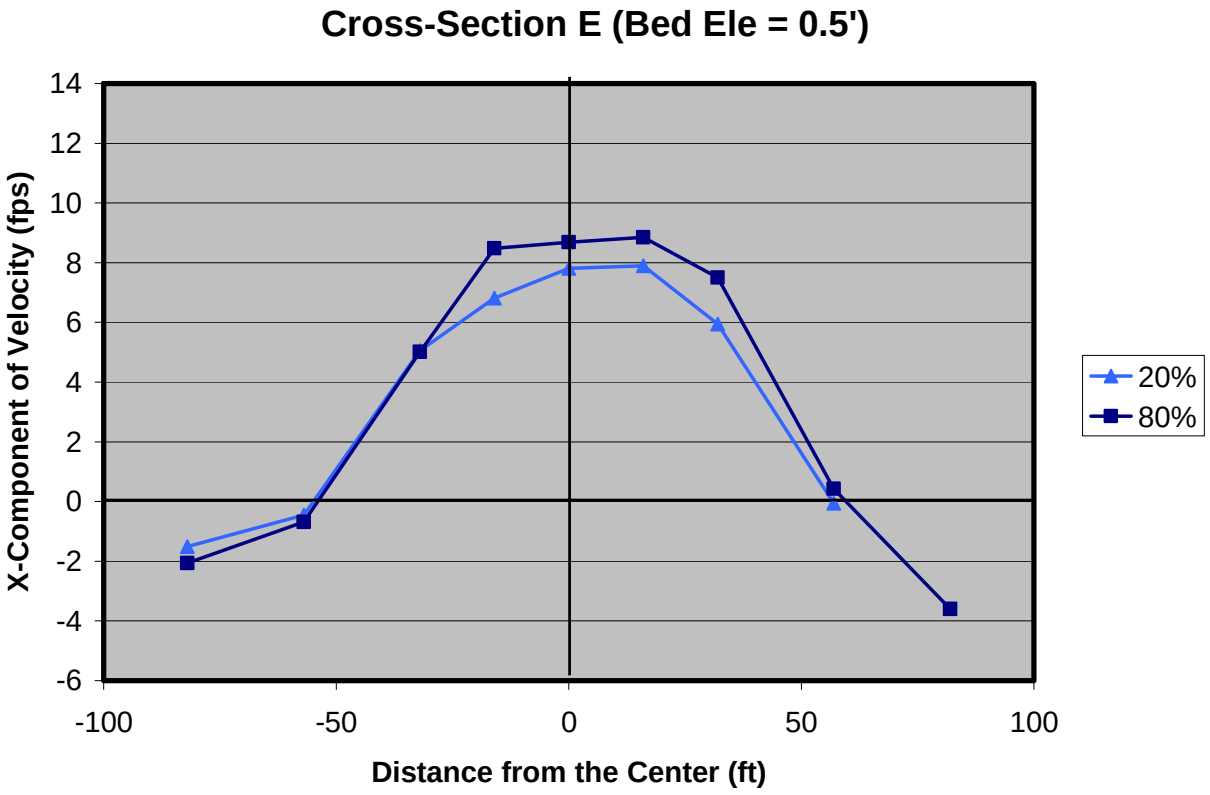

Figure 3.40. X-component of velocity distribution measured at cross-section E under a flow condition of 2285 cfs and a tailwater level of 11.5 ft above the datum. The stilling basin elevation was at 0.5 ft above the datum.

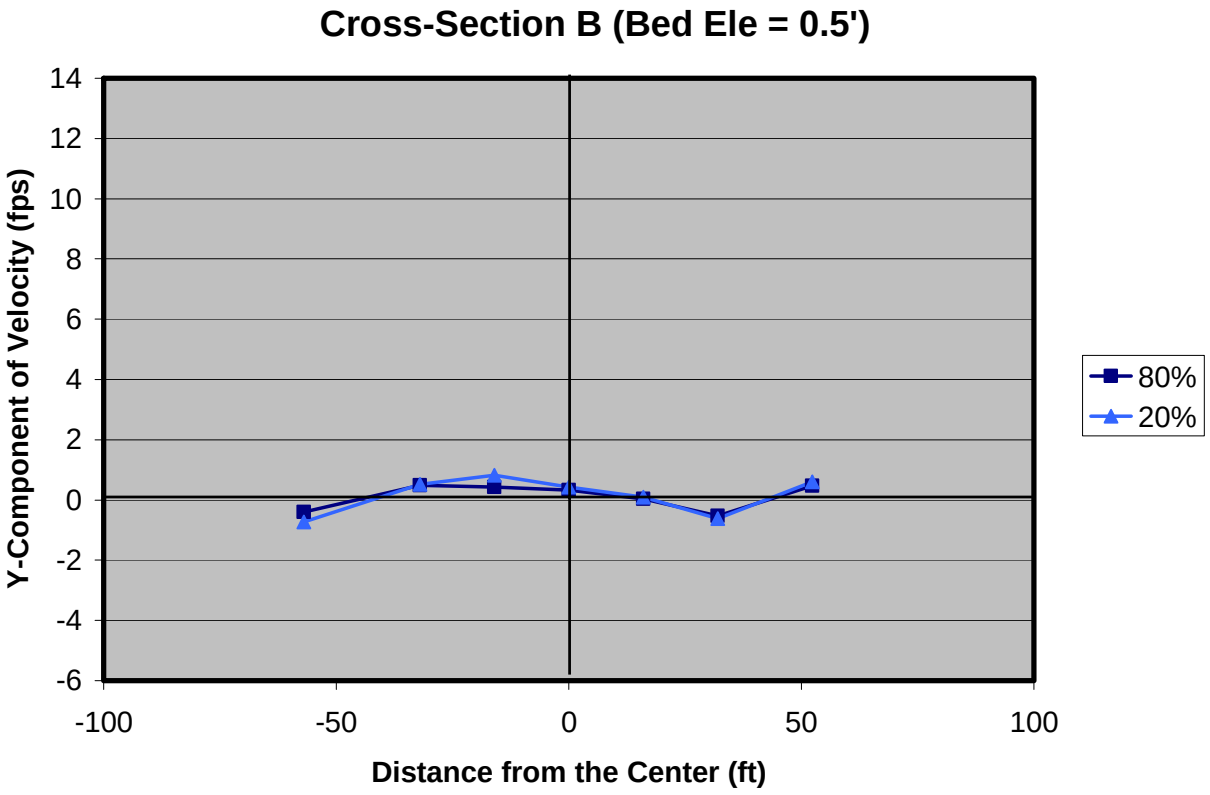

Figure 3.41. Y-component of velocity distribution measured at cross-section B under a flow condition of 2285 cfs and a tailwater level of 11.5 ft above the datum. The stilling basin elevation was at 0.5 ft above the datum.

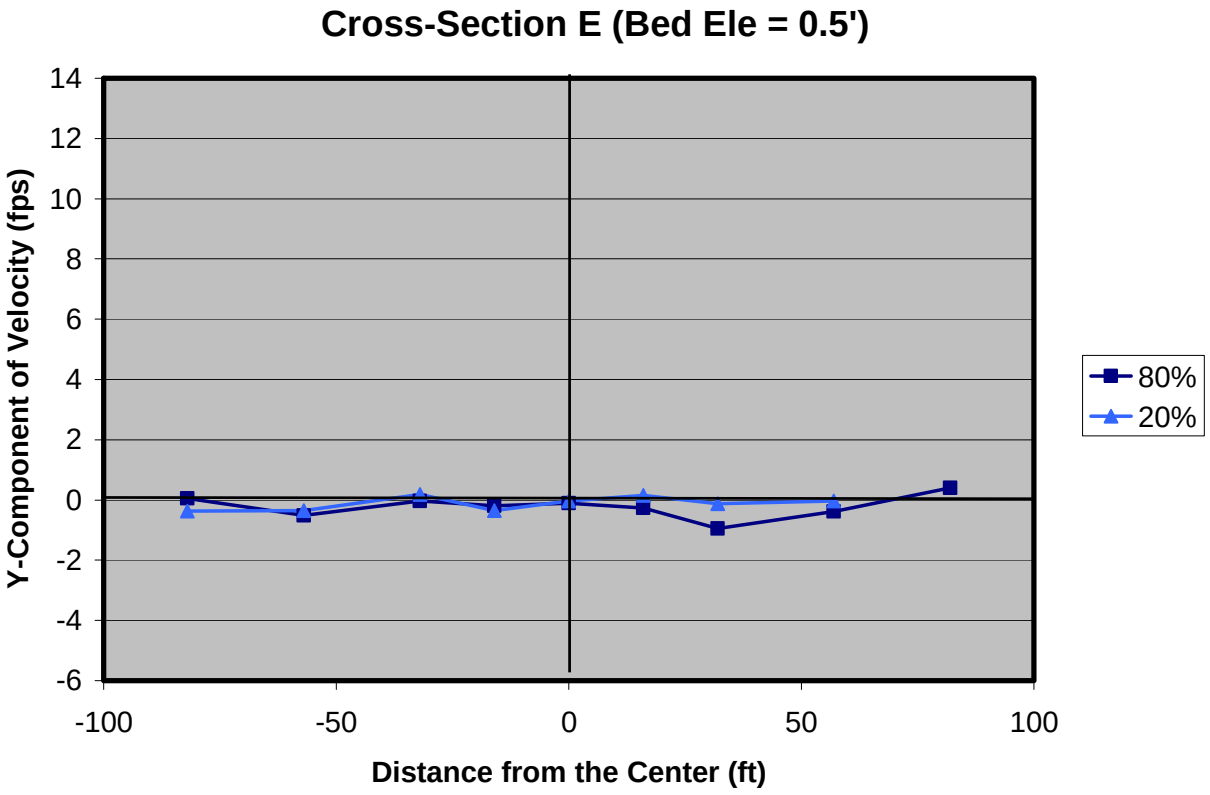

Figure 3.42. Y-component of velocity distribution measured at cross-section E under a flow condition of 2285 cfs and a tailwater level of 11.5 ft above the datum. The stilling basin elevation was at 0.5 ft above the datum.

3.4.3. Production Test Series for the Stilling Basin with Bed Elevation at 1.5 ft above the Datum

According to the last two tests under the drawdown flood condition, a 1-ft change in bed elevation did not have any significant impact on the hydraulic conditions in the downstream channel. Therefore, it was decided that the production tests would be conducted with a bed elevation of 1.5 ft above the datum. In addition, the production tests changed to five tests summarized in Table 3.2.

Table 3.2. Revised discharges and tailwaters of the production tests

Reservoir Elevation (feet)	Spillway Discharge (cfs)	Tailwater Level (ft)	Tailwater Level (ft)
52.1	**4296**	**14.5 (50 year flood)**	**16.0 (500-year flood)**
50.5	**3369**	**13.3 (5-10 year flood)**	**16.0 (500-year flood)**
49.0	**2300**	**7.0 (No tailwater from Colorado River)**	

The first test series was conducted under the flow condition of 4307 cfs and a tailwater of 16 ft. The water surface profile is plotted in Figure 3.43, and the X-components of velocity distributions at cross-sections A and E are plotted in Figures 3.44 and 3.45. Velocity distributions at other cross-sections are given in Appendix A.1. The results of this test series showed that the maximum X-component of velocity distribution at cross-section A was about 11 fps and decreased to 8 fps at cross-section E. The area integrated average velocity[2] at cross-sections A and E were estimated to be 7.2 and 5.4 fps, respectively.

The second test series was conducted under the flow condition of 4248 cfs and a tailwater of 14.5 ft. The water surface profile is plotted in Figure 3.46, and the X-components of velocity distributions at cross-sections A and E are plotted in Figures 3.47 and 3.48. Velocity

[2] The area integrated average velocity was only computed for sections where velocities were positive.

distributions at other cross-sections are given in Appendix A.2. The results of this test series showed that the maximum X-component of velocity at cross-section A was about 13 fps and decreased to 11 fps at cross-section E. The area integrated average velocity at cross-sections A and E were estimated to be 8.8 and 6.8 fps, respectively.

The third test series was conducted under the flow condition of 3367 cfs and a tailwater of 16 ft. The water surface profile is plotted in Figure 3.49, and the X-components of velocity distributions at cross-sections A and E are plotted in Figures 3.50 and 3.51. Velocity distributions at other cross-sections are given in Appendix A.3. The results of this test series showed that the maximum X-component of velocity at cross-section A was about 11 fps and decreased to 7 fps at cross-section E. The area integrated average velocity at cross-sections A and E were estimated to be 5.9 and 3.6 fps, respectively.

The fourth test series was conducted under the flow condition of 3376 cfs and a tailwater of 13.3 ft. The water surface profile is plotted in Figure 3.52, and the X-components of velocity distributions at cross-sections A and E are plotted in Figures 3.53 and 3.54. Velocity distributions at other cross-sections are given in Appendix A.4. The results of this test series showed that the maximum X-component of velocity at cross-section A was about 13 fps and decreased to 10 fps at cross-section E. The area integrated average velocity at cross-sections A and E were estimated to be 9.2 and 6.5 fps, respectively.

The fifth test series was conducted under the flow condition of 2278 cfs and no tailwater, i.e. the drop leaf gate was lowered completely, therefore, the tailwater was a function of the critical depth at the free fall downstream of the model.

The water surface profile is plotted in Figure 3.55. Under no tailwater condition, a hydraulic drop occurred at the downstream end of the stilling basin and the flow regime became supercritical and a second jump occurred 150 ft downstream of the stilling basin.

Due to the presence of supercritical regime, water depths measured at cross-sections B to E were very small and subsequently the flow velocities were very high. Therefore, velocities were measured at 60% depth at all cross-sections except cross-section A. The X-components of velocity distributions at cross-sections A to E are plotted in Figures 3.56 and 3.60. The Y-

components of velocity distributions are given in Appendix A.5. No flow separation was evident near the 45-degree wingwalls due to supercritical regime in the downstream channel. The velocity measurements do not indicate any separation even after the sudden expansion downstream of the wingwalls[3]. The main reason for no separation was the hydraulic drop at the beginning of the expansion, i.e. the 45-degree wingwalls (see Figure 3.15), which redistributed the flow with respect to the angle of expansion. Therefore, due to the parallel direction of flow to the wingwalls, the sudden expansion downstream of the wingwalls did not behave as sudden either.

The results of this test series showed that the maximum X-component of velocity at cross-section A was about 12 fps and increased to about 16 fps at cross-section D. The area integrated average velocity at cross-sections A and E were estimated to be 8.7 and 5.2 fps, respectively.

It should be noted that the surface roughness of the model channel is less than the prototype channel lined with riprap; therefore, it is likely that the length of the prototype channel exhibiting supercritical regime is shorter than that observed in this physical model study. Nevertheless, in order to avoid any erosion of the riprap on the downstream channel, the tailwater in the channel should be about 11.5 ft under the drawdown flood condition.

Water depths were measured along the baffled chute. The maximum water depths occurred under the 4296 cfs flow condition and are summarized in Table 3.3.

Table 3.3. Prototype water depths along the chute under the 4296 cfs flow condition

Location	**Water Depth (ft)**
Upstream of small blocks	4.6
Along small blocks	5.4
Between small and mid size blocks	5.8
Along mid size blocks	6.4
Between Mid size and large blocks	6.6
Along large blocks	6.9

[3] Flow separation does not occur in expansions when the flow regime is supercritical because a high velocity flow cannot coexist with a recirculating flow. Any perturbation in a supercritical flow regime results in occurrence of standing wave fronts, which subsequently redistributes the flow near the wall and prevents any flow separation.

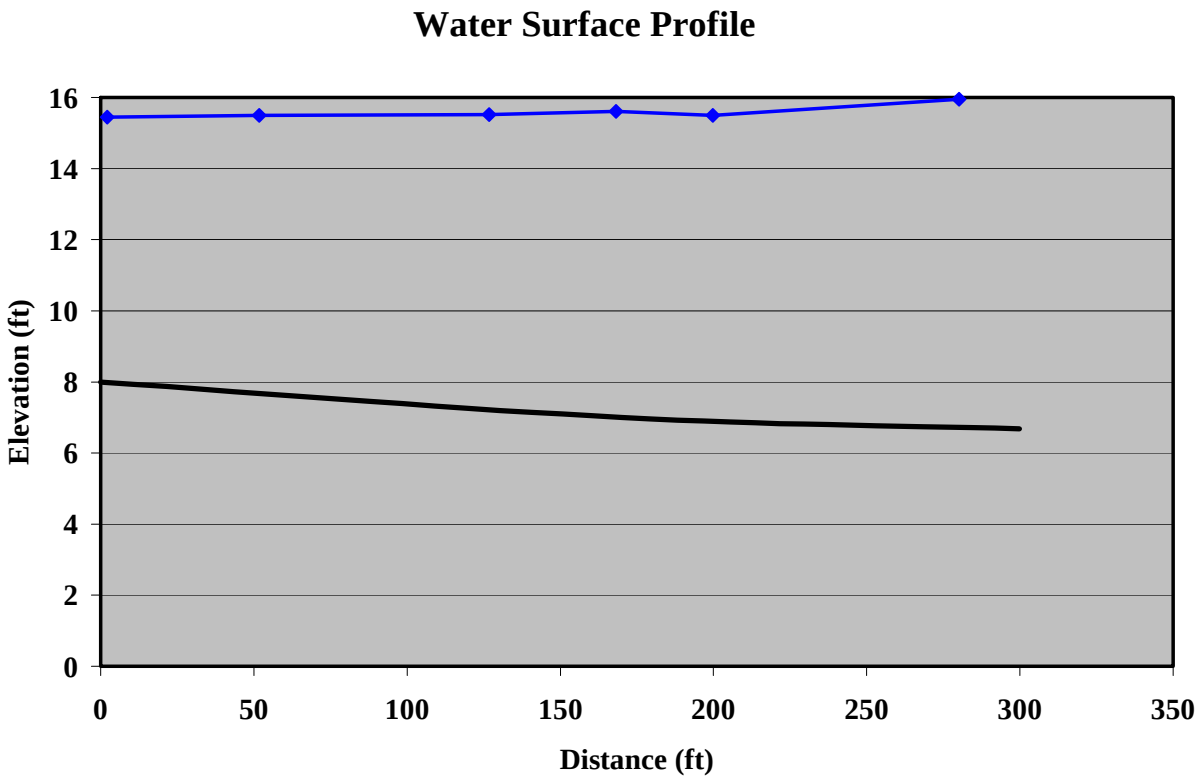

Figure 3.43. Water surface profile in the channel downstream of the stilling basin under a flow condition of 4307 cfs and a tailwater of 16 ft from the datum. The X-coordinate is shown in Figure 3.21.

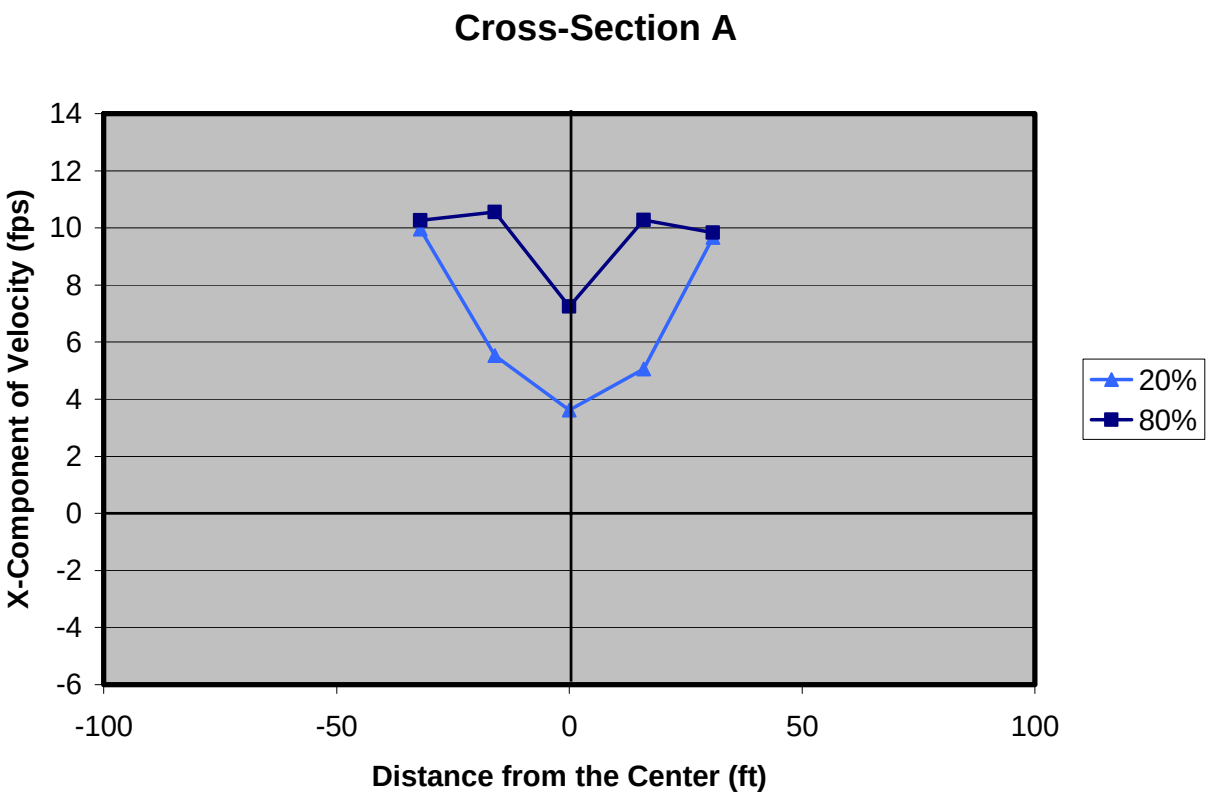

Figure 3.44. X-component of velocity distribution measured at cross-section A under a flow condition of 4307 cfs and a tailwater level of 16 ft above the datum.

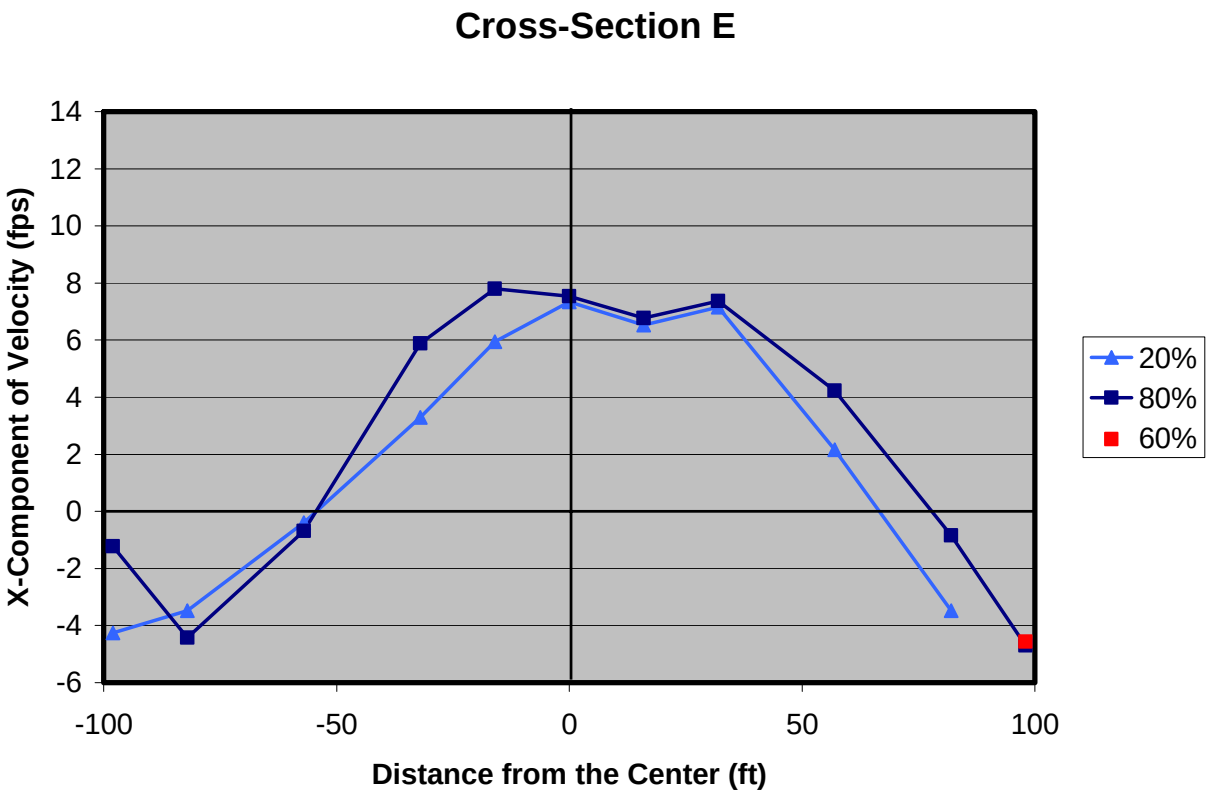

Figure 3.45. X-component of velocity distribution measured at cross-section E under a flow condition of 4307 cfs and a tailwater level of 16 ft above the datum.

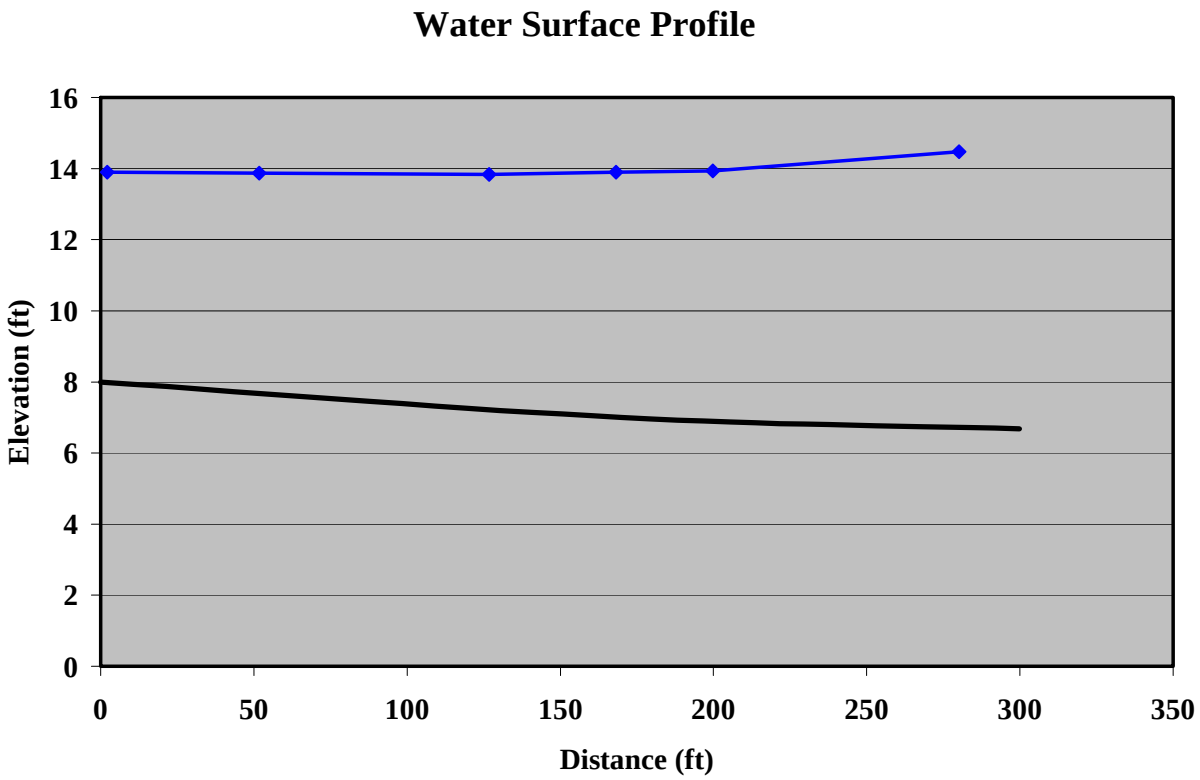

Figure 3.46. Water surface profile in the channel downstream of the stilling basin under a flow condition of 4258 cfs and a tailwater of 14.5 ft from the datum. The X-coordinate is shown in Figure 3.21.

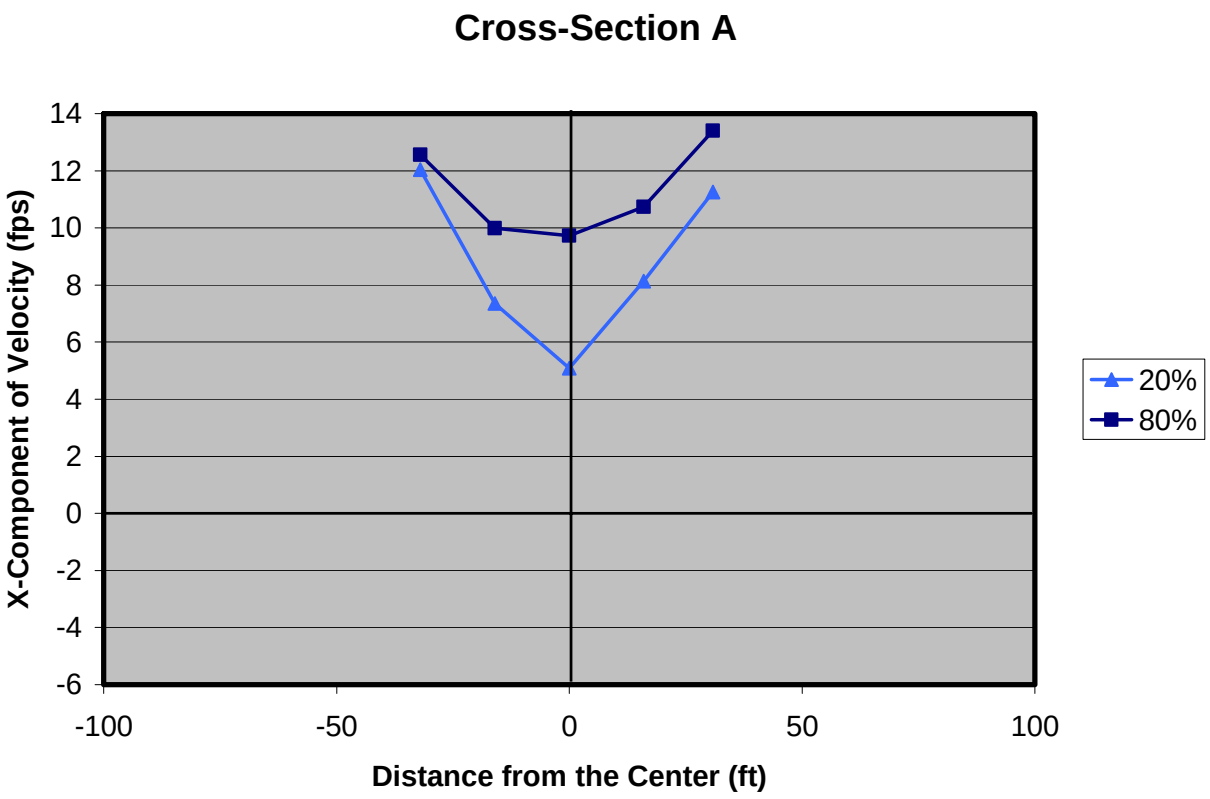

Figure 3.47. X-component of velocity distribution measured at cross-section A under a flow condition of 4248 cfs and a tailwater level of 14.5 ft above the datum.

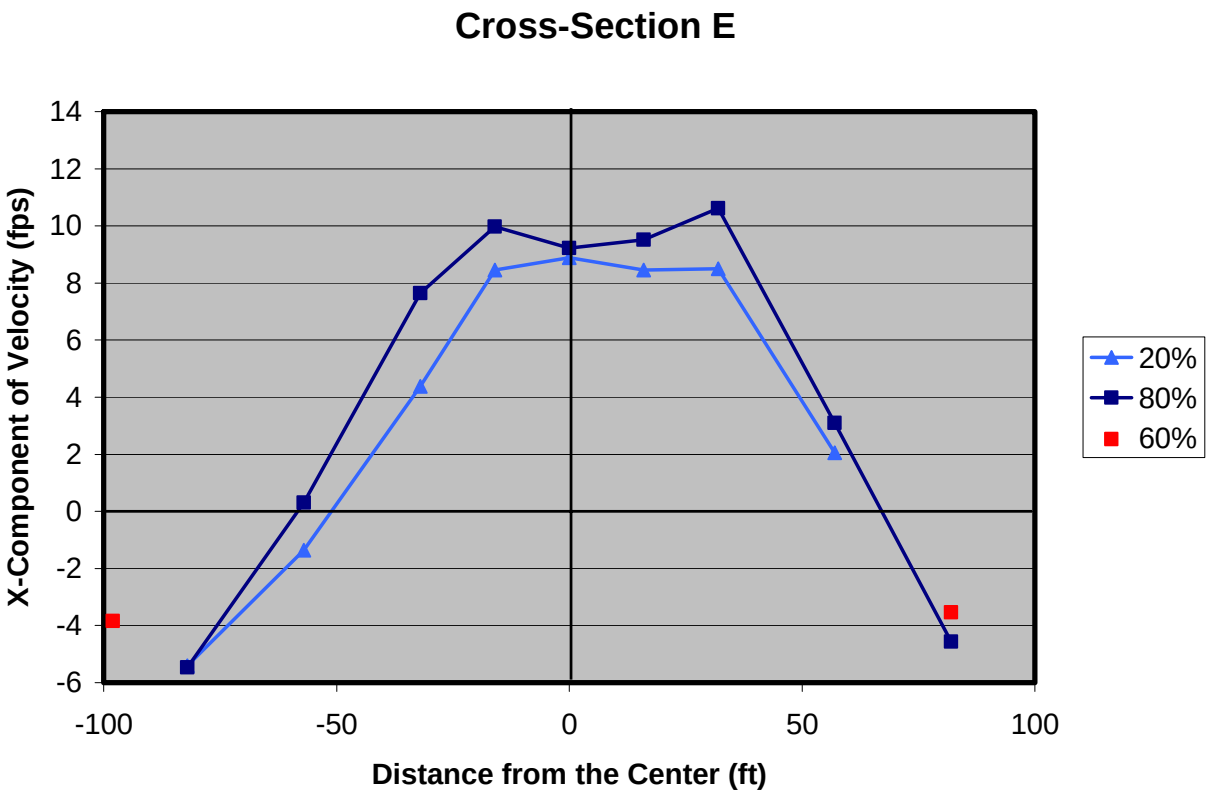

Figure 3.48. X-component of velocity distribution measured at cross-section E under a flow condition of 4248 cfs and a tailwater level of 14.5 ft above the datum.

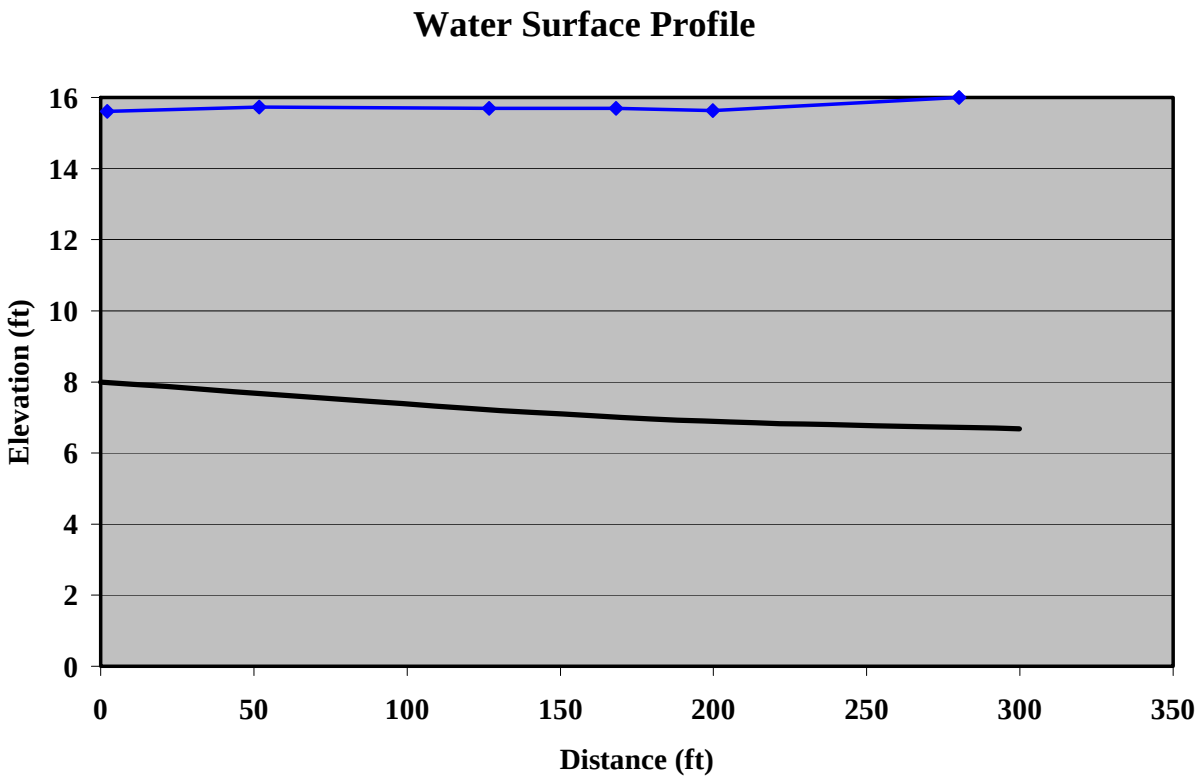

Figure 3.49. Water surface profile in the channel downstream of the stilling basin under a flow condition of 3367 cfs and a tailwater of 16 ft from the datum. The X-coordinate is shown in Figure 3.21.

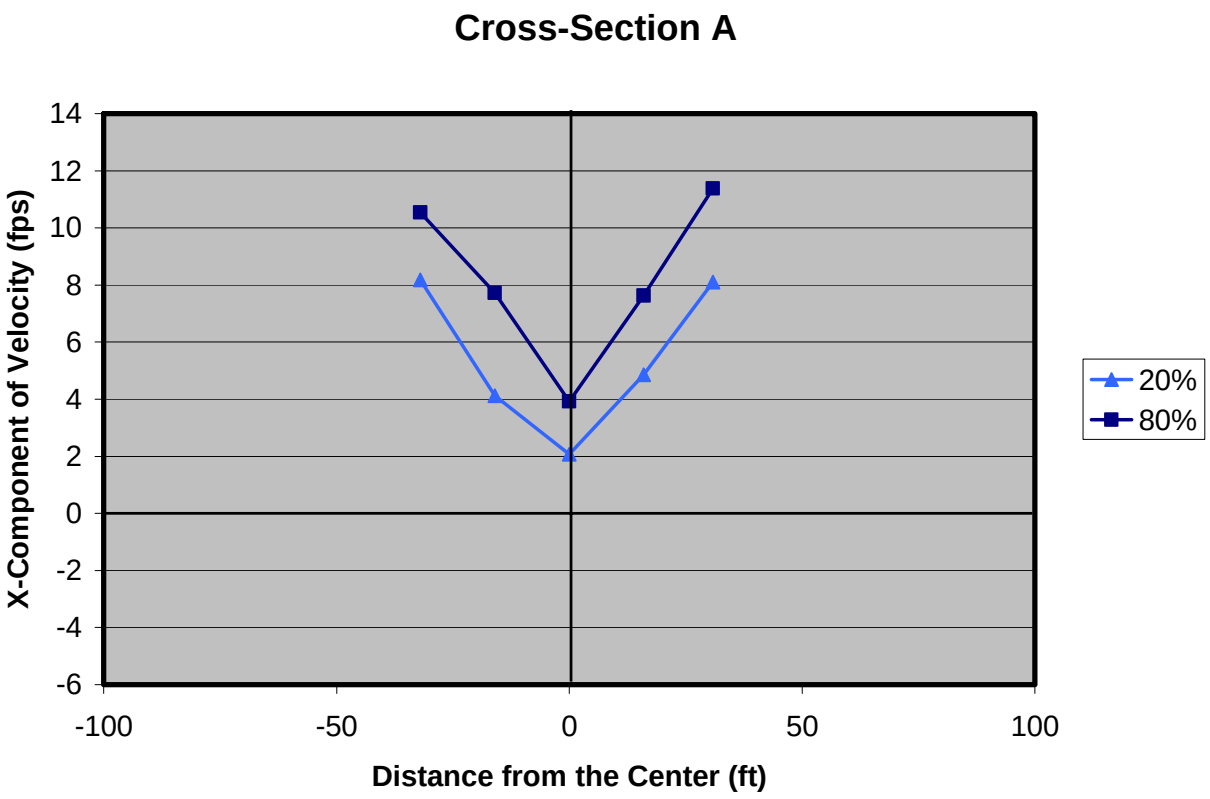

Figure 3.50. X-component of velocity distribution measured at cross-section A under a flow condition of 3367 cfs and a tailwater level of 16 ft above the datum.

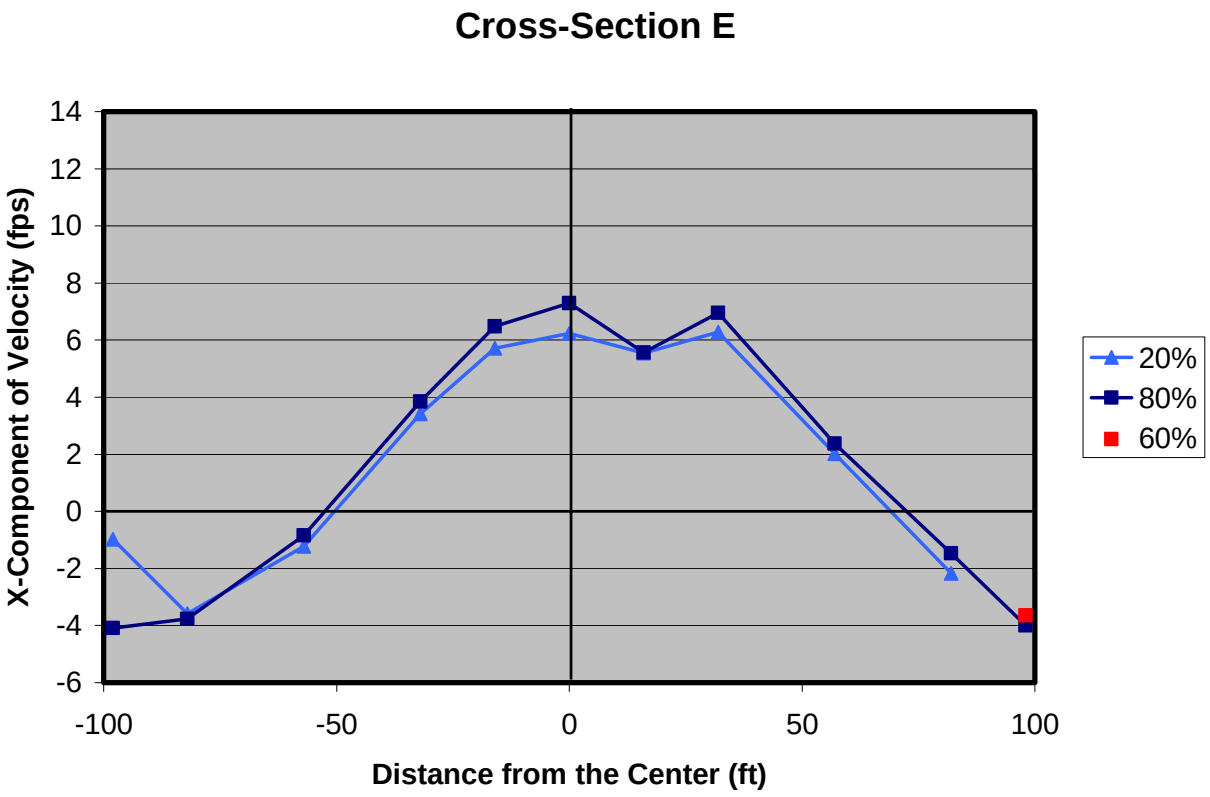

Figure 3.51. X-component of velocity distribution measured at cross-section E under a flow condition of 3367 cfs and a tailwater level of 16 ft above the datum.

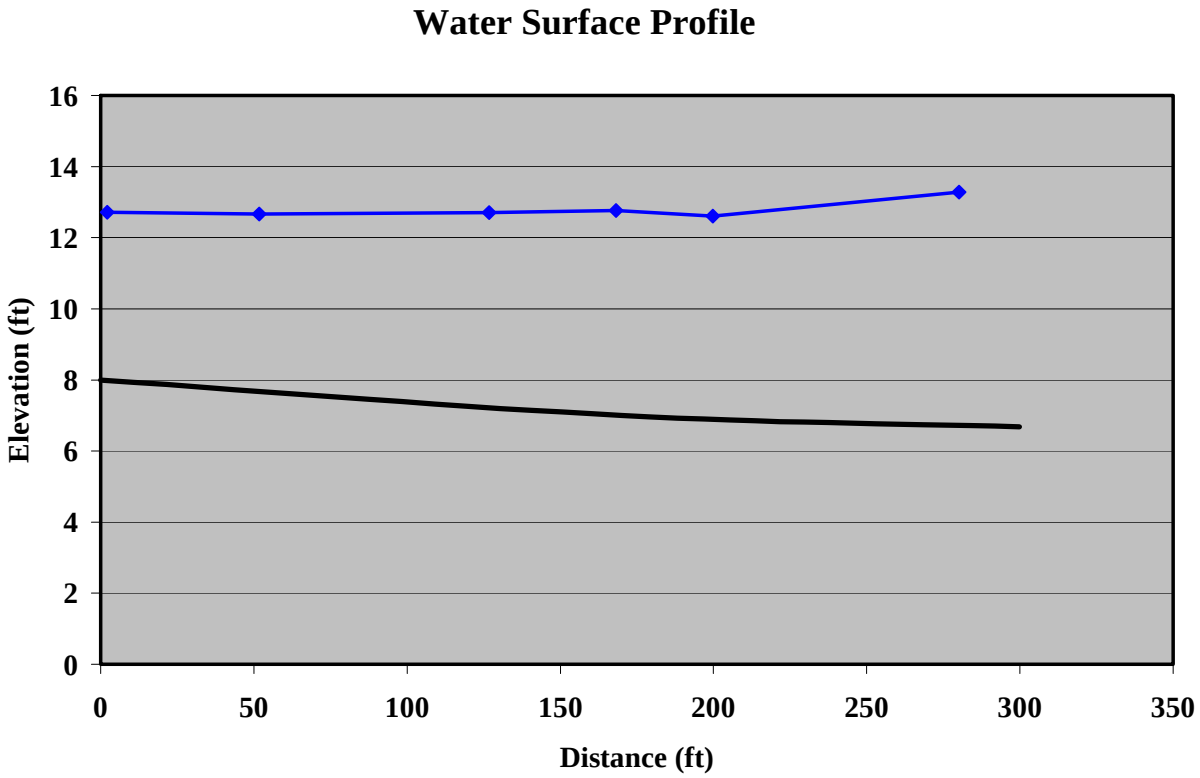

Figure 3.52. Water surface profile in the channel downstream of the stilling basin under a flow condition of 3376 cfs and a tailwater of 13.3 ft from the datum. The X-coordinate is shown in Figure 3.21.

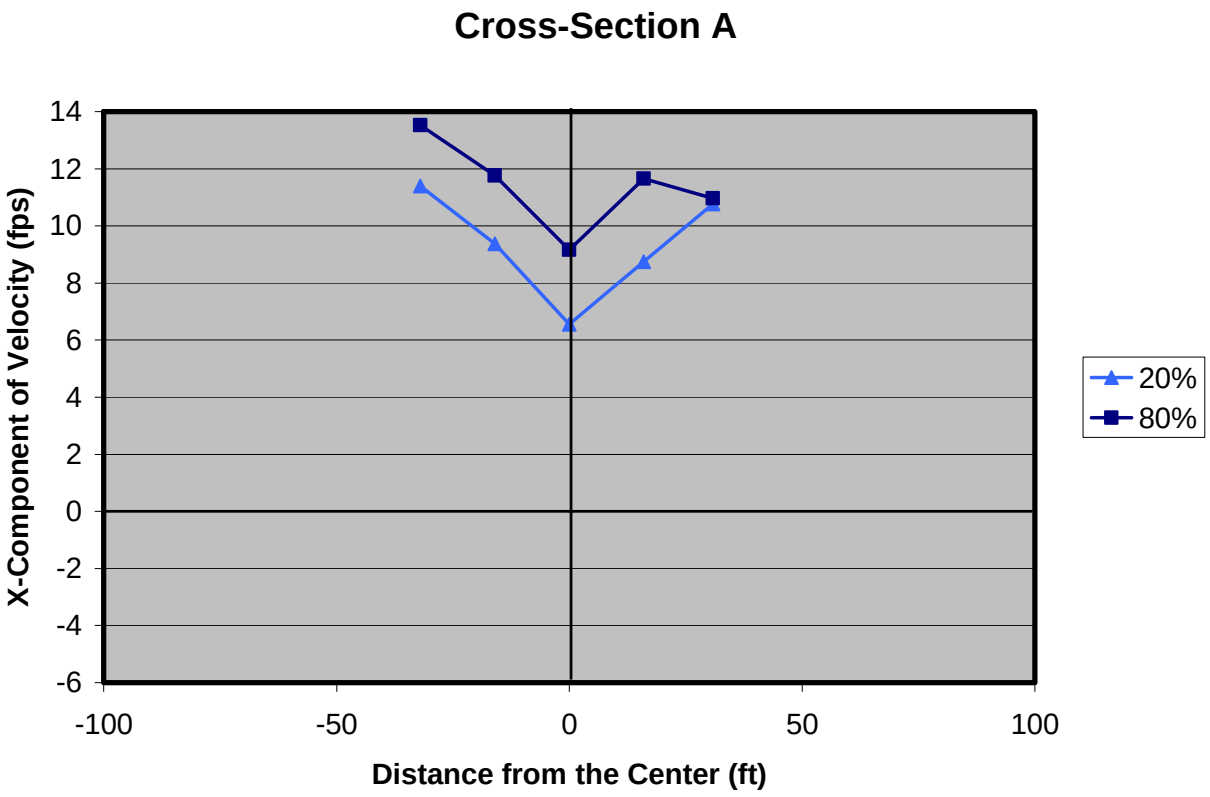

Figure 3.53. X-component of velocity distribution measured at cross-section A under a flow condition of 3376 cfs and a tailwater level of 13.3 ft above the datum.

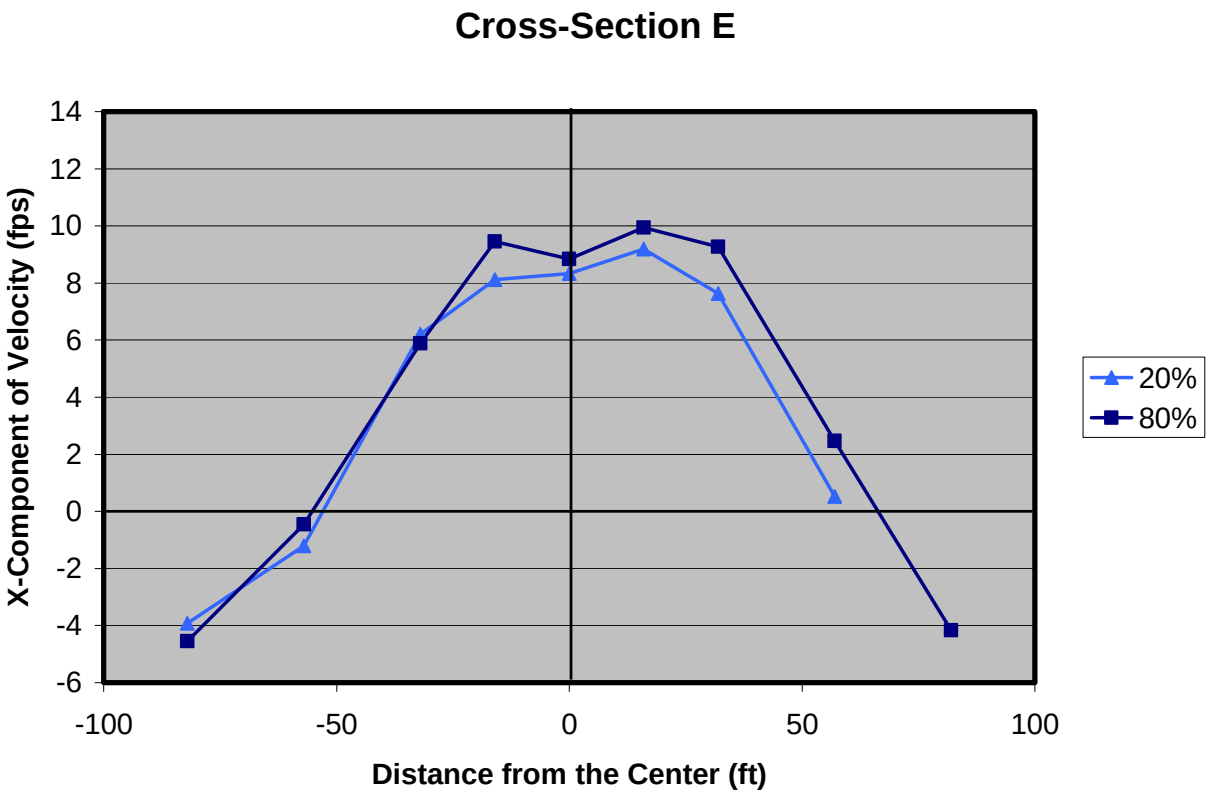

Figure 3.54. X-component of velocity distribution measured at cross-section E under a flow condition of 3376 cfs and a tailwater level of 13.3 ft above the datum.

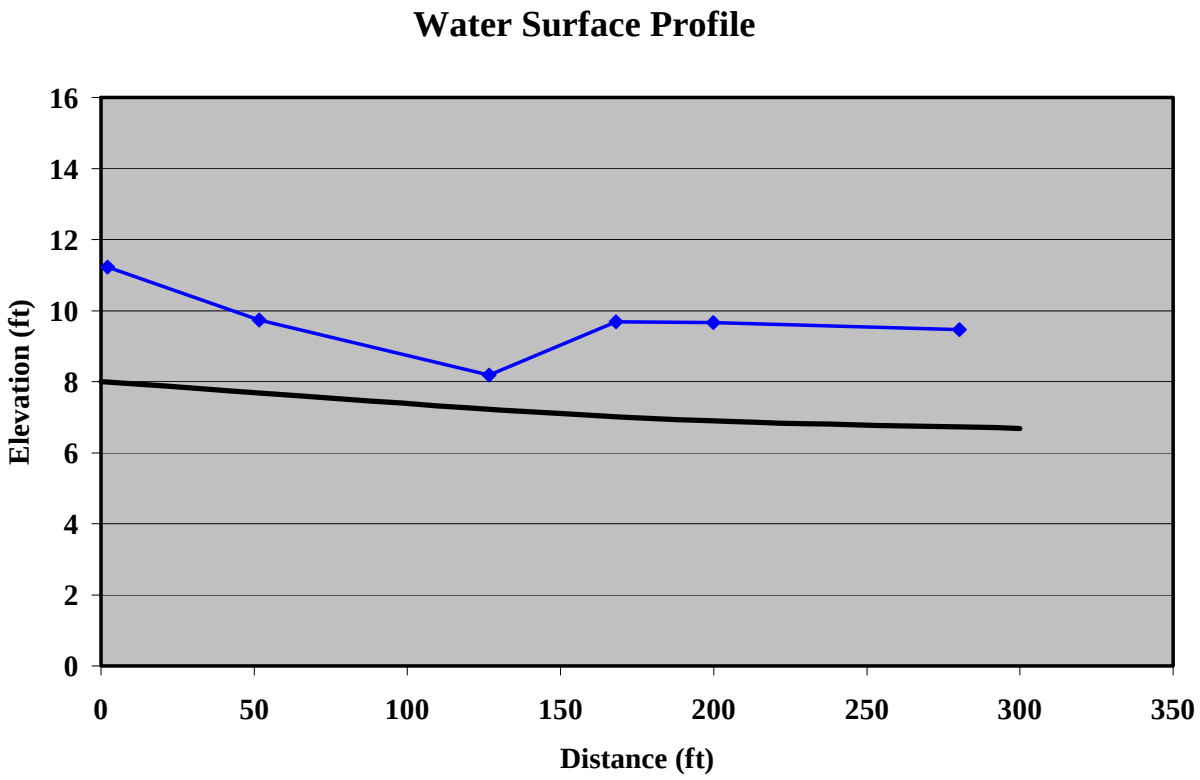

Figure 3.55. Water surface profile in the channel downstream of the stilling basin under a flow condition of 2278 cfs and no tailwater of. The X-coordinate is shown in Figure 3.21.

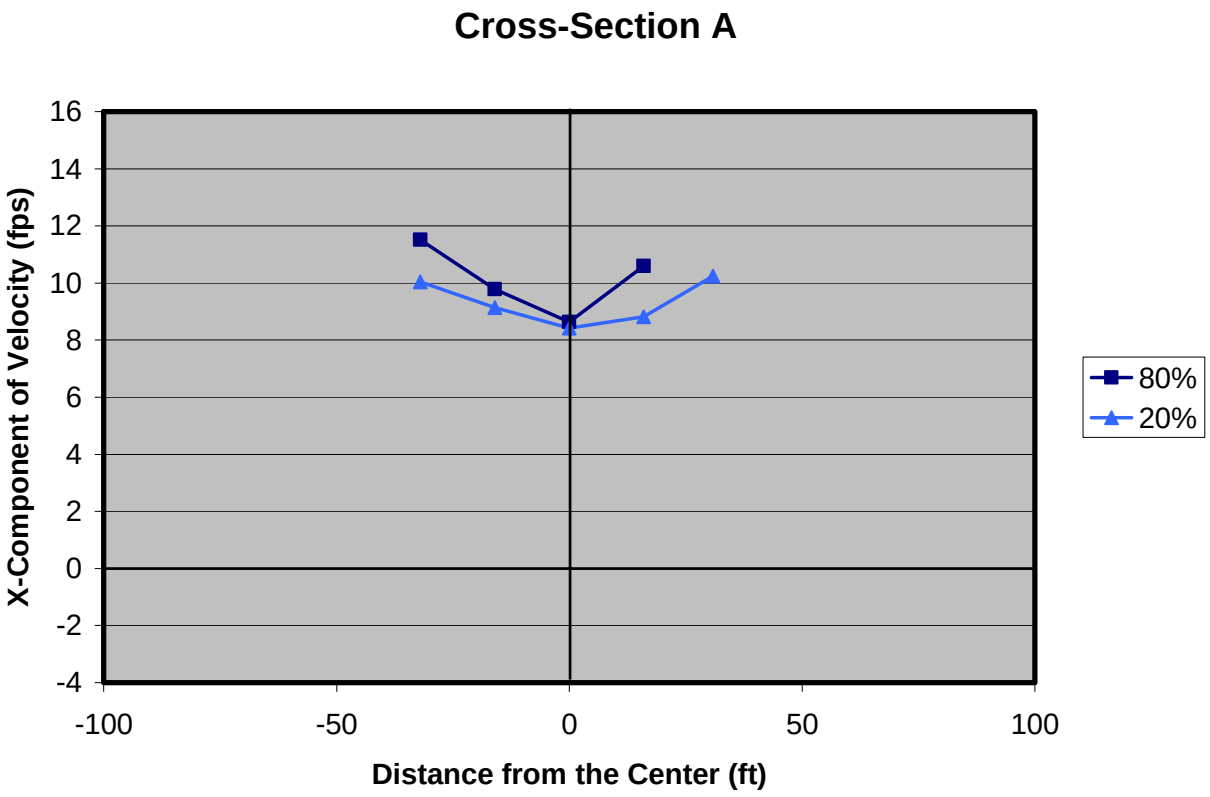

Figure 3.56. X-component of velocity distribution measured at cross-section A under a flow condition of 2278 cfs and no tailwater.

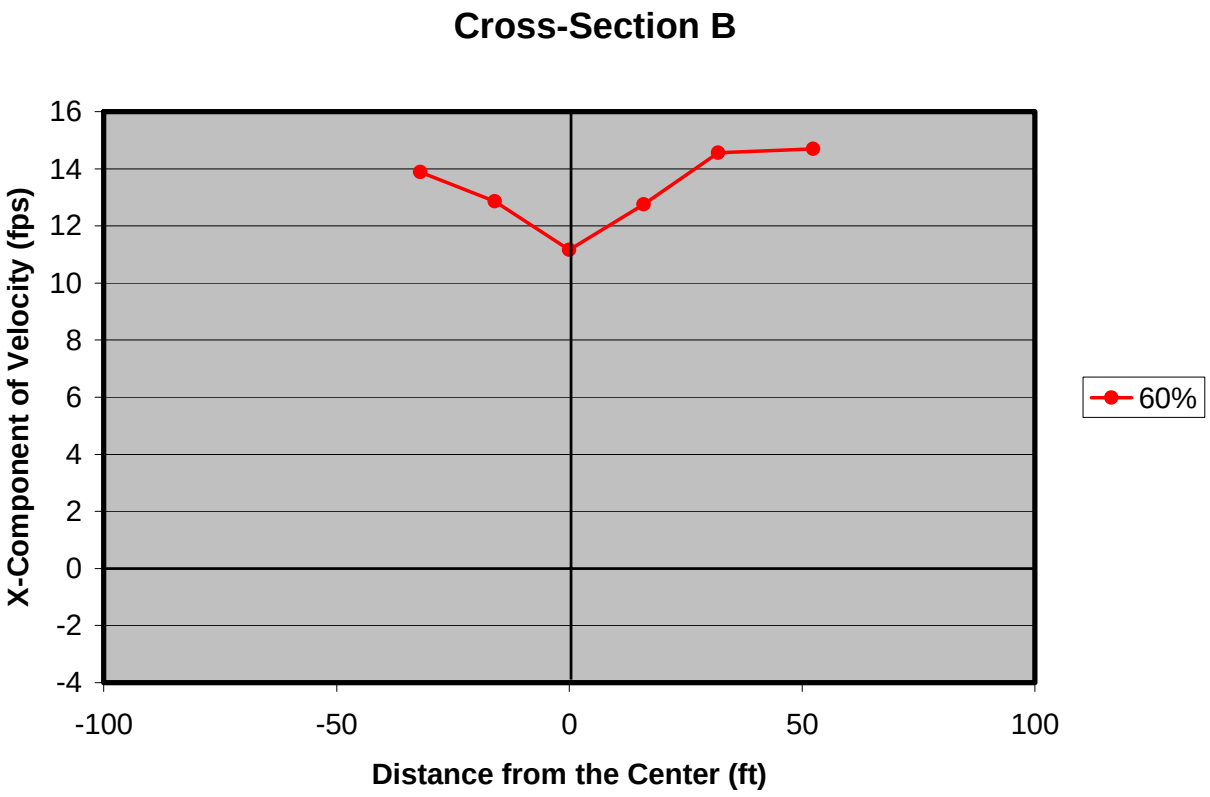

Figure 3.57. X-component of velocity distribution measured at cross-section B under a flow condition of 2278 cfs and no tailwater.

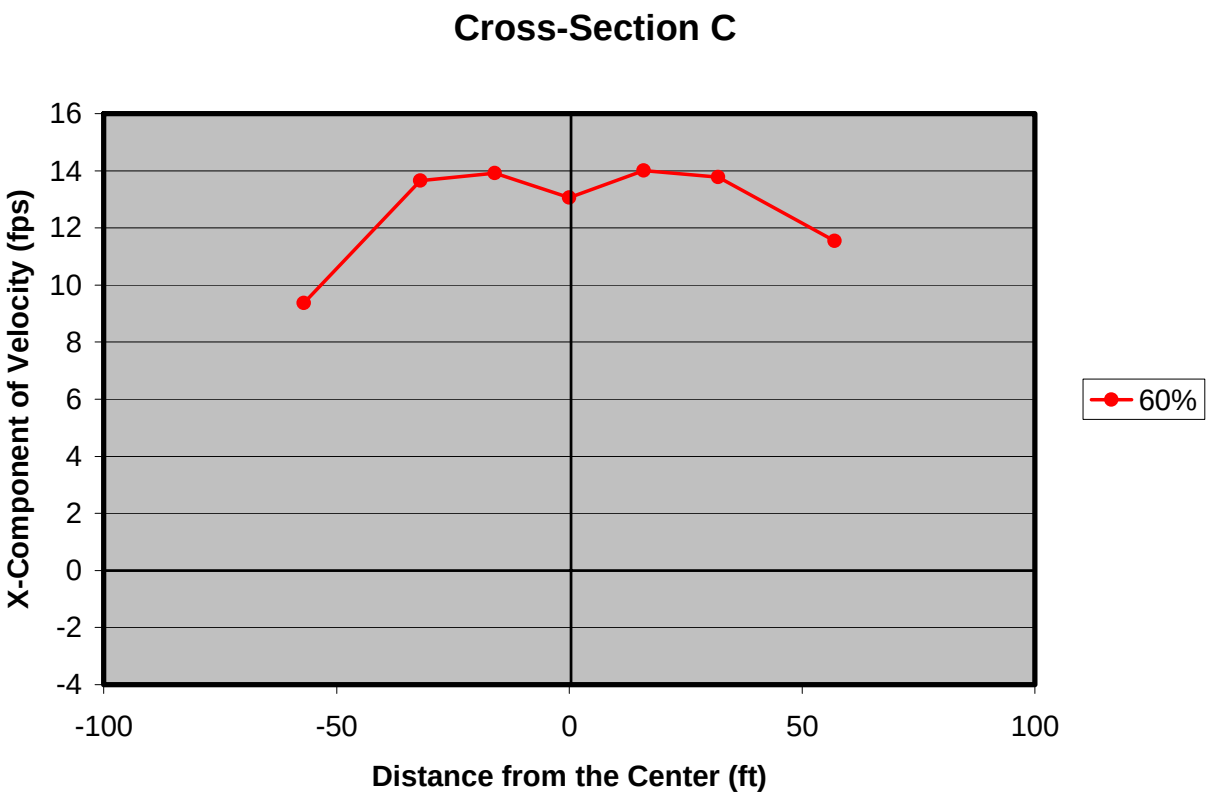

Figure 3.58. X-component of velocity distribution measured at cross-section C under a flow condition of 2278 cfs and no tailwater.

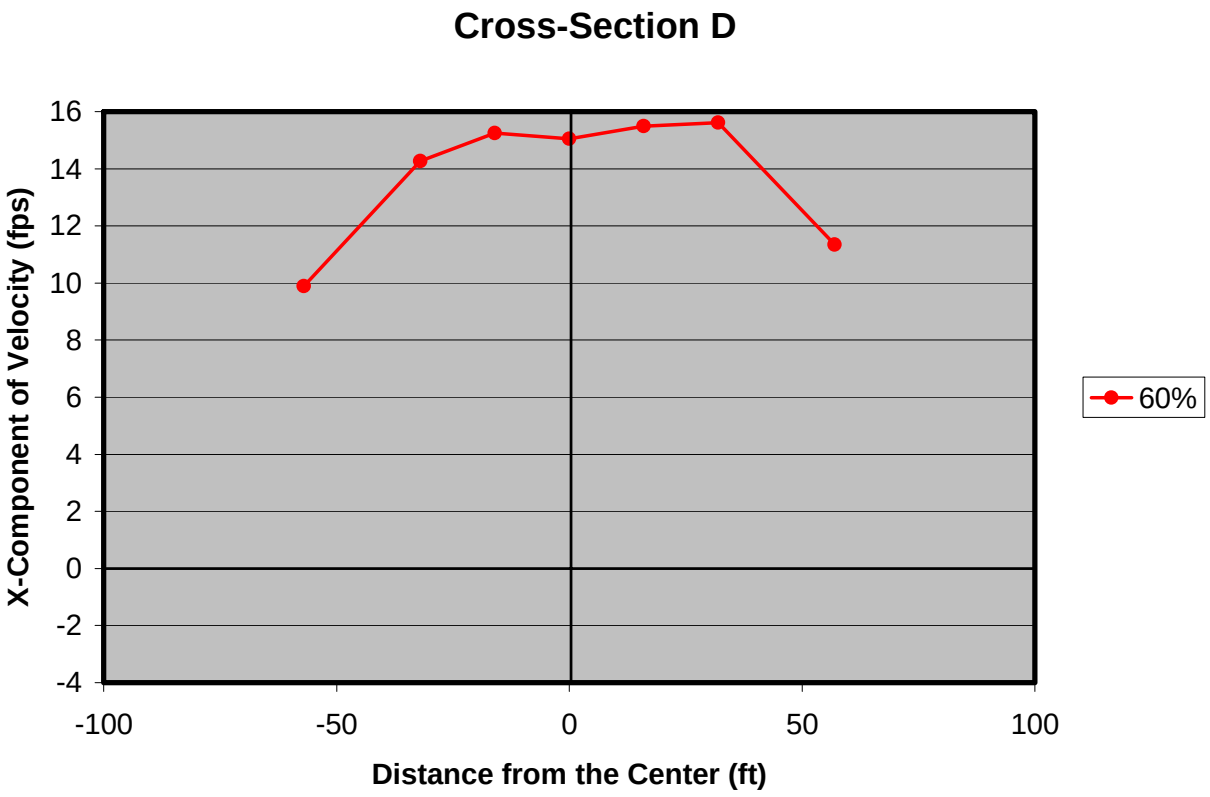

Figure 3.59. X-component of velocity distribution measured at cross-section D under a flow condition of 2278 cfs and no tailwater.

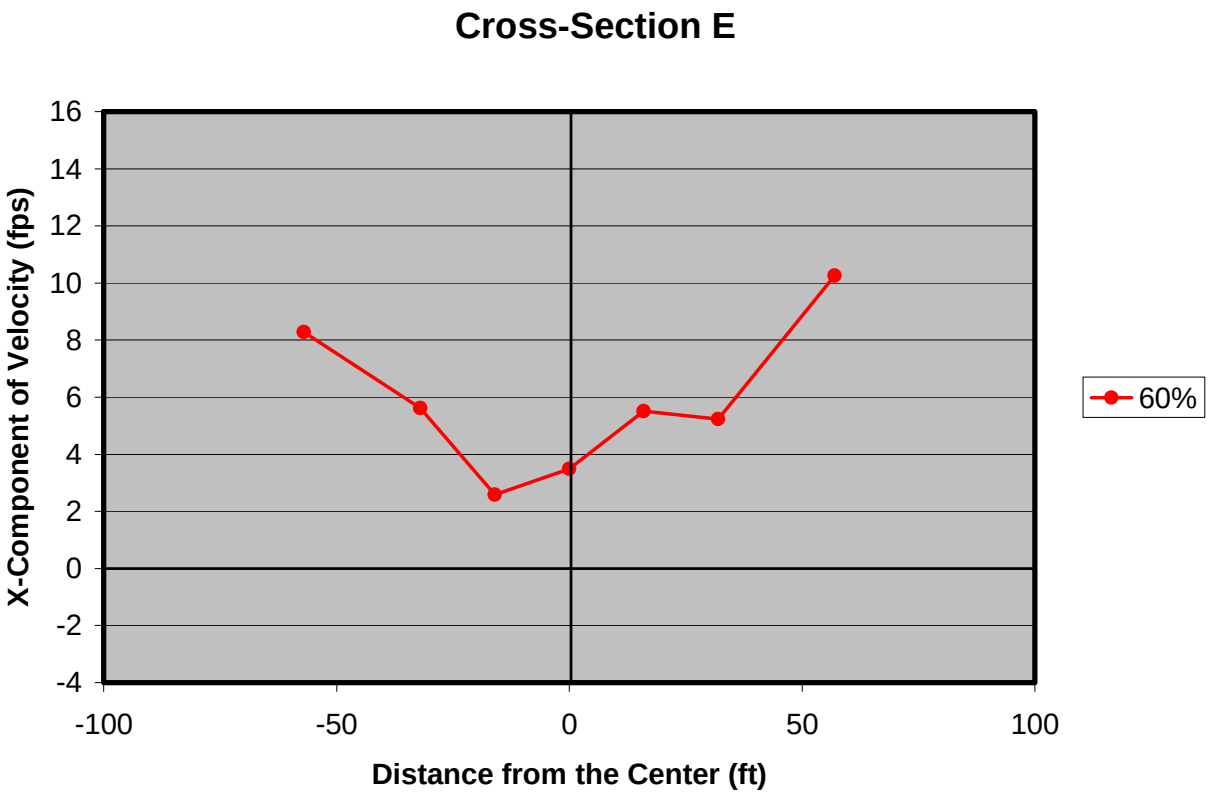

Figure 3.60. X-component of velocity distribution measured at cross-section E under a flow condition of 2278 cfs and no tailwater.

4. Summary

After initial evaluation of the existing stilling basin in the previous physical model study, MWH Americas Inc. requested a new model study of a new design of the stilling basin. The existing stilling basin has a bed elevation of 7 ft below the datum and in order to counteract the excessive pore pressure from seepage water, the stilling basin is currently filled with backfill sand. To avoid the backfill in the stilling basin and to make the stilling basin operational, the stilling basin bed elevation was proposed to be set at 7 ft above the datum, and in order to dissipate the energy an expanding baffled chute was proposed. In this study, overall two major and several minor modifications were proposed and tested. The goal of this physical model study was to assess the performance of the outlet structure under the probable maximum flood, standard project flood, and the reservoir drawdown discharge conditions and different tailwater levels, and to determine the velocity magnitudes downstream of the stilling basin to design the necessary protection measures.

The final design consisted of a baffled chute ending in a stilling basin with a bed elevation 6.5 ft below the channel invert. Eight test series were conducted on the final design. The test series showed that under the probable maximum flood condition with a tailwater level of 14.5 ft above the datum, the maximum average velocity and the maximum velocity are about 8.8 and 13 fps, respectively. Under the standard project flood condition with a tailwater of 13.3 ft above the datum, the maximum average velocity and the maximum velocity are about 9.3 and 13 fps, respectively.

Under the drawdown flood condition with a tailwater of 11.5 ft above the datum, the maximum average velocity and the maximum velocity were about 8.4 and 10 fps, respectively. However, under the drawdown flood condition with no tailwater, a hydraulic drop occurred at the downstream end of the stilling basin and the flow regime became supercritical with a maximum velocity of 16 fps, and a second hydraulic jump occurred about 200 ft downstream of the stilling basin. The surface roughness of the model channel is less than the prototype channel lined with riprap; therefore, the model supercritical flow condition may not be the same as in the prototype. Nevertheless, in order to avoid any erosion of the riprap on the downstream channel, the tailwater in the channel should be about 11.5 ft under the drawdown flood condition.

References

Mohseni, O, Spitael, M. and Stefan, H. 2005. Stilling Basin Hydraulic Model Study. *St. Anthony Falls Laboratory, Project no. 469.*

Appendix A. Production Test Series

A.1. The Flow Condition of 4296 cfs with a Tailwater of 16 ft

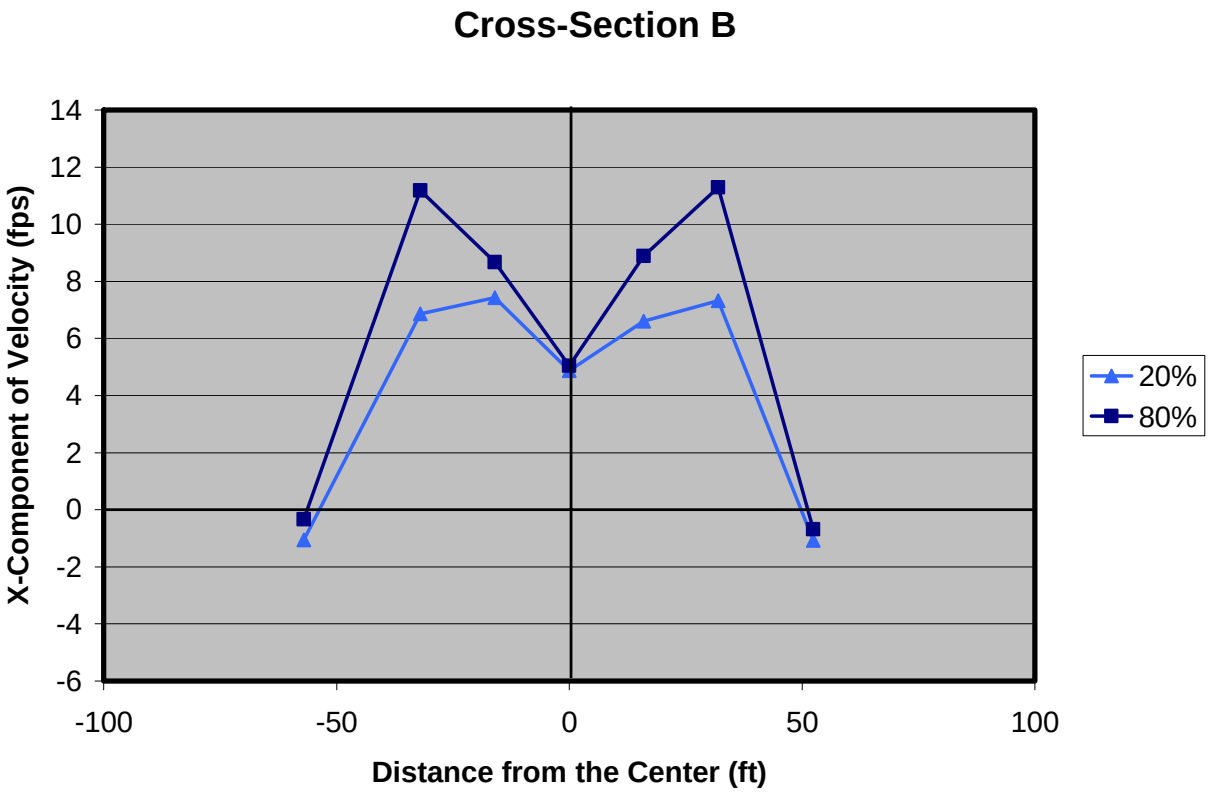

Figure A.1. X-component of velocity distribution measured at cross-section B under a flow condition of 4307 cfs and a tailwater level of 16 ft above the datum.

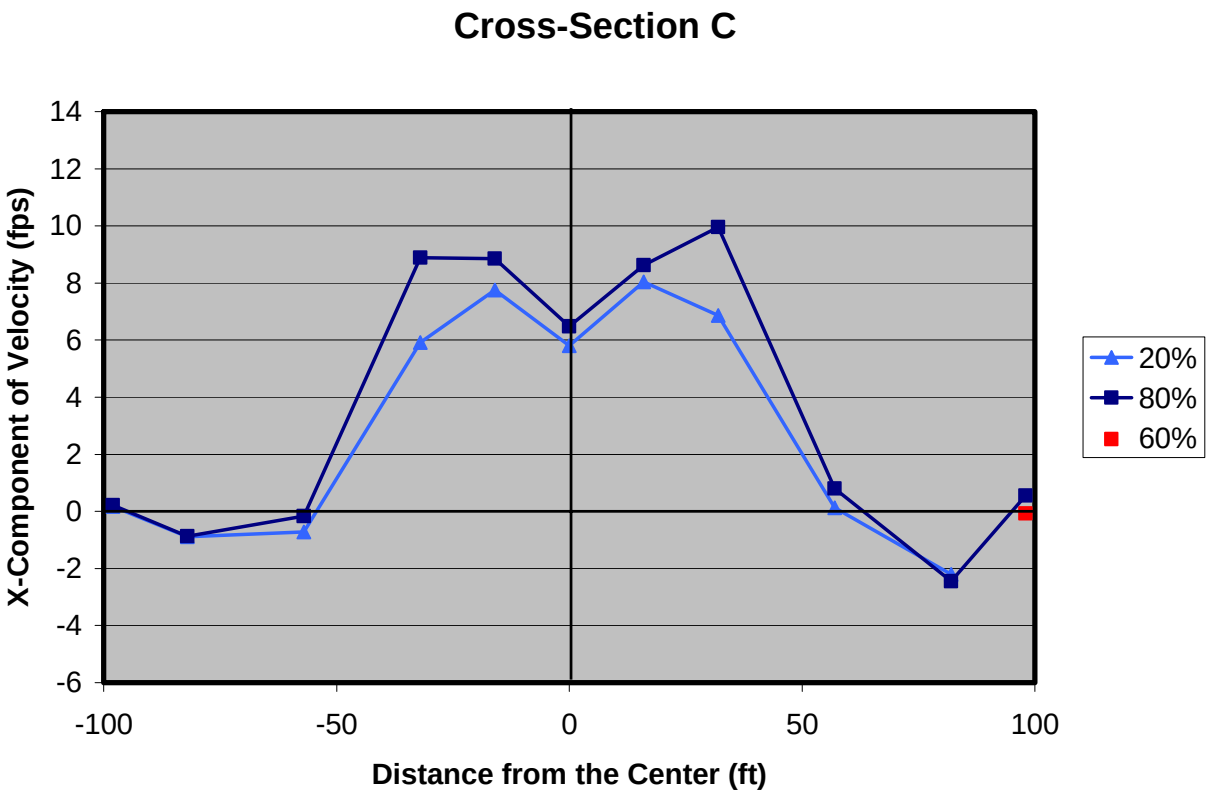

Figure A.2. X-component of velocity distribution measured at cross-section C under a flow condition of 4307 cfs and a tailwater level of 16 ft above the datum.

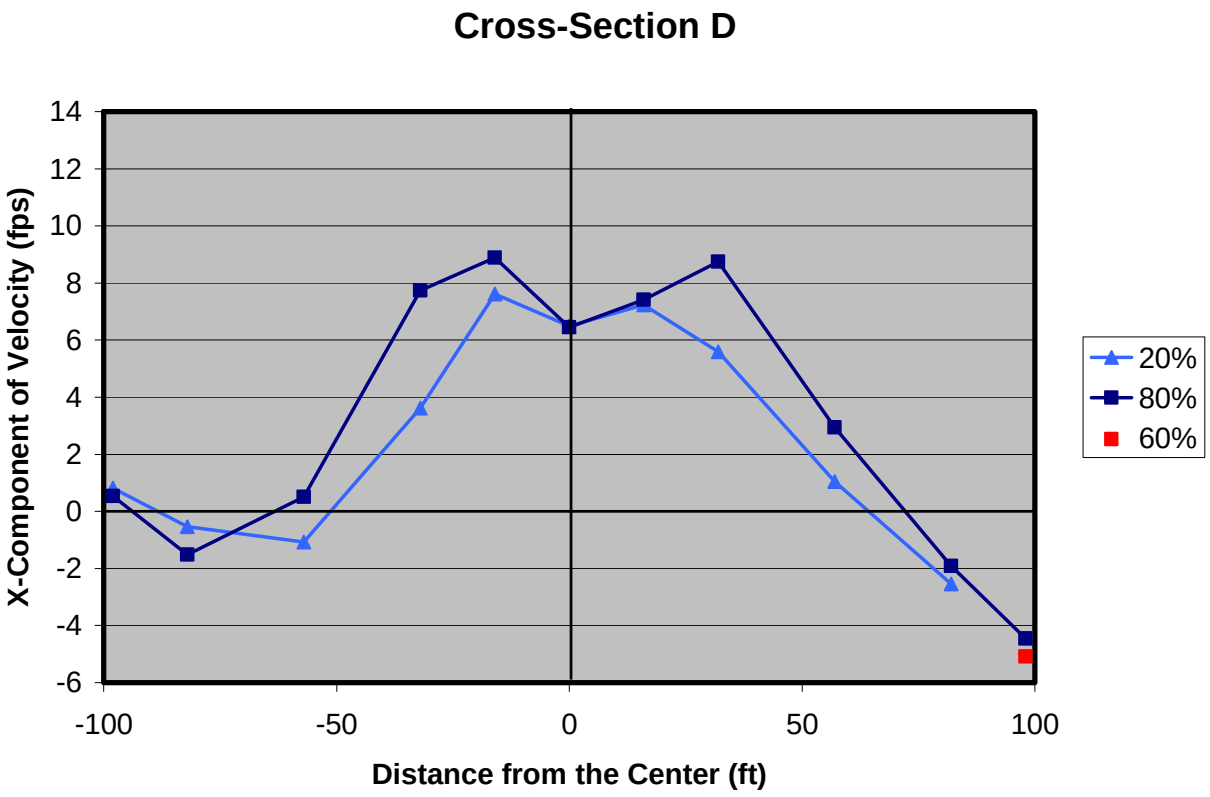

Figure A.3. X-component of velocity distribution measured at cross-section D under a flow condition of 4307 cfs and a tailwater level of 16 ft above the datum.

A.2. The Flow Condition of 4296 cfs with a Tailwater of 14.5

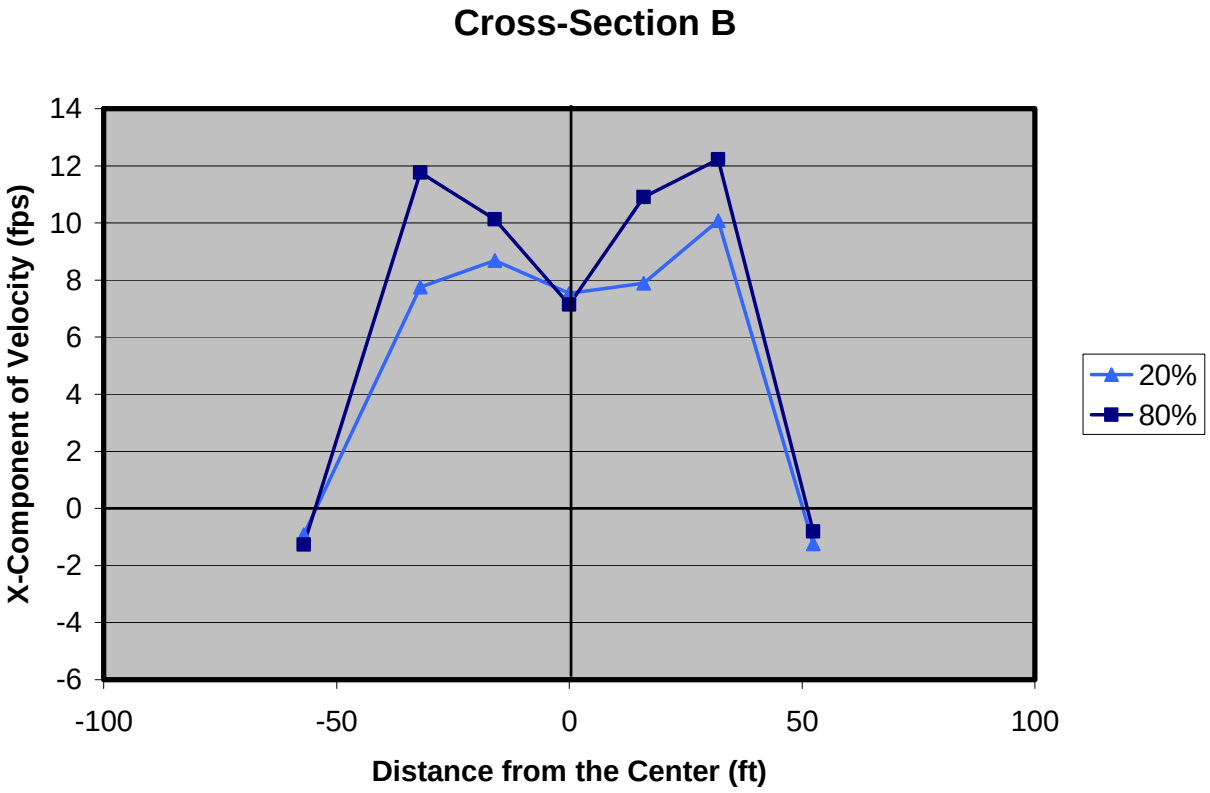

Figure A.4. X-component of velocity distribution measured at cross-section B under a flow condition of 4248 cfs and a tailwater level of 14.5 ft above the datum.

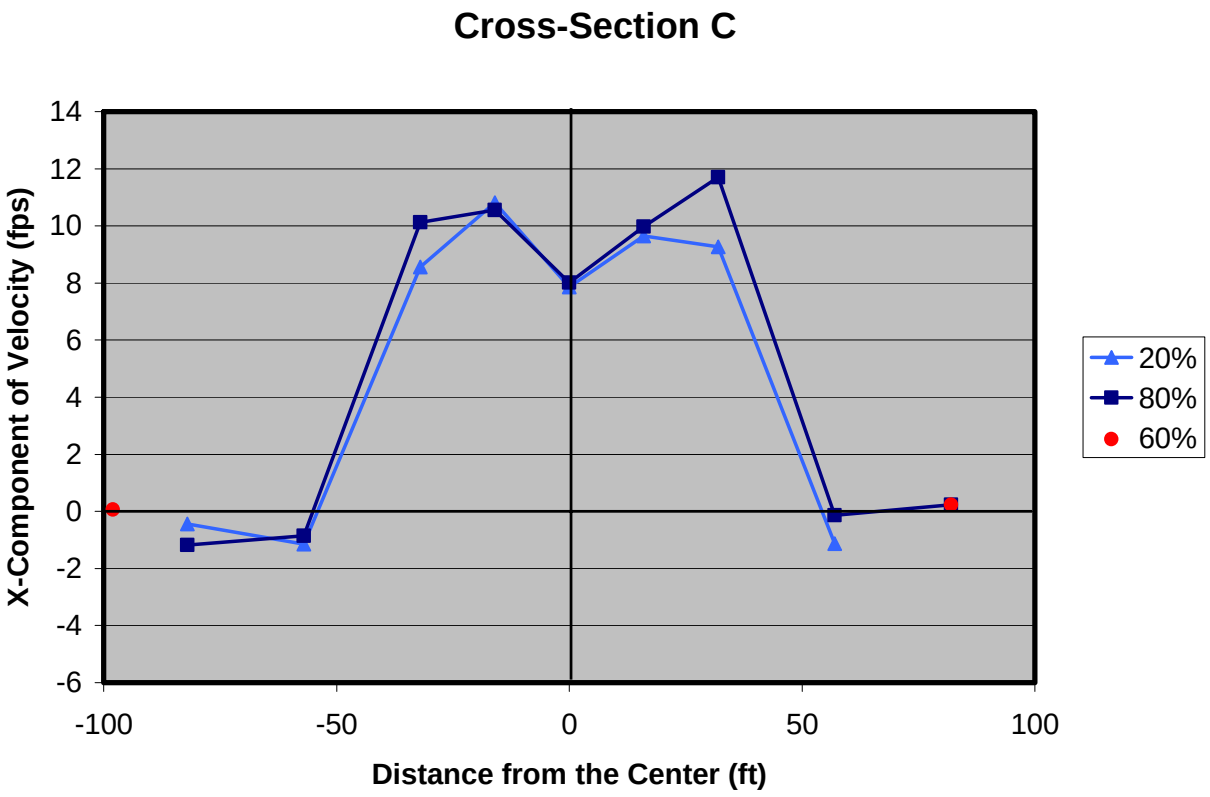

Figure A.5. X-component of velocity distribution measured at cross-section C under a flow condition of 4248 cfs and a tailwater level of 14.5 ft above the datum.

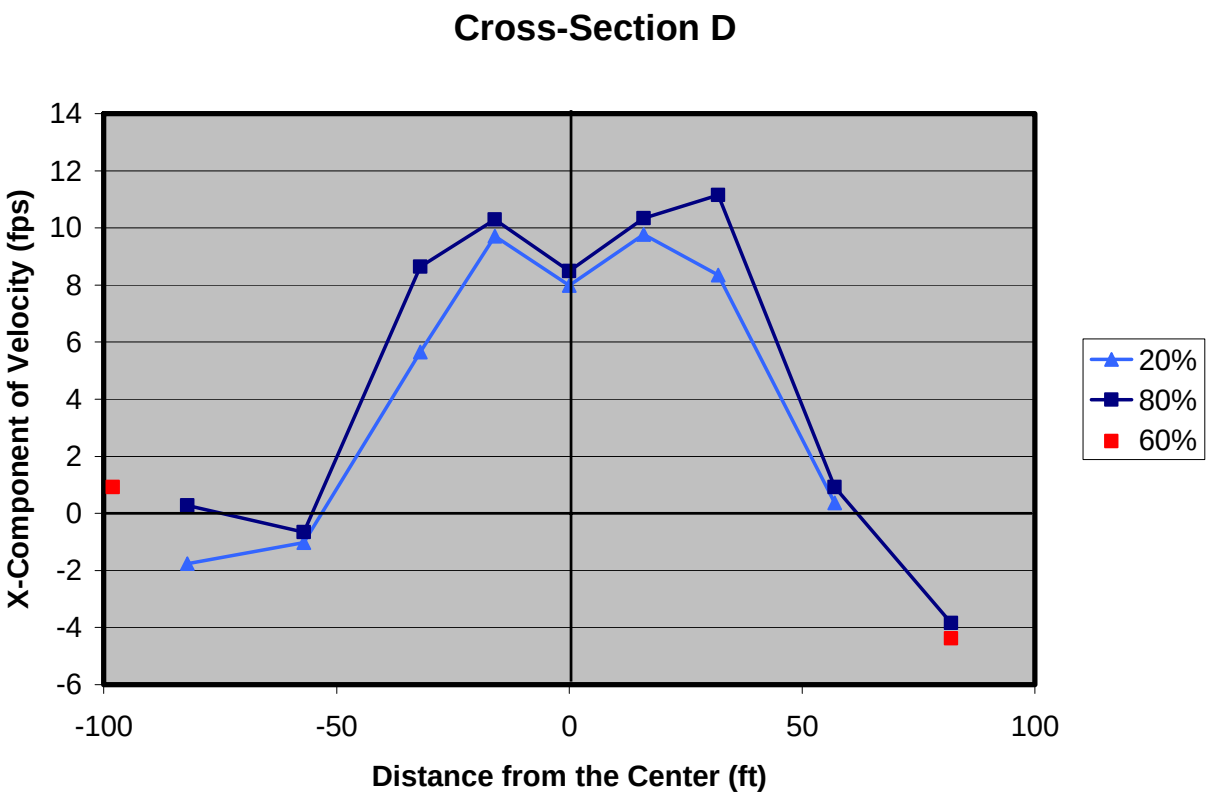

Figure A.6. X-component of velocity distribution measured at cross-section D under a flow condition of 4248 cfs and a tailwater level of 14.5 ft above the datum.

A.3. The Flow Condition of 3369 cfs with a Tailwater of 16 ft

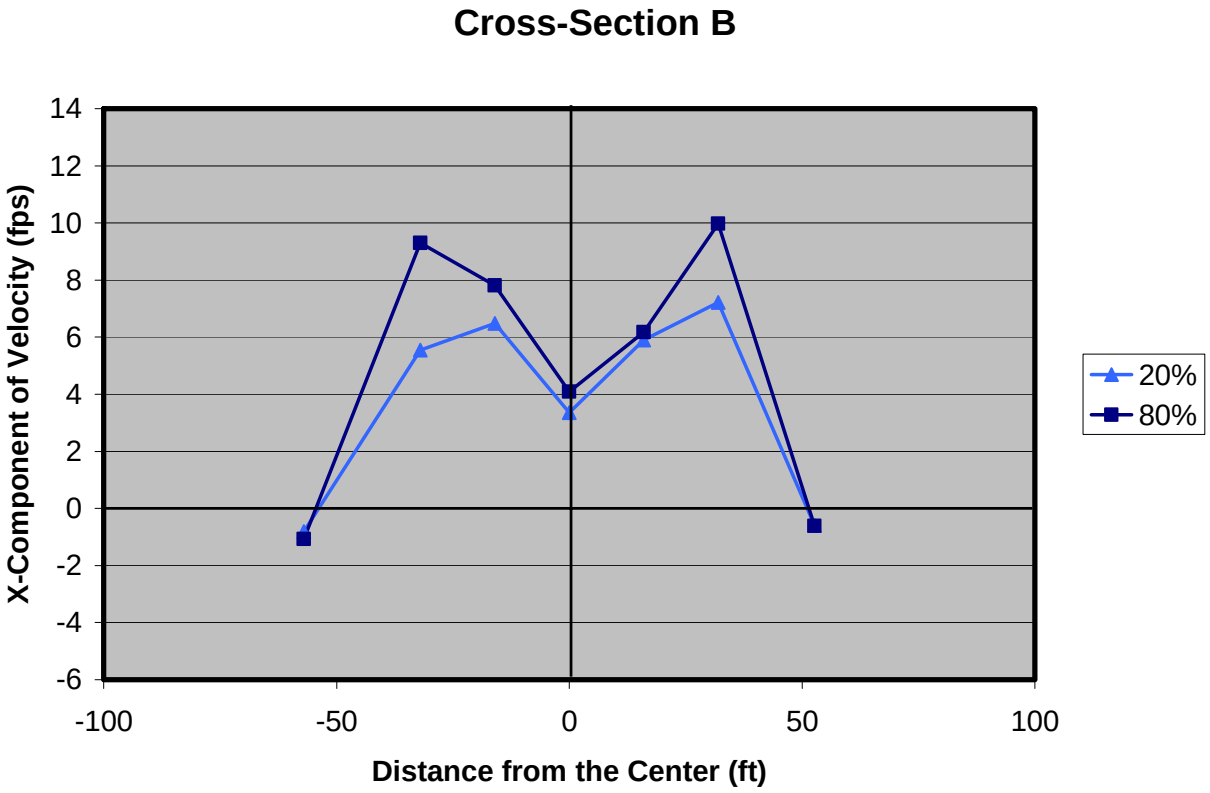

Figure A.7. X-component of velocity distribution measured at cross-section B under a flow condition of 3367 cfs and a tailwater of 16 ft from the datum.

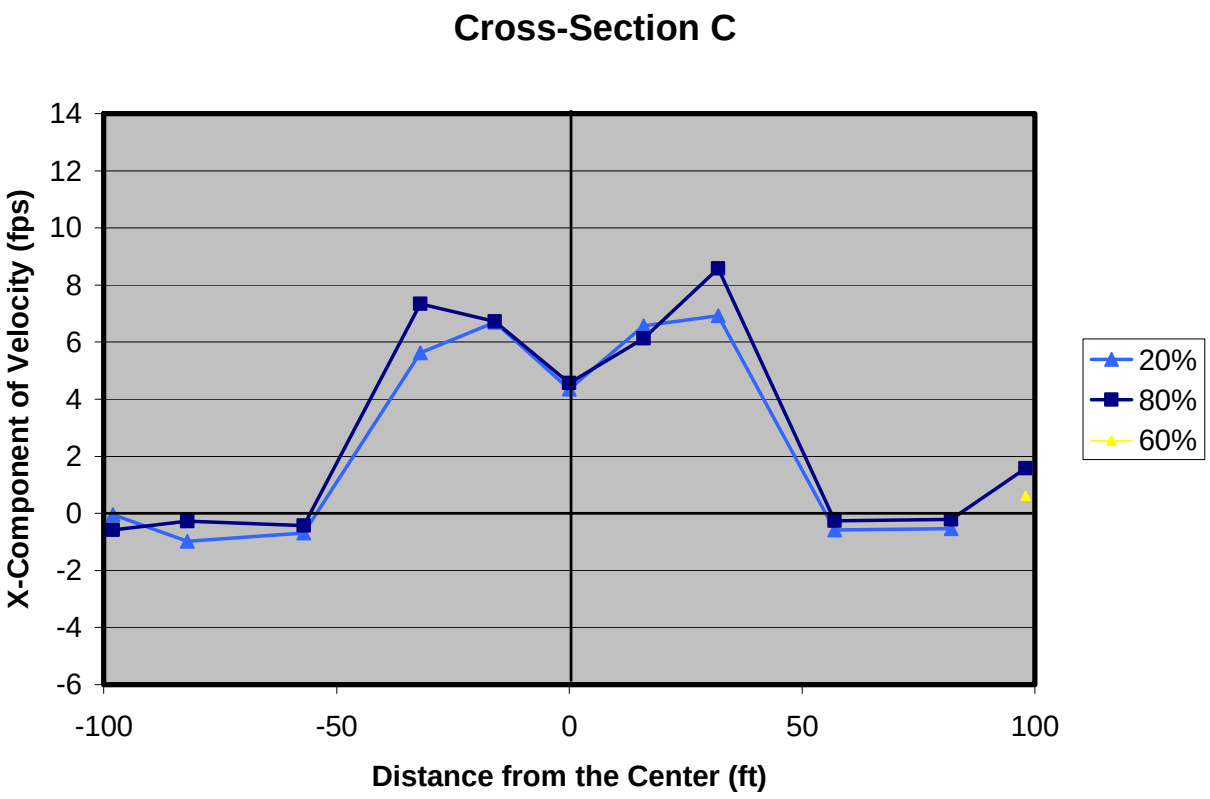

Figure A.8. X-component of velocity distribution measured at cross-section C under a flow condition of 3367 cfs and a tailwater of 16 ft from the datum.

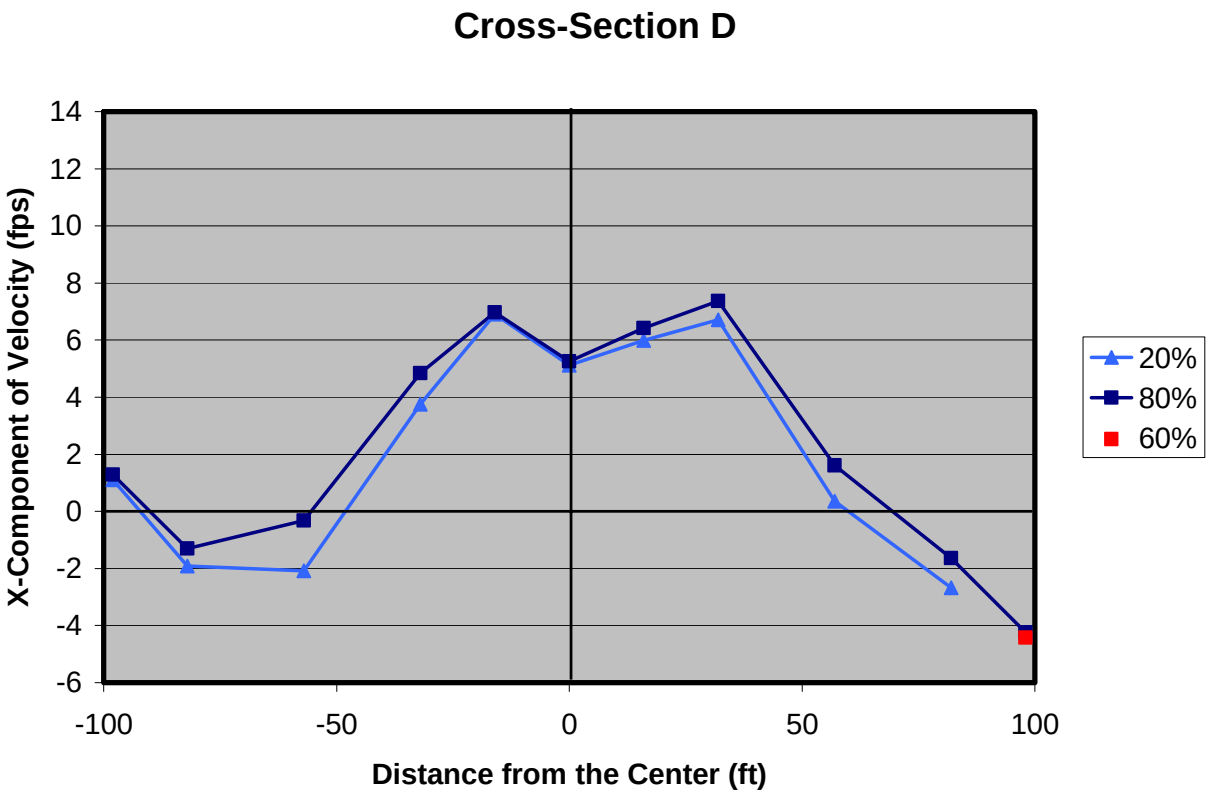

Figure A.9. X-component of velocity distribution measured at cross-section D under a flow condition of 3367 cfs and a tailwater of 16 ft from the datum.

A.4. The Flow Condition of 3369 cfs with a Tailwater of 13.3 ft

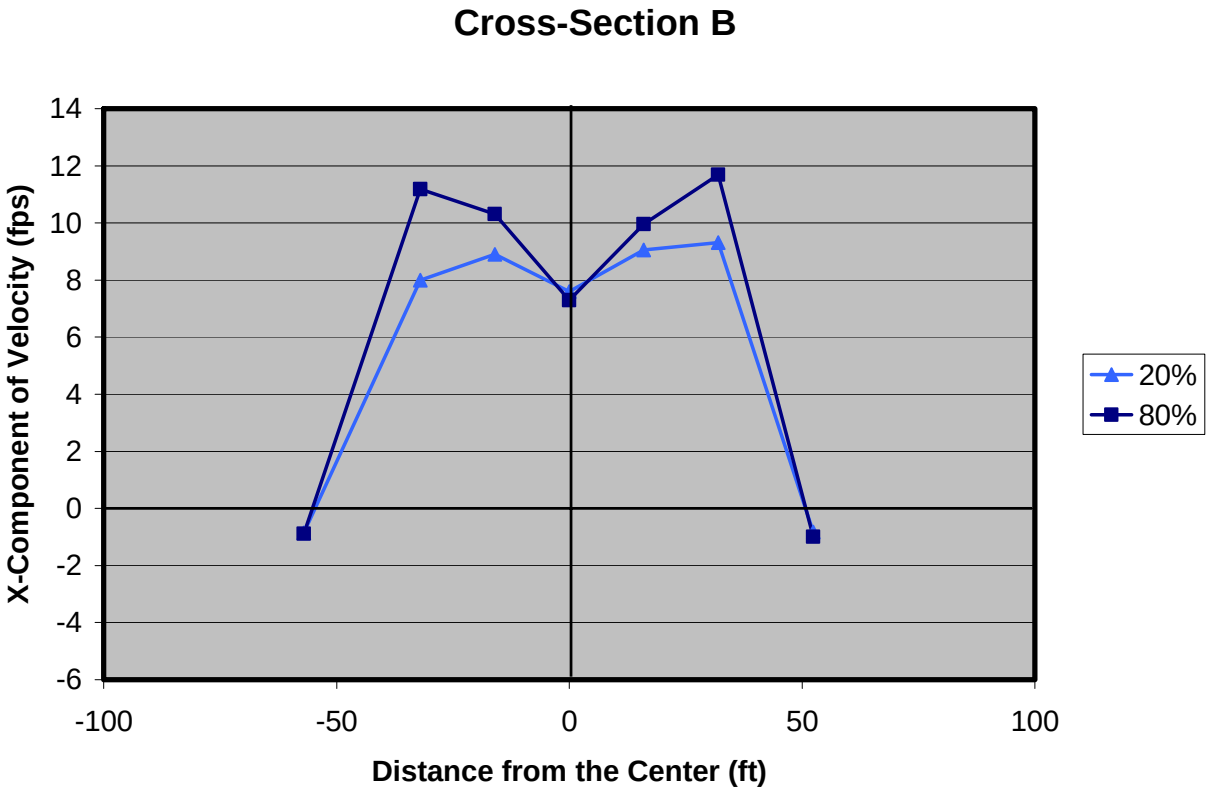

Figure A.10. X-component of velocity distribution measured at cross-section B under a flow condition of 3376 cfs and a tailwater level of 13.3 ft above the datum.

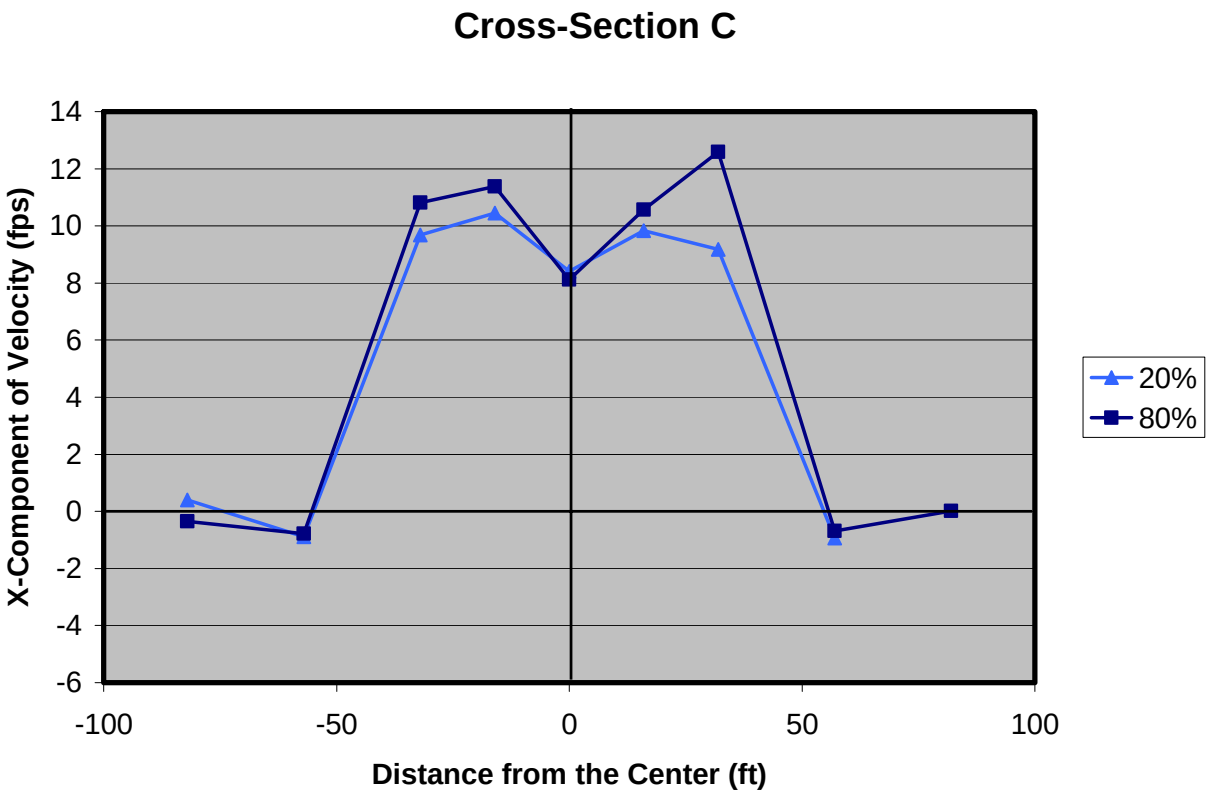

Figure A.11. X-component of velocity distribution measured at cross-section C under a flow condition of 3376 cfs and a tailwater level of 13.3 ft above the datum.

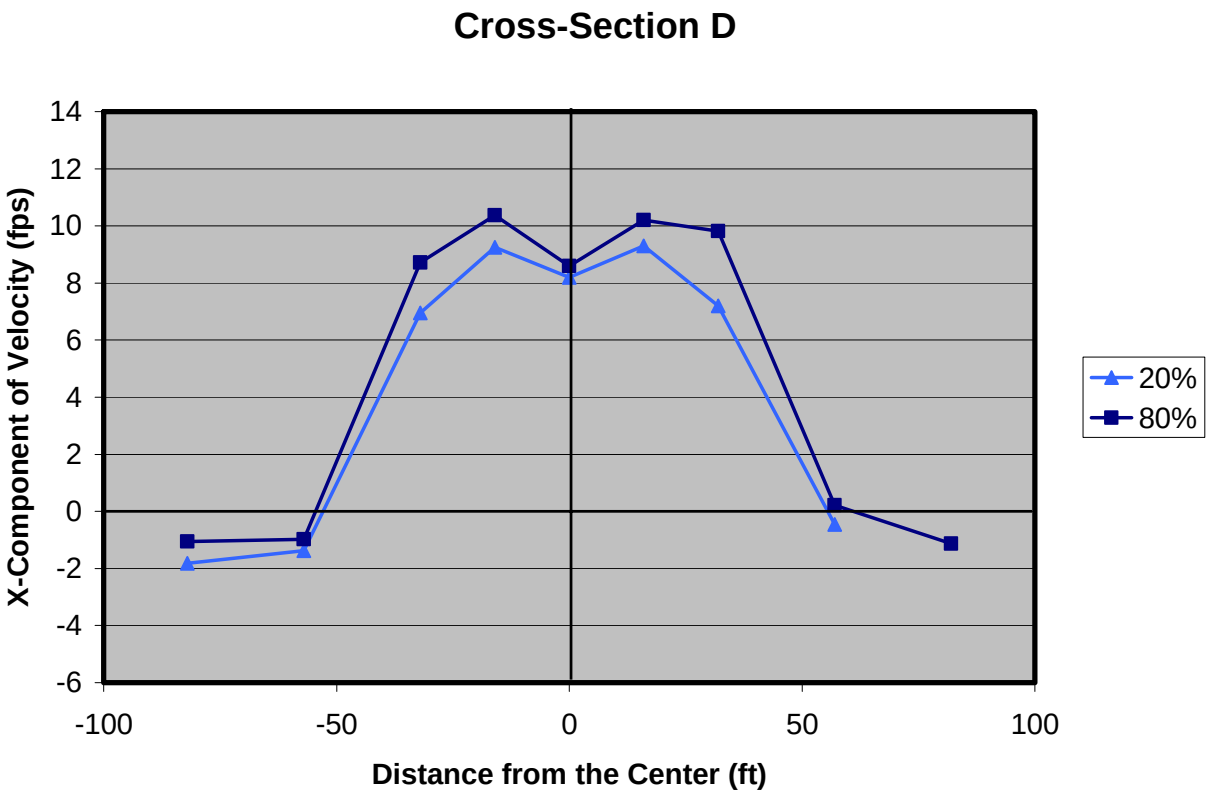

Figure A.12. X-component of velocity distribution measured at cross-section D under a flow condition of 3376 cfs and a tailwater level of 13.3 ft above the datum.

A.5. The Flow Condition of 2300 cfs with no Tailwater

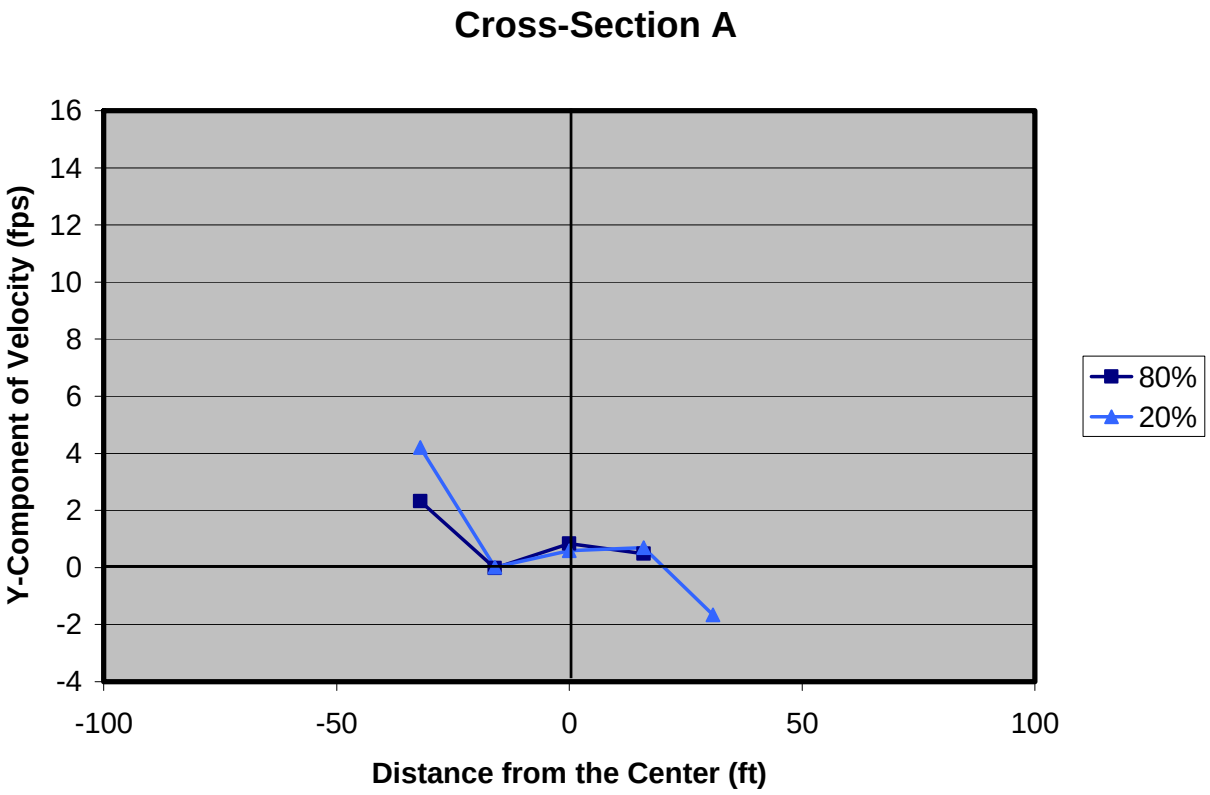

Figure A.13. Y-component of velocity distribution measured at cross-section A under a flow condition of 2278 cfs and no tailwater.

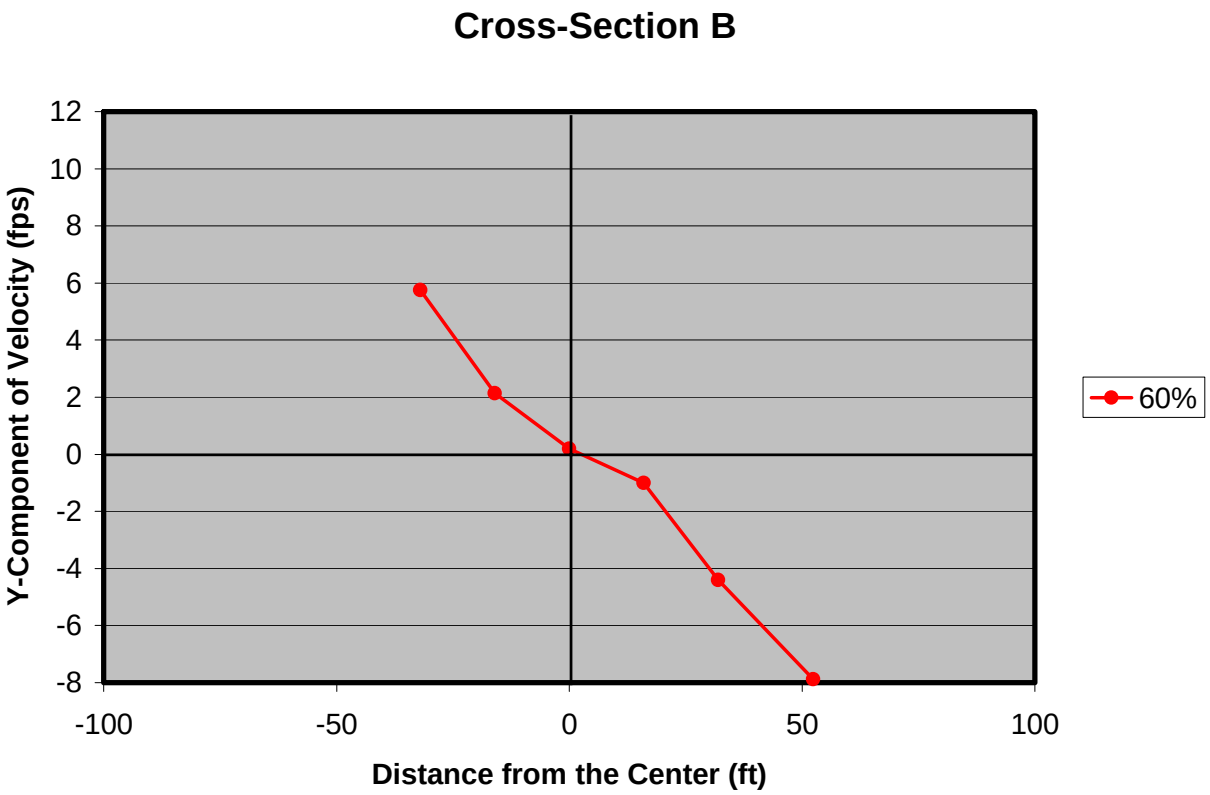

Figure A.14. Y-component of velocity distribution measured at cross-section B under a flow condition of 2278 cfs and no tailwater.

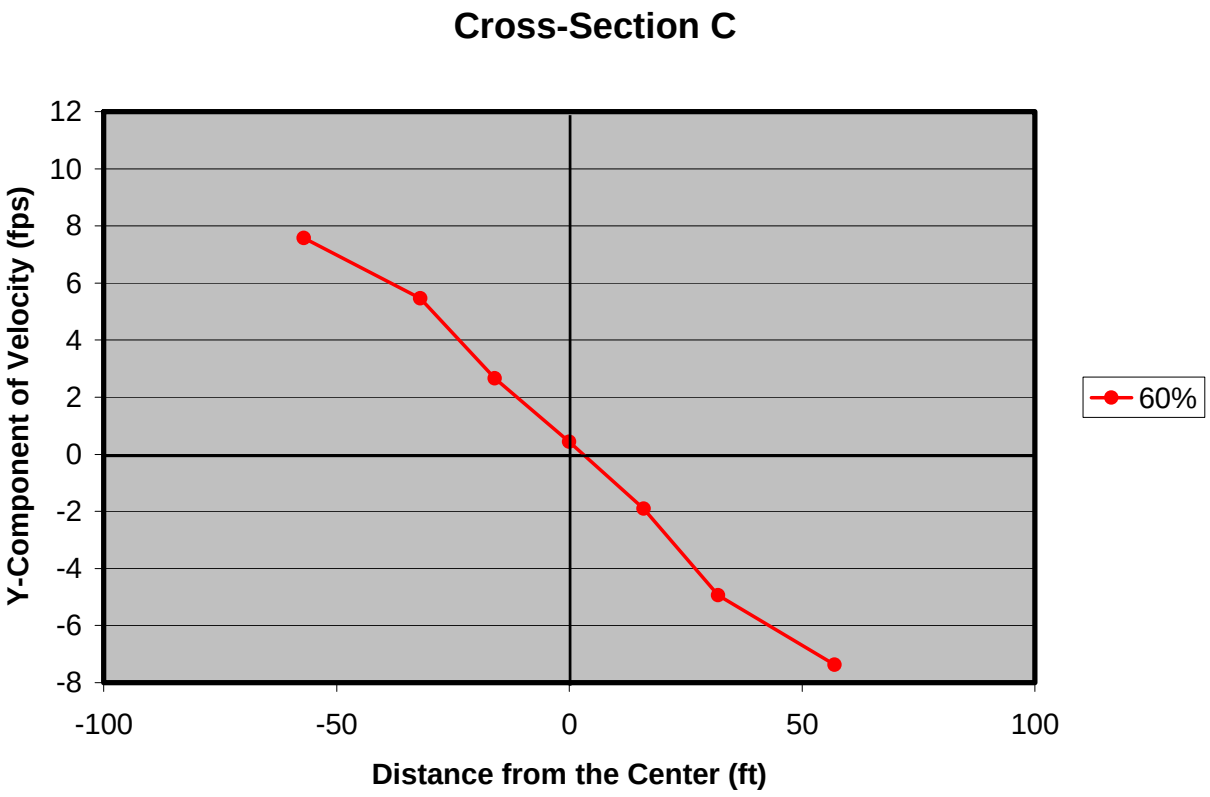

Figure A.15. Y-component of velocity distribution measured at cross-section C under a flow condition of 2278 cfs and no tailwater.

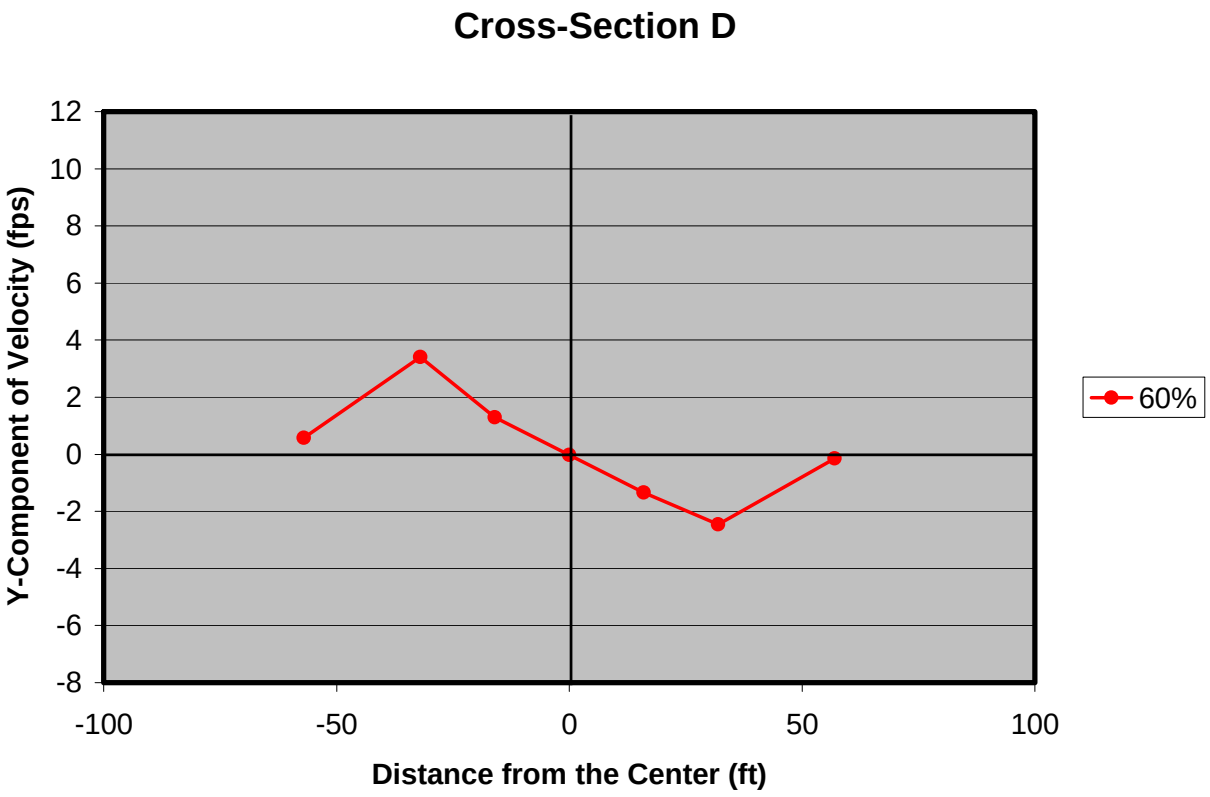

Figure A.16. Y-component of velocity distribution measured at cross-section D under a flow condition of 2278 cfs and no tailwater.

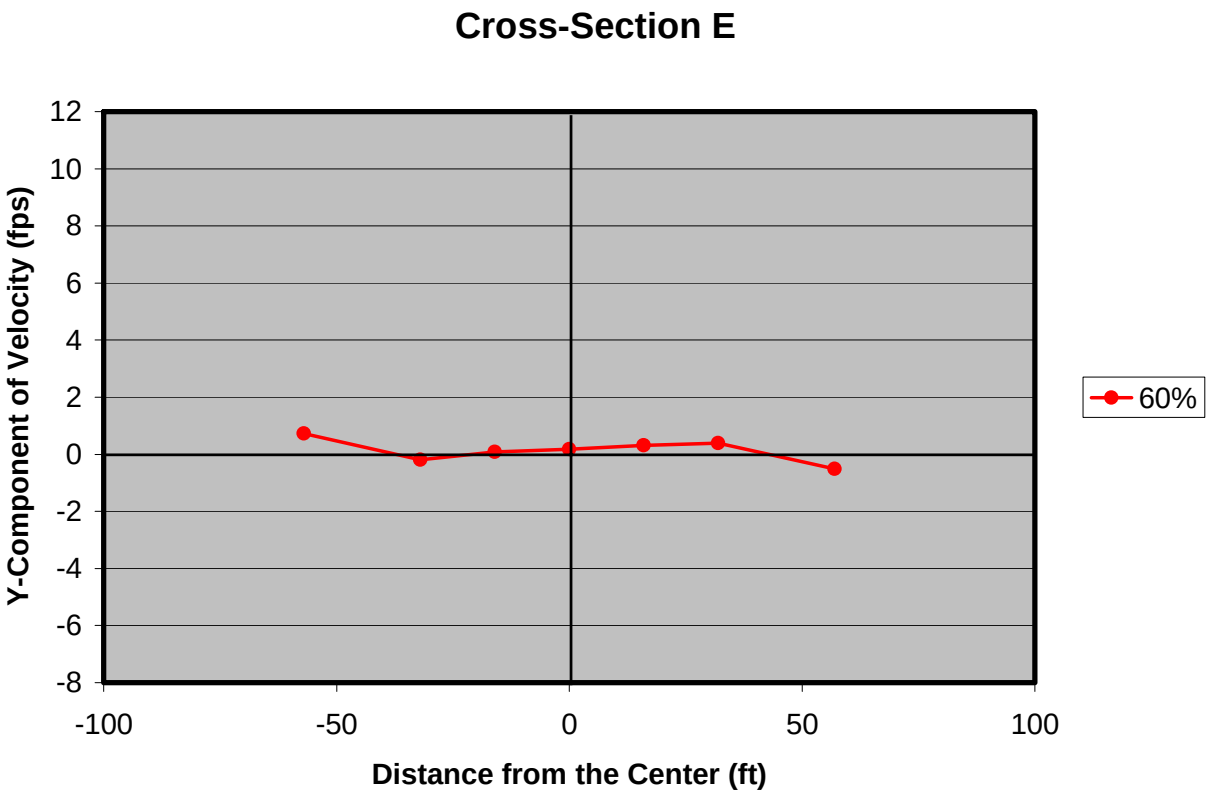

Figure A.17. Y-component of velocity distribution measured at cross-section E under a flow condition of 2278 cfs and no tailwater.